LOS ANGELES PUBLIC LIBRARY

AUG 24 1959

SCIENCE & TECHNOLOGY

ARS JOURNAL

A PUBLICATION OF THE AMERICAN ROCKET SOCIETY

FORMERLY JET PROPULSION

BIND

SURVEY ARTICLE

Space Vehicle Power Systems . . Eugene B. Zwick and Robert L. Zimmerman 553

CONTRIBUTED ARTICLES

Lockheed X-17 Rocket Test Vehicle and Its Applications . . . . Ronald Smelt 565

Aerothermodynamic and Electrical Properties of Some Gas Mixtures to Mach 20 . . . . . W. Chinitz, C. L. Eisen and R. A. Gross 573

Meteoric Ablation Through Interfacial Instability . . . . . .Sin-I Cheng 579

TECHNICAL NOTES

Graphical Computation of Shock and Detonation Waves in Real Gases . . . . . George H. Markstein 585

Magnetic Boundary Layers. . . . . H. F. Ludloff 590

Maximum Ejection Velocity for Return From Satellite Orbits . . . . . Harry Eases 592

Achieving Satellite Rendezvous . . . . . Richard J. Weber and Werner M. Pauson 592

Stability of a Globular Cluster in the Oblate Earth's Equatorial Plane. . . Marvin H. Hewitt 595

Optimum Radiator Temperature for Space Power Systems . . . . . Edward T. Pitkin 596

Optimum Proportioning of Two Propellants to Obtain Maximum Burnt Velocity .R. H. Olds 598

Augmentation of Nuclear Rocket Specific Impulse Through Mechanical-Electrical Means . . . . . Martin Goldsmith 600

Beamed Electromagnetic Power as a Propulsion Energy Source . . . . . Martin I. Willinski 601

Utilization of Stored Energy in Solid Material as an Added Energy Source . John J. Nowgard 603

Optimum Magnetic Field for Stagnation Heat Transfer Reduction at Hypersonic Velocities . . . . . Robert Goulard 604

DEPARTMENTS

Technical Comments 606

Book Reviews 612

New Patents 610

Technical Literature Digest 613

August 1959 Volume 29 Number 8

IMAGINATIVE ENGINEERING

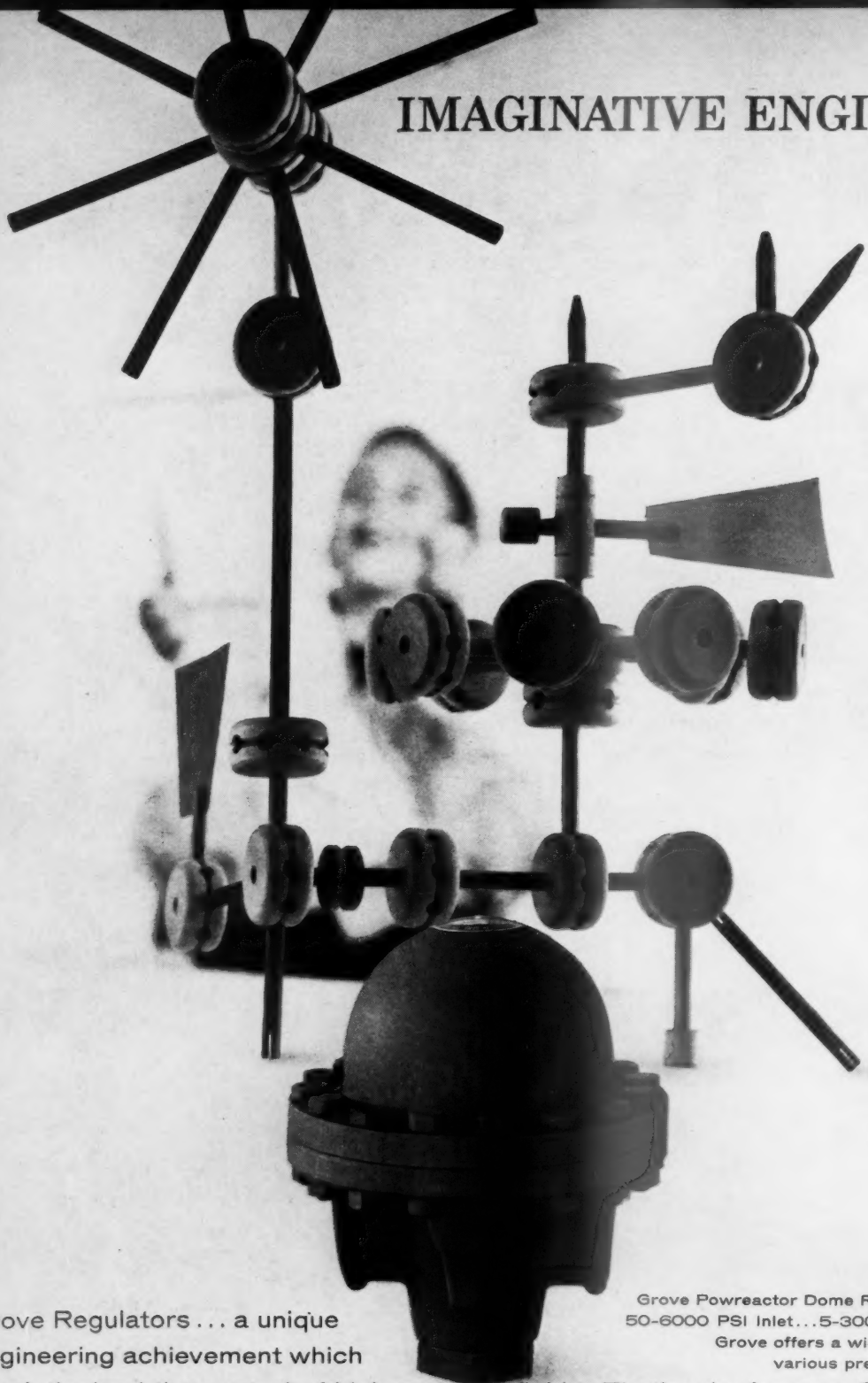

Grove Powreactor Dome Regulator Model GH-408... 50-6000 PSI Inlet...5-3000 PSI Reduced Pressure. Grove offers a wide variety of regulators for various pressure and flow conditions.

Grove Regulators . . . a unique engineering achievement which revolutionized the control of high pressure fluids. That's why for over 20 years—from the first missile experiments in the Navy Experimental Station at Annapolis, to the launching pads of Canaveral and Vandenberg, Grove has been setting the standards for the control of high pressure fluids. Grove Regulators—often imitated but never equalled in design and performance. Unmatched simplicity, accuracy, safety.

GROVE VALVE and REGULATOR COMPANY

3529 Hollis St., Oakland 8, California • 2559 W. Olympic Blvd., Los Angeles 6, California

Offices in other principal cities

Subsidiary of Walworth

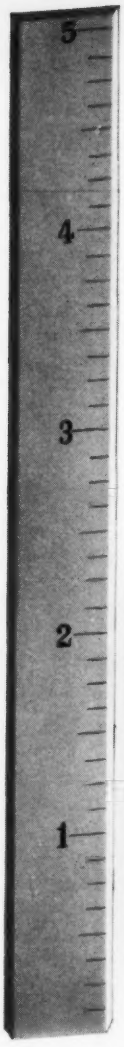

New concepts in modular micro-miniaturization... by Bulova

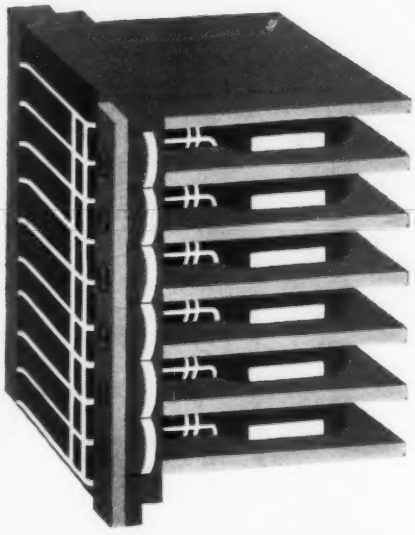

Put Bulova capability behind your program

Bulova is implementing and shaping new concepts in micro-miniaturization, high-density packaging and micro-modular construction.

Bulova craftsmen, toolmaking and production facilities are geared to mass production with tolerances of less than .0003". Watch gaging and quality control techniques provide definite savings in precision assembly.

Experience in precision design, in precision manufacture, is the Bulova capability. Has been for over 80 years. For more information write —

Industrial & Defense Sales, Bulova, 62-10 Woodside Ave., Woodside 77, N.Y.

BULOVA

ARS JOURNAL

A PUBLICATION OF THE AMERICAN ROCKET SOCIETY

FORMERLY JET PROPULSION

EDITOR **Martin Summerfield**

ASSISTANT EDITOR **Barbara Nowak**

ART EDITOR **John Culin**

ASSOCIATE EDITORS

Ali Bulent Cambel *Northwestern University*
Irvin Glassman *Princeton University*
M. H. Smith *Princeton University*

CONTRIBUTORS

Marshall Fisher *Princeton University*
George F. McLaughlin

ADVERTISING AND PROMOTION MANAGER
William Chenoweth

ADVERTISING PRODUCTION MANAGER
Walter Brunke

ADVERTISING REPRESENTATIVES

D. C. Emery and Associates
155 East 42 St., New York, N. Y.
Telephone: Yukon 6-6855

James C. Galloway and Co.
6535 Wilshire Blvd., Los Angeles, Calif.
Telephone: Olive 3-3223

Jim Summers and Associates
35 E. Wacker Dr., Chicago, Ill.
Telephone: Andover 3-1154

R. F. Pickrell and Associates
318 Stephenson Bldg., Detroit, Mich.
Telephone: Trinity 1-0790

Louis J. Bresnick
304 Washington Ave., Chelsea 50, Mass.
Telephone: Chelsea 3-3335

John W. Foster
239 4th Ave., Pittsburgh, Pa.
Telephone: Atlantic 1-2977

American Rocket Society

500 Fifth Avenue, New York 36, N. Y.

Founded 1930

OFFICERS

President	John P. Stapp
Vice-President	Howard S. Seifert
Executive Secretary	James J. Harford
Treasurer	Robert M. Lawrence
Secretary and Asst. Treasurer	A. C. Slade
General Counsel	Andrew G. Haley
Director of Publications	Irwin Hersey

BOARD OF DIRECTORS

Terms expiring on dates indicated

James R. Dempsey	1961	Simon Ramo	1960
Alfred J. Eggers Jr.	1959	H. W. Ritchey	1959
Krafft Ehricke	1959	William L. Rogers	1959
Samuel K. Hoffman	1960	David G. Simons	1961
J. Preston Layton	1960	John L. Sloop	1961
A. K. Oppenheim	1961	Martin Summerfield	1959
William H. Pickering	1961	Wernher von Braun	1960
		Maurice J. Zucrow	1960

TECHNICAL COMMITTEE CHAIRMEN

Lawrence S. Brown, Guidance and Navigation
Milton U. Clauser, Hydromagnetics
Kurt H. Debus, Logistics and Operations
William H. Dorrance, Hypersonics
Herbert Friedman, Instrumentation and Control
George Gerard, Structures and Materials
Milton Greenberg, Physics of the Atmosphere and Space
Stanley V. Gunn, Nuclear Propulsion
Andrew G. Haley, Space Law and Sociology
Samuel Herrick, Flight Mechanics
Max Hunter, Missiles and Space Vehicles
David B. Langmuir, Ion and Plasma Propulsion
Y. C. Lee, Liquid Rockets
Max Lowy, Communications
Harold W. Norton, Test Facilities and Support Equipment
Paul E. Sandorff, Education
William Shippen, Ramjets
John L. Sloop, Propellants and Combustion
Ivan E. Tuhy, Solid Rockets
Stanley White, Human Factors
George F. Wislicenus, Underwater Propulsion
Abe Zarem, Non-Propulsive Power

Scope of ARS JOURNAL

This Journal is devoted to the advancement of astronautics through the dissemination of original papers disclosing new scientific knowledge and basic applications of such knowledge. The sciences of astronautics are understood here to embrace selected aspects of jet and rocket propulsion, space flight mechanics, high-speed aerodynamics, flight guidance, space communications, atmospheric and outer space physics, materials and structures, human engineering, overall system analysis, and possibly certain other scientific areas. The selection of papers to be printed will be governed by the pertinence of the topic to the field of astronautics, by the current or probable future significance of the research, and by the importance of distributing the information to the members of the Society and to the profession at large.

Information for Authors

Manuscripts must be as brief as the proper presentation of the ideas will allow. Exclusion of dispensable material and conciseness of expression will influence the Editors' acceptance of a manuscript. In terms of standard-size double-spaced typed pages, a typical maximum length is 22 pages of text (including equations), 1 page of references, 1 page of abstract and 12 illustrations. Fewer illustrations permit more text, and vice versa. Greater length will be acceptable only in exceptional cases.

Short manuscripts, not more than one quarter of the maximum length stated for full articles, may qualify for publication as Technical Notes or Technical Comments. They may be devoted to new developments requiring prompt disclosure or to comments on previously published papers. Such manuscripts are usually published within two months of the date of receipt.

Sponsored manuscripts are published occasionally as an ARS service to the industry. A manuscript that does not qualify for publication, according to the above-stated requirements as to subject, scope or length, but which nevertheless deserves widespread distribution among jet propulsion engineers, may be printed as an extra part of the Journal or as a special supplement, if the author or his sponsor will reimburse the Society for actual publication costs. Estimates are available on request. Acknowledgment of such financial sponsorship appears as a footnote on the first page of the article. Publication is prompt since such papers are not in the ordinary backlog.

Manuscripts must be double spaced on one side of paper only with wide margins to allow for instructions to printer. Include a 100 to 200 word abstract. State the authors' positions and affiliations in a footnote on the first page. Equations and symbols may be handwritten or typewritten; clarity for the printer is essential. Greek letters and unusual symbols should be identified in the margin. If handwritten, distinguish between capital and lower case letters, and indicate subscripts and superscripts. References are to be grouped at the end of the manuscript and are to be given as follows: For journal articles: authors first, then title, journal, volume, year, page numbers for books: authors first, then title, publisher, city, edition and page or chapter numbers. Line drawings must be clear and sharp to make clear engravings. Use black ink on white paper or tracing cloth. Lettering should be large enough to be legible after reduction. Photographs should be glossy prints, not matte or semi-matte. Each illustration must have a legend; legends should be listed in order on a separate sheet.

Manuscripts must be accompanied by written assurance as to security clearance in the event the subject matter lies in a classified area or if the paper originates under government sponsorship. Full responsibility rests with the author.

Submit manuscripts in duplicate (original plus first carbon, with two sets of illustrations) to the Editor, Martin Summerfield, Professor of Aeronautical Engineering, Princeton University, Princeton, N. J. Preprints of papers presented at ARS national meetings are automatically considered for publication.

ARS JOURNAL is published monthly by the American Rocket Society, Inc. and the American Interplanetary Society at 20th & Northampton Sts., Easton, Pa., U. S. A. Editorial offices: 500 Fifth Ave., New York 36, N. Y. Price: $12.50 per year, $2.00 per single copy. Second-class mail privileges authorized at Easton, Pa. This Publication is authorized to be mailed at the special rates of postage prescribed by Section 132.122. Notice of change of address should be sent to the Secretary, ARS, at least 30 days prior to publication. Opinions expressed herein are the authors and do not necessarily reflect the views of the Editors or of the Society.

© Copyright 1959 by the American Rocket Society, Inc.

NOW!

General Chemical offers Helpful Technical Data on ROCKET FUEL OXIDIZERS

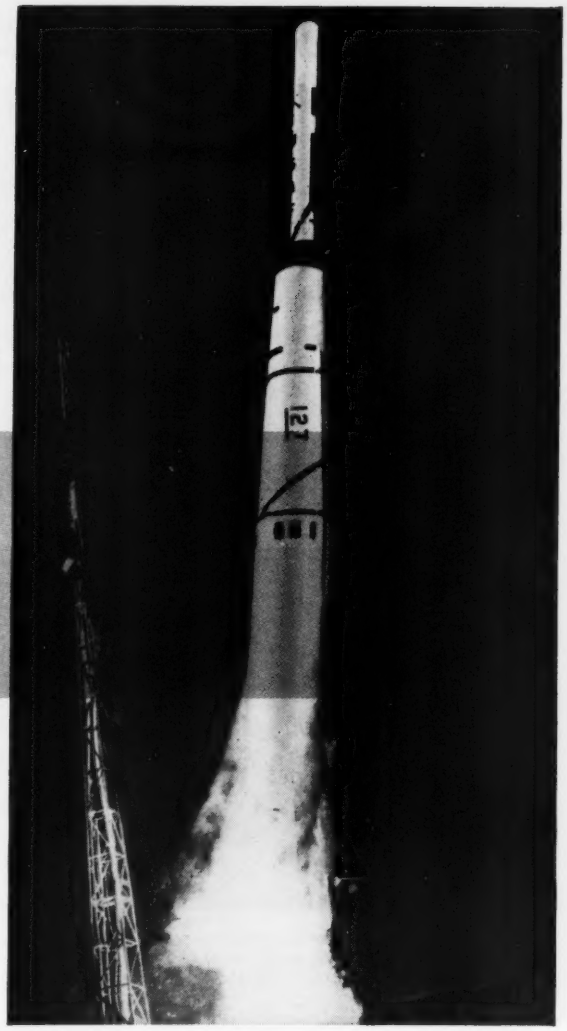

- ✓ **Fuming Nitric Acid**
- ✓ **Liquid Fluorine**
- ✓ **Chlorine Trifluoride and other Halogen Fluorides**

To assist specialists working in the field of rocket and missile propulsion, General Chemical now offers a valuable set of product information bulletins packed with physical and chemical data, tables and graphs. This information is based on General Chemical's extensive experience with these products as America's leading producer of fluorine and fluorine-based chemicals, and one of the nation's primary producers of nitric and other mineral acids. The questions our customers ask most often about these products are answered here.

Here are the specific bulletins offered:

"Nitric Acid, Fuming"—29 pages—Including detailed product description of both red and white fuming nitric acid, chemical and physical properties, corrosion data, directions for storage and handling.

"Fluorine"—21 pages—Including extensive data on the chemical and physical properties of this most powerful oxidizing agent, a description of materials and equipment for handling gaseous and liquid fluorine, safety precautions.

"Chlorine Trifluoride"—35 pages—Including the chemical and physical properties of chlorine trifluoride and other halogen fluorides, recommended materials for use in halogen fluoride systems, directions for safe handling.

Also available are bulletins on:

Handling Elemental Fluorine Gas In The Laboratory
Liquid Fluorine Unloading Procedure
Chlorine Trifluoride Vapor Pressures

Mail coupon now for your free copy of any or all 6 of these valuable technical bulletins.

Allied Chemical

GENERAL CHEMICAL DIVISION
40 Rector Street, New York 6, N. Y.

GENERAL CHEMICAL DIVISION ARS-89
ALLIED CHEMICAL CORPORATION
40 Rector Street, New York 6, N. Y.

Please send the following General Chemical Technical Bulletins:

- ☐ "Nitric Acid, Fuming" (PD-TA-70751)
- ☐ "Fluorine" (PD-TA-85413)
- ☐ "Handling Elemental Fluorine Gas In The Laboratory" (PD-TA-85413A)
- ☐ "Liquid Fluorine Unloading Procedure" (PD-TB-85411)
- ☐ "Chlorine Trifluoride" (TA-8532-2)
- ☐ "Chlorine Trifluoride Vapor Pressures" (DA-85321)

Name_____

Title_____

Company_____

Address_____

City_____ Zone_____ State_____

Historical Achievements at JPL

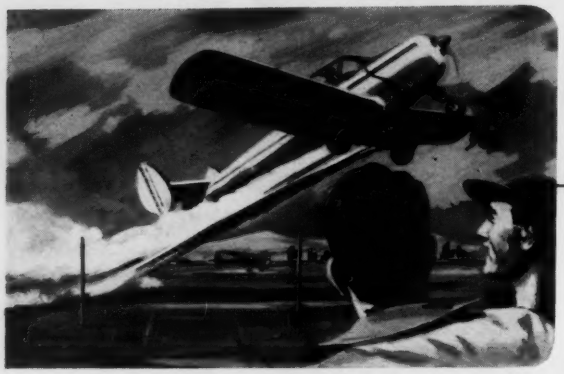

JATO UNITS...The nation's first successful jet-assisted takeoff (JATO) units were originated and developed in 1941 at the Jet Propulsion Laboratory, and sparked the development of future rocket vehicles.

THE WAC-CORPORAL...fired in flight from a V-2 rocket, established a world's altitude record of 250 miles in 1949. The combination was known as the Bumper-Wac.

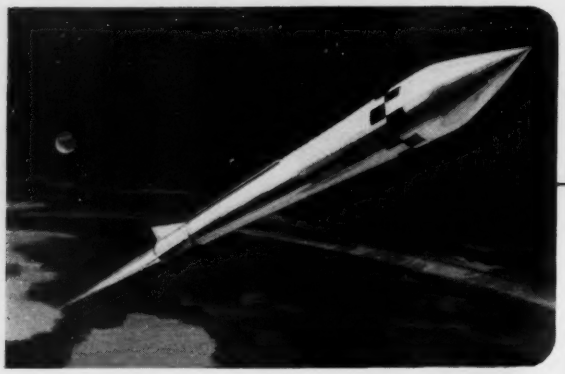

THE CORPORAL...this country's first ballistic surface-to-surface guided missile, now an operational weapon of the U.S. Army, was pioneered and developed by the Jet Propulsion Laboratory.

THE SERGEANT... A second-generation solid propellant missile developed by JPL for the U.S. Army. The SERGEANT is now being readied for production.

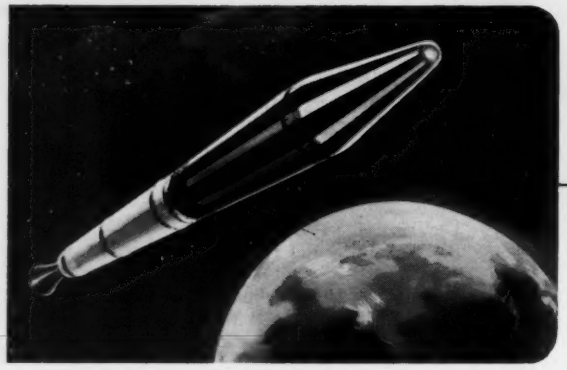

EXPLORER I...The United States' first successful earth satellite, launched January 31, 1958, was developed by JPL in collaboration with the Army Ballistic Missile Agency.

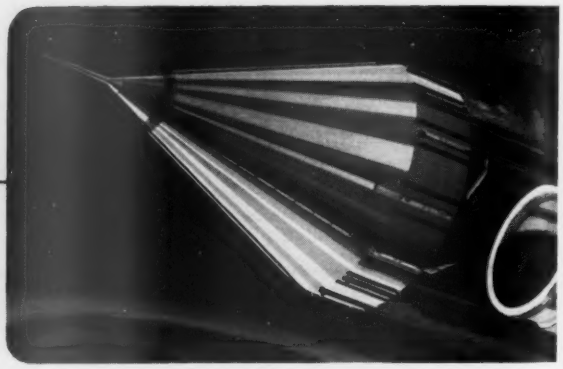

PIONEER IV... America's first successful moon-space probe, launched March 3, 1959, was developed by the Jet Propulsion Laboratory in collaboration with the Army Ballistic Missile Agency and the National Aeronautics and Space Administration.

jpl

CALIFORNIA INSTITUTE OF TECHNOLOGY

JET PROPULSION LABORATORY

A Research Facility operated for the National Aeronautics and Space Administration

PASADENA, CALIFORNIA

Employment opportunities for Engineers and Scientists interested in basic and applied research in these fields:

INFRA-RED, OPTICS, MICROWAVE, SERVOMECHANISMS, COMPUTERS, LIQUID AND SOLID PROPULSION, STRUCTURES, CHEMISTRY, INSTRUMENTATION, MATHEMATICS, AND SOLID STATE PHYSICS

Send professional resume', with full qualifications and experience, for our immediate consideration

Space Vehicle Power Systems

EUGENE B. ZWICK[1] and
ROBERT L. ZIMMERMAN[2]

Sundstrand Turbo Division
Pacoima, Calif.

Mr. Zwick is in charge of the Research Branch at Sundstrand Turbo. He received his B.S. in Physics from California Institute of Technology. Before joining Turbo in 1954 he was with Marquardt Aircraft Co. where he was engaged in the fields of aerodynamics and combustion.

Mr. Zimmerman is in charge of the Systems Integration Branch at Sundstrand Turbo which handles all development projects. Mr. Zimmerman received his B.S. degree from University of California at Berkeley and before joining Turbo in 1953 had spent a number of years with Hughes Aircraft Co. as a specialist in electronic systems.

PRESENTED herein is a review of systems which can be utilized for the generation of secondary and/or propulsion power for advanced space vehicles. The power systems considered are:

Chemically-fueled power supplies; open and closed cycle.
Solar power supplies, closed cycle.
Nuclear power supplies, closed cycle.
Thermionic and thermoelectric power supplies.
Solar photo-voltaic and solar recycling fuel cell power supplies.

Included also in the review are the results of an initial program relating to the optimum temperature ratio, collector and radiator size for general power systems when used with nuclear, chemical or solar energy sources. The performance of the conversion devices *per se* as a function of the collector or radiator environment is not included.

Descriptions are presented of a number of typical power systems. An attempt is made to describe the general physical construction as well as to indicate the limitations of the system. Analyses and estimates have been prepared in order to determine the system weight as a function of power level and duration.

Comparison of some of the systems studied is presented. Weights and sizes of the significant components are tabulated for 1- and 100-kw systems. Variation of system weight with time and power level is plotted to determine the optimum system from a weight standpoint for various applications.

System selection for various missions is summarized, and the role of turbomachinery in space vehicle power systems is noted.

Description of Systems

Many devices which are usable for conversion of energy to electrical power have been given serious consideration by various research groups and industry within this country and Europe. These devices, which are reviewed herein, can be categorized either as: Thermal engines including turbines, thermionic and thermoelectric generators; electrochemical engines including fuel cells and solar regenerated fuel cells; and quantum engines including photo-voltaic cells.

The energy sources for these devices can be derived from a nuclear reactor, the combustion or decomposition of chemicals, the thermal energy from a solar source, or from a discreet quantum of energy at a particular frequency.

Future space vehicles, depending on the application, can utilize the conversion devices or energy sources that have been mentioned. The determination of the most suitable device for the advanced space vehicle depends on factors, such as watts per pound, duration, reliability of the device, effect of a malfunction on the society living within the regime of the device (such as a malfunction of a nuclear reactor at launch when used as a space vehicle power supply), availability of the system and, of course, cost, environment and other usual considerations.

The power requirements for space vehicles can be divided into two categories, the secondary and propulsion requirements. The secondary power requirements are shown in Table 1. These range from 1 to 200 kw for periods of 4 hr to 1 year.

For electrical propulsion systems, however, depending on the length of the mission and the boost thrust available, the power will vary from 50 to 600 kw. The power as a function of specific impulse is shown in Fig. 1. The mass flow rate is inversely proportional to the specific impulse. The power, and therefore the prime mover weight, however, is proportional to the specific impulse. Therefore, the prime mover weight will increase as the total requirement for working fluid increases (extended missions) and the weight rate decreases. An optimum power level exists which depends on the duration of the mission.

The important fact is that power ranging from one to hundreds of kilowatts for periods from a few hours to years will be required.

Systems considered are:

An open cycle chemically-fueled power supply wherein oxygen and hydrogen are used as an energy source. The combustion products are used to drive a rotary prime mover and thence to generate electrical power.

A closed cycle chemically-fueled power supply wherein oxygen and hydrogen are used as an energy source to vaporize a working fluid (liquid sulphur). The recirculated working fluid is used to drive a rotary prime mover and thence to generate electrical power.

A closed cycle solar power supply wherein energy from the sun is collected and concentrated by a parabolic mirror. The concentrated energy is supplied to a boiler to heat the working fluid and then to generate power using the same mechanism as in the closed cycle chemically-fueled power supply.

Presented at the ARS Semi-Annual Meeting, June 8–11, 1959, San Diego, Calif.

[1] Assistant Chief Engineer, Research Branch. Member ARS.
[2] Assistant Chief Engineer, Systems Integration Branch.

Table 1 Power requirements for space vehicles

Mission	Time	kw
manned satellite	4–30 hr	1–15
cislunar vehicle (manned)	150 hr	3–30
lunar orbit probe (unmanned)	300 hr	1–2
circumlunar vehicle (manned)	300 hr	3–30
soft lunar landing and return (manned)	300 hr	10–50
interplanetary probe to Mars	300 days	2–200
interplanetary vehicle (manned)	300 days	10–200

A closed cycle nuclear power supply wherein the energy from a nuclear reactor is transferred to the working fluid. The energy in the working fluid is used in the same manner as it is in the closed cycle chemically-fueled and solar power supply systems.

A solar cell power supply wherein the incident photons from the sun are used to displace electron-hole pairs in a semiconductor and thus generate power. The solar cells are connected in banks to provide the desired terminal voltage and current.

A fuel cell-solar energy power supply wherein incident quanta from the sun are used to dissociate the reaction products from a fuel cell. The reactants, after separation, are recycled to the fuel cell to produce electrical power.

A thermoelectric power supply wherein a temperature difference (Seebeck effect) is used to generate electrical power statically. The thermoelectric power for individual devices is extremely low; thus, hundreds of units operating at high temperature must be used to provide power at practical voltages. The heat source for these devices can be derived either from a nuclear reactor or solar collector system.

A thermionic power supply wherein thermal energy is used to release electrons from a thermionic cathode. High cathode temperatures are utilized to obtain efficiencies comparable with other heat engines. Banks of thermionic generators are required for practical applications. The heat source for these devices can be derived either from a nuclear reactor or solar collector system.

Open Cycle Chemically-Fueled Power Supply

Open cycle power supplies use the hot exhaust gases from propellants to drive a prime mover, which provides shaft power for the generation of mechanical or electrical energy. Such units can use cryogenic propellants as well as the more conventional mono- and bipropellant liquids and the solid propellants. Fig. 2 is a block diagram of an open cycle system which utilizes, for this example, cryogenic propellants. The system consists of: Propellant tanks, combustion chamber, a turbine as a prime mover, an alternator and controls.

A study of power supplies for long duration space vehicles indicates that, for an open cycle system, the minimum propellant weight is attained from the use of liquid hydrogen and liquid oxygen as the propellants.

A simple open cycle system which utilizes cryogenic propellants may be pressurized by supplying heat to the propellant tanks. The power into the heater is controlled as a function of the tank pressure with a pressure sensitive switch.

The hydrogen leaving the storage tanks is used as a coolant to absorb the heat generated in the rotating equipment as a result of inefficiencies. The waste heat from the prime mover exhaust is used to raise the hydrogen temperature so that the hydrogen can be used to heat the oxygen. The hydrogen and oxygen are heated to equal temperatures by passing these gases through a concurrent heat exchanger before entering the constant-pressure regulator; thus, gas is supplied to the reaction chamber at a fixed mixture ratio producing a 2200 F hot gas to drive a turbine. The gas temperature is maintained below a stoichiometric temperature by utilizing a hydrogen-rich mixture of six times the stoichiometric requirements.

The gases, after being expanded through the nozzle, impinge on the buckets of a multistage single or multiple disk turbine. Although the general system described uses a turbine as a prime mover, substitution of a positive displacement device for a turbine would not materially affect the overall concept or the performance. Table 2 represents a study of the characteristics of a 1-hp, 324-hr, open cycle prime mover with an optimum propellant. Studies indicate that, for short duration chemically-fueled open cycle systems, an

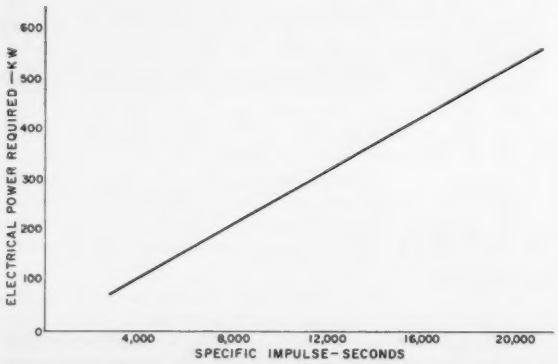

Fig. 1 Ion propulsion. Power vs. specific impulse for 1-lb thrust

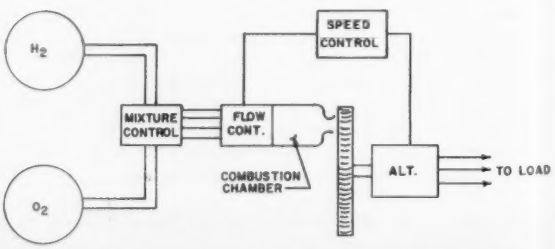

Fig. 2 Open cycle chemical power supply

optimum system would weigh approximately 600 lb, and the volume would be approximately 60 ft³. The information in Table 2 has been scaled and presented in Fig. 15 to facilitate comparison with other systems.

Closed Cycle Chemically-Fueled Power Supply

The closed cycle system is very similar to the open cycle system described previously except that, in this case, the energy from the reaction is utilized to heat a working fluid which drives the prime mover. In the open cycle system, the hot gas products from the propellant were used to drive the prime mover directly. For the closed cycle chemically-powered system, a cryogenic oxygen-hydrogen bipropellant is best. In contrast to the open cycle system, the propellants are now burned stoichiometrically in order to obtain the maximum energy per pound from the reaction.

Stress considerations limit the temperature of the prime mover to about 2000 F. The mass flow of the propellants to the burner is controlled so that the turbine working fluid does not exceed this temperature.

The closed cycle system which is represented in Fig. 3 consists of:

Oxygen-hydrogen tanks which provide the chemical energy to the system.

A bipropellant constant-pressure regulator to control the pressure to the gaseous propellants.

A boiler which uses heat energy from the propellants to vaporize the working fluid.

A turbine which transforms the energy available in the gas to mechanical power to drive an alternator.

A condenser which radiates the unused heat in the cycle.

A pump which returns the working fluid from the condenser to the boiler for recirculation in the system.

The oxygen and hydrogen are supplied from their respective tanks by thermal pressurization. Tank pressure is controlled by varying the power to the tank heaters. The hydrogen gas is utilized as a coolant for the rotating machine so that its temperature can be maintained at a prescribed level. Both the gaseous oxygen and hydrogen after passing through concurrent heat exchangers are supplied to the bipropellant pressure regulator and then to the reaction chamber portion of the boiler. The working fluid which is supplied to the boiler from the condenser is vaporized by the heat transferred from the reaction. The high pressure high temperature working fluid is expanded through the nozzle and impinges on the turbine. The superheat in the exhaust gas and the latent heat of condensation are radiated to the background temperature of space. The resulting liquid working fluid at the outlet from the condenser is passed through an alternator cooling jacket and then to the boiler.

The closed cycle system, in addition to the basic elements which have been considered, also requires controls for the liquid content of the boiler, the boiler pressure and the turbine speed.

The selection of a working fluid for a Rankine engine depends on a number of factors. The most important of these are the temperatures to be utilized in the cycle. In order to achieve a high thermal efficiency, it is important that the

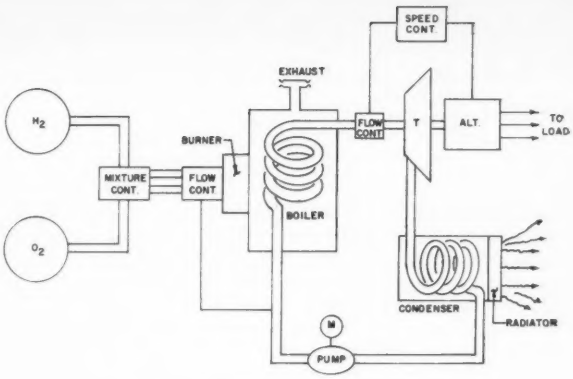

Fig. 3 Closed cycle chemical power supply

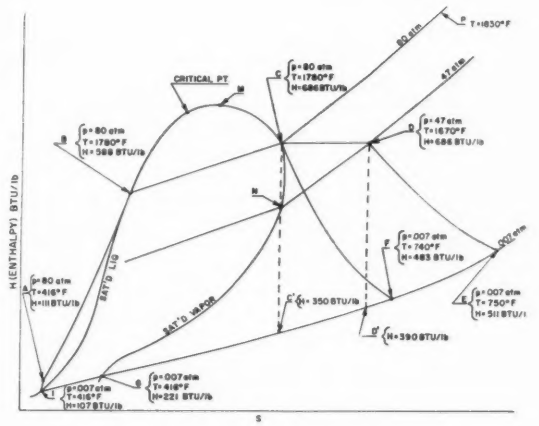

Fig. 4 Enthalpy-entropy diagram for sulphur

critical temperature of the working fluid be at or above the maximum temperature to be utilized in the cycle. Superheating above the critical temperature results in little gain in thermal efficiency but a very considerable increase in material problems. It is, of course, important that the fluid remain liquid down to the minimum temperature to be utilized in the cycle. An additional fluid property which is of considerable significance in system design and durability is the shape of the Mollier diagram. It is quite desirable to have a fluid on whose Mollier diagram the saturated vapor line shows a positive slope. Comparison of a number of fluids, including water and mercury, led to the selection of sulphur as a closed cycle working fluid. It has a relatively low melting point, 240 F; its critical temperature is high, approximately 1900 F, and its Mollier diagram indicates a positive slope of the saturated vapor curve up to approximately 80 atm as indicated in Fig. 4.

A study program for a 324-hr, 1-hp, closed cycle system

Table 2 Chemical open cycle system performance, O_2 and H_2 power supply

Prime mover		Shaft power, 1.0 hp / Total energy, 324 hp hr — Propellant					
Type	Weight, lb	Type	S.F.C., lb/hp hr	Weight, lb	Volume, ft³	Tank weight, lb	Total weight, lb
four stage turbine	20	H_2-O_2	1.8	556	62.0	50	626

Table 3 Chemical closed cycle system performance, O_2 and H_2 power supply

Rotational speed, rpm	S.F.C., lb/hp hr	Fuel weight, lb	Fuel volume, ft³	Tank weight, lb	Prime mover weight, lb	Total system weight, lb
24,000	1.68	545	22.4	24	60	640
64,000	1.33	433	17.8	20	37	508

which utilized sulphur as the working fluid and hydrogen and oxygen as the propellants has been completed. Table 3 indicates the weight and volume characteristics of this system.

The table indicates that for the closed cycle compared with the open cycle system, the machinery weight is higher, but the superior performance results in a total system weight approximately 10 per cent less. The volume, for this oxygen-hydrogen system operating stoichiometrically, is a factor of three less than the open cycle requirements.

Closed Cycle Solar Power Supply

The closed cycle solar power supply will be identical to the chemical closed cycle system except for the energy source. For the solar power system, a parabolic mirror is used to collect the incident solar energy and focus this energy into a boiler. The latent heat of condensation and superheat, in a manner identical to the chemical closed cycle system, is radiated to space (Fig. 5).

The incident energy available to a collector in the vicinity of the Earth's surface is 440 Btu/hr-ft². This corresponds to approximately 0.13 kw/ft². The energy available at the collector is less than 440 Btu/hr-ft² by the amount that is reradiated by the boiler. The boiler access area, which in the limit is determined by the diameter of the sun's image at the focus, in practical applications will be the area required to accommodate the various aberrations in the mirror system.

The mirror size can be determined from the Carnot and device efficiency. The Carnot efficiency

$$\eta_{lc} = \frac{T_H - T_R}{T_H}$$

is the maximum thermal efficiency obtainable from a heat engine working between a high temperature T_H and a low temperature T_R. Device efficiency is defined here as the ratio of the actual thermal efficiency of the device in question to that achievable by a Carnot engine. This ratio f is a useful means of comparing various heat engines. The value of f tends to remain constant for a given cycle over a wide range of operating points. Maximum thermal efficiency (product of Carnot and device efficiency) results in a minimum size collector. The Carnot efficiency is dependent on the boiler temperature, which is limited by material considerations, and the radiator temperature. Low radiator temperatures, however, result in large radiator area requirements, since radiant heat rejection is proportional to the fourth power of the radiator temperature.

A preliminary study was made to determine the optimum temperatures for the boiler and radiator. Expressions for the weight of the collector and radiator (as a function of temperature ratio, area, specific weights, device efficiency and temperature) were optimized for minimum weight. The results of the study are presented in Figs. 6, 7 and 8.

Fig. 6 permits the computation of a parameter R which depends on T_H, the high temperature in the cycle; W_1 and W_2 the specific weights of the collector and radiator; η_K the efficiency of the collector, and ϵ the emissivity of the radiator. Inefficient collection yields high values of R; inefficient radiation yields low values of R.

In Fig. 7 the optimum radiator temperature is presented. α, the ratio of T_R to T_H is given as function of R with the device efficiency f as a parameter. For high values of R (collector size problems) the radiator optimizes at low temperatures.

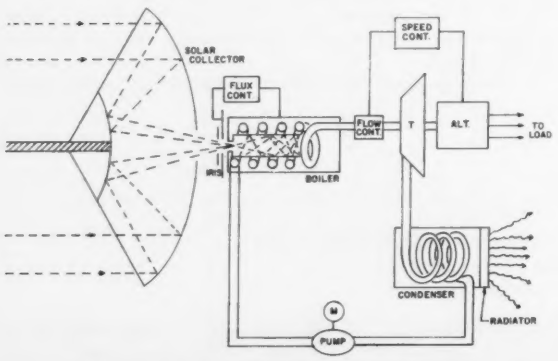

Fig. 5 Closed cycle solar power supply

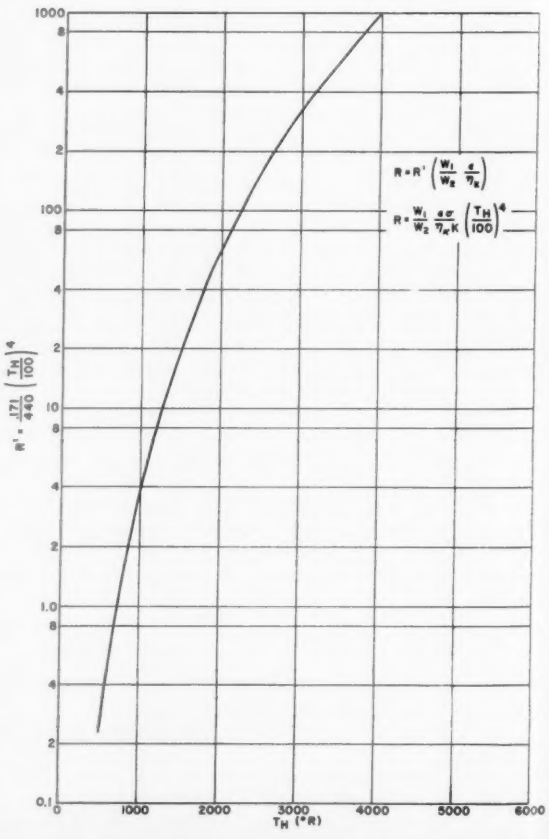

Fig. 6 R' vs. maximum cycle temperature for a power system with a solar collector, prime mover and radiator

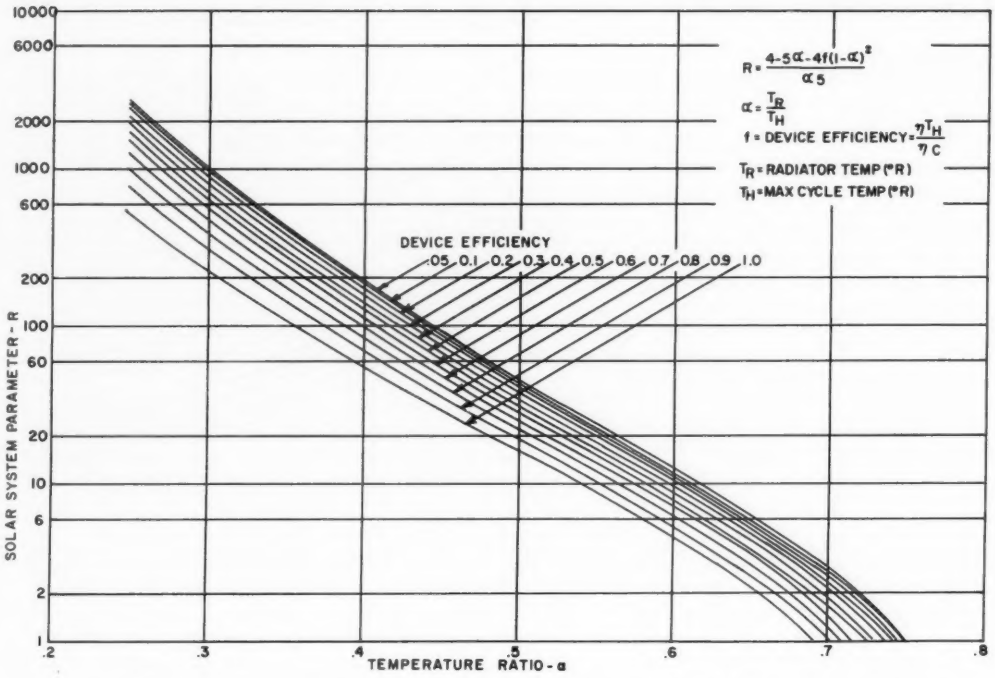
SOLAR SYSTEM PARAMETER - R
TEMPERATURE RATIO - α
DEVICE EFFICIENCY
.05 0.1 0.2 0.3 0.4 0.5 0.6 0.7 0.8 0.9 1.0
R = 4-5α-4f(1-α)²/α5
α = T_R/T_H
f = DEVICE EFFICIENCY = ηT_H/η C
T_R = RADIATOR TEMP (°R)
T_H = MAX CYCLE TEMP (°R)

Fig. 7 Optimum temperature ratio for a power system with a solar collector, prime mover and radiator

which yields relatively high thermal efficiency. For low values of R, the radiator optimizes at high temperatures which tends to minimize radiator area.

Fig. 8 presents the combined collector and radiator weight as a function of R and device efficiency. The weight is normalized here by the specific weight of the collector and the collector efficiency.

An example of the use of the curves for a 100-kw system follows. Fig. 6

$$T_H = 2240 \text{ R}$$
$$R' = 100$$
$$W_1/W_2 = 0.4$$
$$\epsilon/\eta_K = 1$$

thus

$$R = 40$$

Fig. 7

$$R = 40$$
$$f = 0.68$$

thus

$$\alpha = 0.465$$
$$T_R = 0.465 \times 2240$$
$$T_R = 1030$$

Fig. 8

$$R = 40$$
$$f = 0.68$$
$$W' = 28$$
$$\eta_K = 0.9$$
$$W_1 = 0.2$$

thus

$$W = 6.5 \text{ lb/kw (collector + radiator)}$$
$$\eta_{TH} = f(1 - \alpha) = 36.5 \text{ per cent}$$
$$P_{IN} = 100\text{kw}/0.36 = 275 \text{ kw}$$
$$A_c = \frac{275\text{kw}}{0.9 \times 0.13\text{kw/ft}^2} = 2370 \text{ ft}^2$$
$$W_c = 2370\text{ft}^2 \times 0.2 = 474 \text{ lb}$$
$$W_R = 650 - 474 = 176 \text{ lb}$$

The results from the curves do not consider variations in the performance of the prime mover in the systems. An actual system would have to take into account the H-S curve for the working fluid as well as the relationship between device efficiency and pressure ratio.

The weights of closed cycle power systems, using the data of the collector-radiator study and including the weight of other equipment, such as turbines, alternators and boilers established in prior studies, are presented in Fig. 16 as a function of power for time invariant systems. The same information is presented in Fig. 15 at powers of 1 and 100 kw, so that it can be compared with time variant systems.

Practical considerations will limit the application of solar energy. Before a 100-kw device can be made feasible, it will be necessary to devise erecting schemes and mechanical configurations so that large, low weight parabolic mirrors can be unfolded in space. The mirror, for the 100-kw system for example, must be 60 ft in diameter.

Closed Cycle Nuclear Power Supply

The closed cycle nuclear power supply shown in Fig. 9 is similar to the closed cycle solar and closed cycle chemical power supplies in that it uses a Rankine cycle heat engine to convert thermal energy into electrical power. Heat is sup-

$$W = W_1' \frac{W_1}{\eta_K} = \frac{\text{COLLECTOR WT} + \text{RADIATOR WT}}{K \cdot W_\cdot}$$

$$W = \frac{3413\, W_1}{f}\left\{\frac{1}{f}\left[\frac{4-4f+3\alpha f}{(4-5\alpha)-(1-\alpha)^2 4f}\right]\right\}$$

$$R = \frac{W_1}{W_2}\frac{\epsilon\sigma}{\eta_K K}\left(\frac{T_H}{100}\right)^4$$

σ = STEFAN BOLTZMANN CONST = 0.1713

K = SOLAR CONST = 440 BTU/FT^2 HR

ϵ = RADIATOR EMISSIVITY

η_K = COLLECTOR EFFICIENCY = 0.9

W_1 = COLLECTOR SPECIFIC WT (lb/FT^2) = 0.2

W_2 = RADIATOR SPECIFIC WT (lb/FT^2) = .5 TO 2

f = DEVICE EFFICIENCY

$\alpha = \frac{T_R}{T_H}$

T_R = RADIATOR TEMP (°R)

T_H = MAXIMUM CYCLE TEMP (°R)

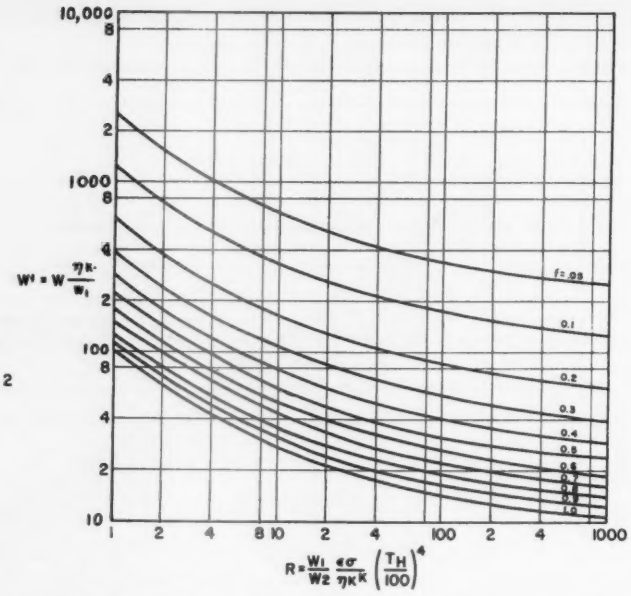

Fig. 8 Optimum radiator and collector per unit specific weight for a power system with a solar collector, prime mover and radiator

plied to the working fluid from a nuclear reactor and is rejected to outer space by radiation. The reactor for this application will be a small nuclear reactor, with or without shielding, depending on the mission for which the power supply is to be utilized.

Current technology indicates that small nuclear reactors using sulphur as the working fluid can achieve a thermal output of approximately 2 megawatts (2000 kw) per ft^3 with a weight of approximately 300 lb per ft^3, exclusive of shielding. The minimum reactor size which may be made critical is approximately $\frac{1}{2}$ ft^3. Thus, for any space vehicle power supply using nuclear energy there will be a minimum of 1 megawatt (1000 kw) of thermal energy available from a $\frac{1}{2}$-ft^3 reactor weighing 150 lb. Using a cycle efficiency of 35 per cent obtainable from closed cycle sulphur systems, up to 350 kw can be provided by the use of this minimum 1 megawatt heat source.

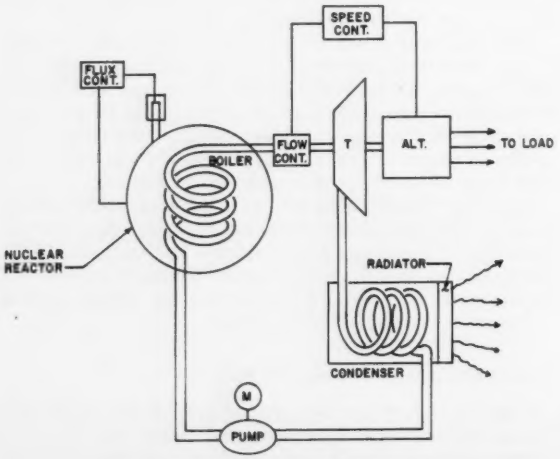

Fig. 9 Closed cycle nuclear power supply

For large power outputs, the weight of the radiator is the dominant factor in total system weight. A study was made to determine the criteria for minimizing the radiator area as a function of the maximum cycle temperature and the device efficiency. The thermal efficiency is given by the product of the Carnot and device efficiency.

The results of this study show that for a device efficiency of 1.0, the minimum radiator area is achieved when the ratio of radiator to maximum temperature is 0.75 (see Figs. 10 and 11). The thermal efficiency for this condition is 0.25. For device efficiencies approaching zero, the optimum temperature ratio approaches 0.8 and the thermal efficiency approaches 0.2f. An example of the use of the curves for a 400-kw system is, from Fig. 10

$$P_0 = 400 \text{ kw}$$
$$= 0.8$$

$$\alpha = 1 - \frac{8}{\eta_T}\left[1 - \sqrt{1 - \frac{15f}{25}}\right]$$

$$\eta_{TH} = \frac{8}{9}\left[1 - \sqrt{1 - \frac{15f}{25}}\right]$$

$\alpha = \frac{T_R}{T_H}$

$\eta_{TH} = \eta_C f$

$\eta_C = \frac{T_H - T_R}{T_H}$

f = DEVICE EFFICIENCY

T_R = RADIATOR TEMP (°R)

T_H = MAX CYCLE TEMP (°R)

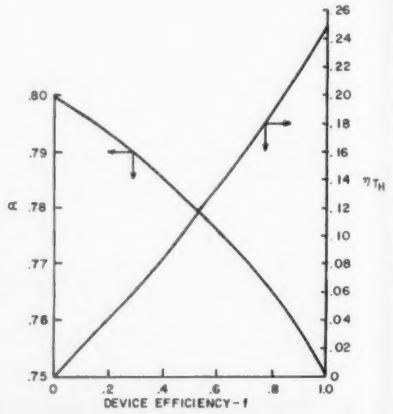

Fig. 10 Optimum temperature ratio and thermal efficiency for a power system with an internal heat source, prime mover and radiator

thus

$$\alpha = 0.765$$
$$\eta_e = 1 - \alpha = 0.235$$
$$\eta_{TH} = 0.19$$

from Fig. 11

$$T_H = 1750 \text{ R}$$
$$A_R = 3 \text{ ft}^2/\text{kw}$$

Fig. 16 shows the power vs. weight for the unshielded nuclear closed cycle system. For power levels less than 350 kw, the weight increases due to increases in the prime mover and radiator weight. For power levels in excess of 350 kw, the reactor size as well as the prime mover increases proportionally to the output. The comparison with time variant systems is shown in Fig. 15.

Specific weights for the radiator calculations were assumed to be 2.0 lb per ft² for a power level of 1 kw, and 0.5 lb per ft² for power levels in excess of 100 kw.

Solar Cell Power Supply

Solar cells have recently been used as direct converters of solar energy for power applications. These cells have been introduced commercially by a number of companies.

The semiconductor solar cells consist of P-type and N-type silicon. The N-type silicon has an excess electron due to the doping of the silicon with a material which has five electrons in the valence orbit. The P silicon has a lack of electron or a hole due to the doping of this part of the cell with a material with three electrons in the valence orbit. When photons from the sun impinge upon the surface of the solar converter they are absorbed with a resultant displacement of electron-hole pairs. The displacement of an electron or a hole near the junction will result in a continuous shift of electrons and holes within the complete lattice and through the load, thus providing electrical current.

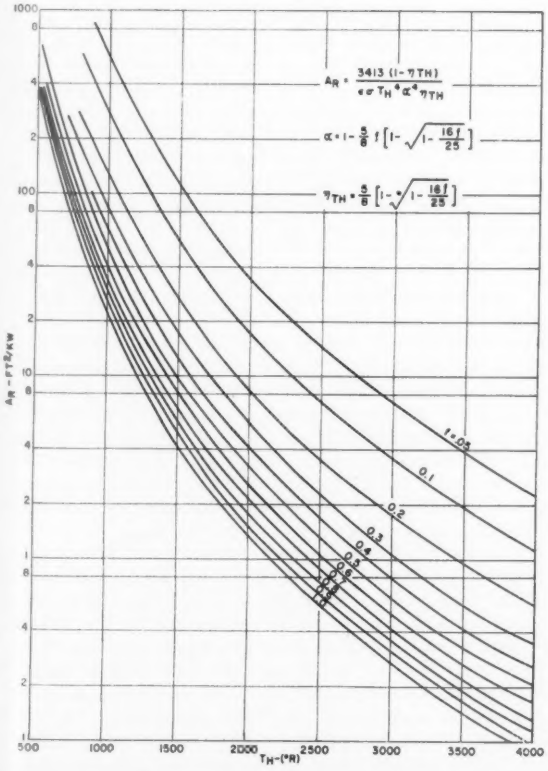

Fig. 11 **Optimum radiator area for a power system with an internal heat source, prime mover and radiator**

Solar converters presently provide output with a conversion efficiency of approximately 10 per cent. Thus for a 100-w solar conversion system, approximately 8 ft² of silicon cells will be necessary. The figure of merit for solar cells has been reported to vary from 0.1 to 0.25 lb per w. The lower value is used for large multikilowatt converters. Current research is directed at increasing the conversion efficiency of solar cells by variation of composition and stacking. This latter technique involves the interception of light passing through one cell by a second cell placed behind it which is sensitive to wave lengths to which the surface cells are transparent. These gains in efficiency will, of course, be accompanied by an increase in weight per unit area and a reduction in area requirements. Series parallel connections are necessary to provide the required voltage and current from solar cells. For a 3-kw system, approximately 100,000 cells with a total weight of 600 lb will be required.

Solar cells have an advantage over the systems discussed previously, in that they can be assembled into systems of very low power level with little fixed weight penalty. Thus a 10-w system will require approximately two times the weight of a 5-w system. In contrast, the weight of turbomachinery at low power levels tends to approach an irreducible minimum independent of power level, so that a 10-w solar closed cycle system would probably weigh substantially the same as a 50- or a 5-w system.

For systems which operate without incident solar energy, it is necessary to utilize electrochemical batteries in conjunction with the solar cell. The batteries for this type of a configuration will be charged during the period when the solar collector can be oriented toward the sun and discharged during the dark part of the orbit.

For alternating current requirements it will be necessary to use either a rotary-type inverter or a static transistorized inverter.

The regime wherein the solar cell configuration is optimum is shown in Figs. 16 and 18.

Fuel Cell-Solar Energy Power Supplies

The fuel cell-solar energy system makes use of two sources of energy. These are the exothermic energy available from the reaction of the stored reactants of the fuel cell system and the energy available as radiant energy to reconstitute the product of the reaction to the original form.

The fuel cell does not differ from a conventional battery in its theory of operation. The difference is physical; in a conventional battery the chemicals are stored on the plate materials, whereas in the fuel cell the chemicals are stored externally in separate containers.

A typical space vehicle, one possible application for a fuel cell, might require power for only a small part of each day spent in space. Thus, in a conventional cell, the reactants would have to be available for the total expected power-time product delivered to the end item (a transmitter, television camera, space surveillance equipment or other).

However, if solar energy is utilized, the large power pulse can be furnished by the reaction of the stored reactants. The dissociation of the product, charging the fuel cell system, is accomplished over a longer period of time with a comparatively small solar collector. The block diagram shown in Fig. 12 represents a typical solar energy charging system. Proper mechanization of the system will result in the overall conversion of solar energy into electricity with an electrochemical process as an intermediate step.

The solar conversion scheme is in the research stage, and, as such, no information is available pertaining to the weight,

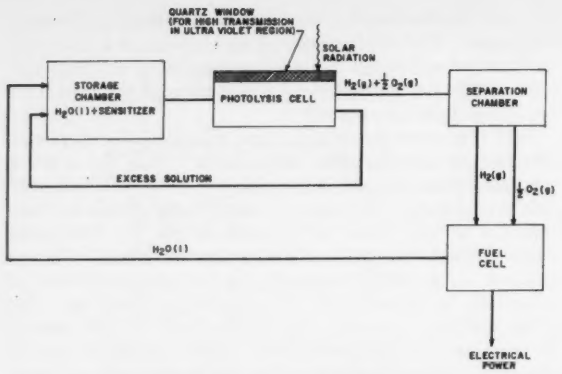

Fig. 12 Diagram of recycling fuel cell using solar energy to photo-dissociate product of fuel cell

volume or, indeed, the practical feasibility of such a device.

In order for the fuel cell-solar conversion scheme to be practical and competitive, it will be necessary for this device to make maximum use of the available energy from the sun. The silicon solar cell presently provides 100 w per m², and the closed cycle solar-turbines provide approximately 350 w per m² of collector area. The fuel cell-solar system must provide more than 100 w per m² in order to compete with the simple solar cell.

Conventional photolysis techniques for dissociating the reaction products are effective for wave lengths less than 3100 Å. The incident energy, however, to 3100 Å is only 27 w per m². If the photolysis range is extended to 4100 Å and thence to 5100 Å by the use of sensitizers, the incident power increases to 134 and 330 w per m², respectively.

A type of fuel cell which has received considerable research attention for the past 100 years uses the hydrogen-oxygen reaction. It should be emphasized that hydrogen and oxygen reactants provide an electrochemical device with minimum weight and volume from a stored chemical viewpoint. A number of other possibilities exist, such as a nitric oxide-chlorine reaction or a lithium-hydrogen reaction which, from a system point of view, might provide a better solar regenerated fuel cell end item.

In particular, the nitric oxide-chlorine reaction has a much wider spectral sensitivity for photochemical dissociation than hydrogen-oxygen and appears very attractive. The system would consist of a cell utilizing the reaction product nitrosyl chloride as a solvent for a suitable electrolyte. Overall conversion efficiency of the nitric oxide-chlorine solar regenerative fuel cell will be comparable to silicon solar cells. Advantages of this system include the ease with which large systems can be fabricated together with the inherent storage capabilities of the system.

The fuel cell differs in one major respect from the other closed or open cycle systems. Each of the other systems is limited by the Carnot efficiency. The fuel cell *per se* is not Carnot-limited and theoretically can achieve 100 per cent efficiency. Fuel cells using hydrogen-oxygen have been reported with efficiencies of 60 to 70 per cent. The major disadvantage is the weight. Present estimates range from 130 to 400 lb per kw for 600 psi, 240 C and 15 psi, 50 C batteries.

Thermoelectric Power Supply

Recent advances in the technology of materials have made feasible the generation of power by thermoelectric methods. P- and N-type materials compounded from high atomic weight substances, such as lead, bismuth, tellurium and mercury have been investigated. Research studies indicate that theoretical device efficiencies of 5 to 7 per cent for bismuth telluride-bismuth and P- and N-type bismuth telluride are obtainable.

Research activity has been directed toward materials which provide high thermoelectric power (mv/deg C) with minimum resistivity and thermal conductivity. It is desired to optimize these parameters in order to maximize the generated voltage and to minimize the internal power (I^2R) and thermal conductivity losses.

Two schemes have been considered which use a thermoelectric generator for space application. One method uses a nuclear reactor to provide the thermal energy and a radiator to maintain the temperature of the cold junction. The second method uses a solar mirror to focus the incident energy on to the junction. These systems are presented in Figs. 13 and 14.

The efficiency for these heat engines, like the closed cycle turbine or reciprocator, can be expressed as the product of the device and Carnot efficiencies

$$\eta_{TH} = \frac{T_H - T_R}{T_H} f$$

Expressions for f have been derived which involve the thermoelectric power of the materials used S, the product of the resistivity ρ and the thermal conductivity k

$$f_{\text{opt}} = \frac{M - 1}{M + (T_R/T_H)}$$

where

$$M = \sqrt{1 + \frac{v}{2}\left(\frac{T_H + T_R}{T_R}\right)}$$

and

$$v = \frac{(S_1 + S_2)^2 T_R}{(\sqrt{k_1\rho_1} + \sqrt{k_2\rho_2})^2}$$

Static thermoelectric engines are presently limited in temperature difference as well as maximum temperature. The reported thermal efficiency for laboratory devices operating at 2000 F with a ΔT of 990 deg is approximately 2 per cent. The output voltage for these devices is approximately 0.2 mv per deg C. One hundred and eighty-seven couples will be required for a 20-v bank with a ΔT of 990 F. The devices, in addition, may require pumps and motors to circulate the working fluid and coolant, and thus approach a rotating closed cycle heat engine in complexity without providing the performance. The reliability of static devices may be low due to the requirements for large numbers of high temperature connections.

The parameter R (Fig. 6) for a hot junction temperature of 2460 R, a radiator weight of 2.0 lb per ft², an emissivity of 0.9 and a collector at 0.2 lb per ft² with 90 per cent efficiency is equal to 15. An examination of Fig. 8 for a device efficiency of 5 per cent indicates $W' = 600$, which yields, for the collector and radiator, a specific weight of 133 lb per kw. The specific weight for the generator is reported to be approximately 1000 lb per kw; accordingly, the system would weigh 1133 lb to produce 1 kw.

A somewhat different set of operating conditions is required if the static thermoelectric generator is used with a nuclear heat source. There will, in general, be a temperature limitation to the reactor, say for example 1500 F. For this temperature and an efficiency equal to 5 per cent of the Carnot efficiency ($f = 0.05$), a radiator area of 36 ft² is required at an emissivity of 1.0 (see Fig. 11). Assuming $\epsilon = 0.9$, 40 ft² will be needed. At 2 lb per ft², the radiator weight will be 80 lb. The minimum size nuclear heat source is about a $\frac{1}{2}$-ft³ device and will weigh about 150 lb. The total system weight including auxiliary equipment, will be approximately 1230 lb for a 1-kw system.

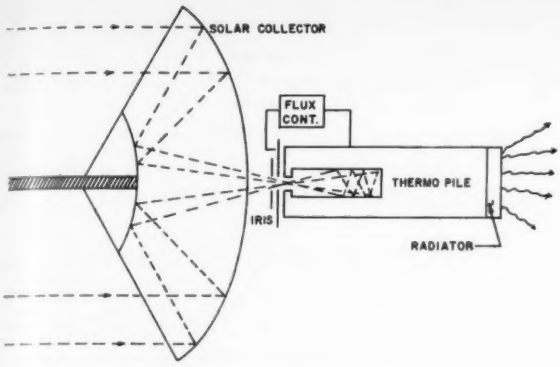

Fig. 13 Thermoelectric solar power supply

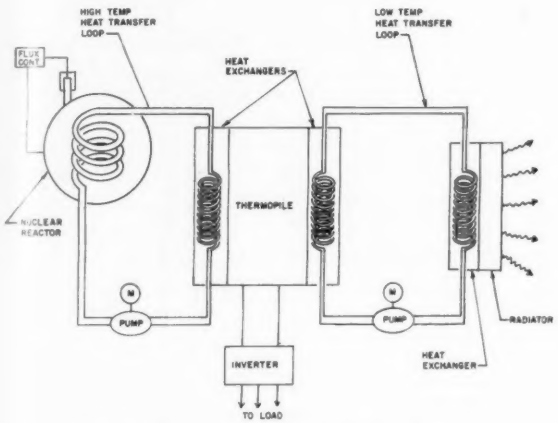

Fig. 14 Thermoelectric nuclear power supply

Thermionic Power Supply

The thermionic generator is similar to the thermoelectric device except that a thermionic cathode is used instead of P-N junctions. Physically, the thermionic device consists of an anode and cathode with finite spacing. The potential from the device is dependent on the thermochemical potential, the thermoelectric power and the voltage drop due to lead resistance. The current is a function of the temperature, the work function for the materials and the space charge.

Efficiency expressions have been derived for these devices which are identical to the expressions for the thermoelectric engine for the limiting case wherein ΔT approaches zero. The thermal efficiency may again be expressed as a product of the thermal efficiency of a Carnot engine and a device efficiency

$$\eta_{TH} = \eta_c f$$

The device efficiency is in turn a function of a parameter Z

$$f = \frac{(\sqrt{Z+1} - 1)}{(\sqrt{Z+1} + 1)}$$

where Z is a function of the open circuit voltage, the temperature and the Boltzmann constant.

Laboratory evaluation indicates that thermal efficiencies of 13 per cent can be attained with cathode temperatures of 2300 F and anode temperatures of 1000 F. The device efficiency is approximately 28 per cent. The terminal voltage at this optimum efficiency (for this configuration) was 0.5 v. The current density was approximately 1 amp per cm^2.

A 1-kw unit, considering the present state of the art, would thus require approximately 54 series units with 50 units in parallel for a total of 2700 units (assuming 1-cm^2 cathodes and 24 v). Space applications would be similar to the thermoelectric generator (Figs. 13 and 14). No realistic weight estimates for a practical thermionic device are available.

System Comparisons

The characteristics of some of the various systems described in the preceding sections are tabulated in Table 4. In this table 1- and 100-kw systems have been considered with estimates for the weight and the size of the power supplies and their significant components. All the significant assumptions are tabulated in the notes listed. Several systems which have been discussed in the text have been omitted from the tabulation and the subsequent comparisons in Figs. 15 and 16. The thermionic systems and the solar regenerative fuel cell systems were omitted due to the unavailability of weight estimates for practical systems at the present time. The thermoelectric systems have been omitted because the available weight estimate of 1000 lb per kw for a thermocouple device seems unreasonably high, and no more realistic weight estimates were available.

Several important features of Table 4 are discussed below. It will be observed, for example, that the turbine weight does not change in going from a 1-kw system to a 100-kw system. Virtually the same turbine would be used with the difference in power level resulting from a combination of increased arc of admission and higher back pressure. In the closed cycle systems, this higher back pressure corresponds to a higher condenser temperature, which is indicated in the notes. Thus an increase in exhaust density by a factor of 10 and an increase in the arc of admission from 10 to 100 per cent yields roughly a 100 to 1 increase in the power generated.

Another item noted in Table 4 which needs a word of explanation is the alternator weight assumed. Although the alternator never represents a large fraction of the total system weight, it should be noted that a decrease in specific weight from 2 to 0.3 lb per kw has been assumed as the power increases from 1 to 100 kw. Recent experimental work[3] demonstrated a 22-kw alternator weighing 11 lb. This was not a fully developed device, but it is certainly indicative of the future trends in rotating electromagnetic machinery. Electrostatic generators have been reported in the literature with similar weight estimates.

The radiator temperatures, sizes and weights do not correspond to the optimum temperatures indicated in the analytical studies presented in Figs. 6, 7, 8, 10 and 11. The differences arise from practical considerations of the vapor pressure characteristics of the working fluid and the effect of back pressure on turbine performance.

The information presented in Table 4 together with suitable interpolations and extrapolations are presented in Figs. 15 and 16. In Fig. 15 a comparison of system weights as a function of time is presented. The question at issue here is whether or not there is any application for the chemically-fueled space vehicle power supply. We find that the chemical open cycle system is lighter than all other systems at the 1-kw level up to about 10-hr duration, at which point the solar closed cycle powerplant takes over. For durations longer than 10 hr, this solar powerplant is optimum from a weight viewpoint. At the 100-kw level, the chemical open cycle powerplant maintains a weight superiority up to approximately 2 hr where the unshielded nuclear closed cycle device becomes the optimum powerplant for longer durations. It should be noted that the chemical closed cycle machine is superior to the chemical open cycle machine for durations in excess of 35 hr at the 1-kw level, but for this duration the solar powerplant is lighter than either one of them.

[3] At Sundstrand Turbo Division.

Table 4 Power supply characteristics

TYPE	CHEMICAL OPEN CYCLE		CHEMICAL CLOSED CYCLE		SOLAR CLOSED CYCLE		NUCLEAR CLOSED CYCLE		SOLAR CELLS	
Energy Source	Liq. H_2 - Liq. O_2		Liq. H_2 - Liq. O_2		Solar		Unshielded Nuclear Reactor		Solar	
Power Level	1 Kw	100 Kw	1 Kw	100 Kw	1 Kw	100 Kw	1 Kw	100 Kw	1 Kw	100 Kw
WEIGHT										
Energy Source	2.8 #/Hr	170 #/Hr	2.1 #/Hr	160 #/Hr	6#	480#	150#	150#	250#	10,000#
Prime Mover										
Turbine	20#	20#	20#	20#	20#	20#	20#	20#	--	--
H Ex	--	--	5#	20#	5#	100#	--	--	--	--
Alternator	2#	30#	2#	30#	2#	30#	2#	30#	--	--
Radiator	--	--	18#	170#	18#	170#	24#	170#	--	--
TOTAL WEIGHT	22# + 2.8 #/Hr	50# + 170 #/Hr	45# + 2.1 #/Hr	240# + 160#/Hr	51#	800#	196#	370#	250#	10,000#
VOLUME OR SIZE										
Energy Source	0.32 ft^3/Hr	19.2 ft^3/Hr	0.092 ft^3/Hr	5.65 ft^3/Hr	30 ft^2	2400 ft^2	0.5 ft^3	0.5 ft^3	82 ft^2	8200 ft^2
Prime Mover										
Turbine	200 $in.^3$	200 $in.^3$	200 $in.^3$	200 $in.^3$	200 $in.^3$	200 $in.^3$	200 $in.^3$	200 $in.^3$	--	--
H Ex	250 $in.^3$	875 $in.^3$	500 $in.^3$	1 ft^3	15 $in.^3$	520 $in.^3$	--	--	--	--
Alternator	8 $in.^3$	120 $in.^3$	8 $in.^3$	120 $in.^3$	8 $in.^3$	120 $in.^3$	8 $in.^3$	120 $in.^3$	--	--
Radiator	--	--	9 ft^2	340 ft^2	9 ft^2	340 ft^2	12 ft^2	340 ft^2	--	--
NOTES:	η_+ = 48% Alt - 2# / Kw	η_+ = 80% Alt - 0.3# / Kw	η_+ = 60% Alt - 2# / Kw	η_+ = 80% Alt - 0.3# / Kw	η_+ = 60% Alt - 2# / Kw	η_+ = 80% Alt - 0.3# / Kw	η_+ = 60% Alt - 2# / Kw	η_+ = 80% Alt - 0.3# / Kw	4 watts / #	10 watts / #
	η_{alt} = 85% T_H = 2200°F 40% H_2 - 60% O_2 by weight		T_H = 1780°F T_C = 400°F W_{rad} = 2#/ft^2	T_H = 1780°F T_C = 540°F W_{rad} = 0.5#/ft^2	T_H = 1780°F T_C = 400°F W_{rad} = 2# / ft^2	T_H = 1780°F T_C = 540°F W_{rad} = 0.5# / ft^2	T_H = 1600°F T_C = 400°F W_{rad} = 2# / ft^2	T_H = 1600°F T_C = 540°F W_{rad} = 0.5# / ft^2	η = 10%	
	Pressure Ratio - 150	Pressure Ratio - 1000								
			η_{alt} = 85% 11% H_2 - 88% O_2 by weight Working Fluid - Sulfur		η_{alt} = 85% coll. = 0.2# / ft^2 coll. = 90% Working Fluid - Sulfur		η_{alt} = 85% Reactor: 2 Mw/ft^3 300#/ft^3 1/2 ft^3 min Working Fluid - Sulfur			

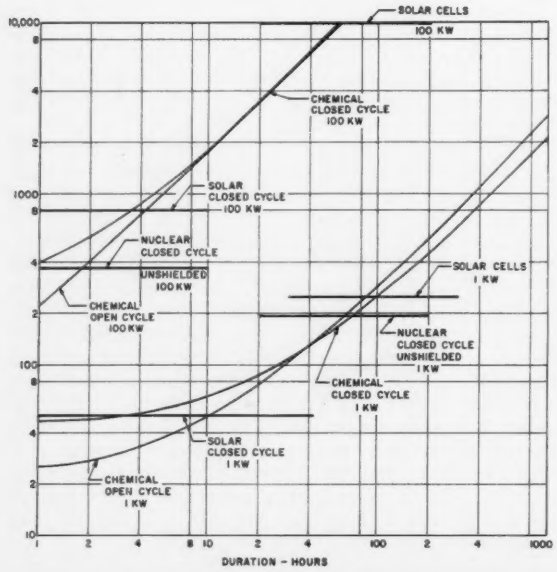

Fig. 15 Comparison of space vehicle power systems

There are many considerations which might alter the exact crossover points for these various powerplants; for example, no provision has been made in the solar powerplant for heat storage on the dark side of an orbit. Similarly, no provision for shielding has been made for the nuclear powerplants. Such considerations will undoubtedly vary the crossover time and perhaps the powerplant selection for particular applications. The significance to be drawn from Fig. 15 is that, at least from a weight point of view, the open cycle chemical power supply has a place in the sun, but only for relatively short duration missions. For those missions where erecting a mirror or carrying a nuclear powerplant are not permitted, the choice between the open and closed cycle powerplants will depend on the relative importance of powerplant weight and size. There is roughly a 3 to 1 propellant-volume ratio in favor of the closed cycle machine, which may be significant for the longer durations.

The variation of system weight with power level for those systems whose weight is essentially independent of time is presented in Fig. 16. Here again, the merit in such a plot lies in the estimation of approximate power levels at which the weight crossovers occur. Allowing for the uncertainty in the present state of the art in solar cells together with some optimism in the closed cycle solar powerplant weight, we would estimate a crossover between these two at about 100 w. The crossover between the closed cycle solar powerplant and the closed cycle nuclear powerplant occurs at ap-

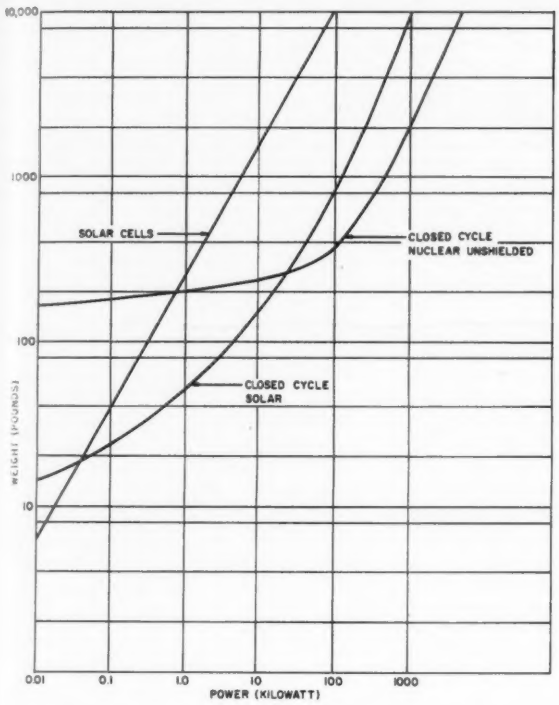

Fig. 16 Space vehicle power systems weight vs. power

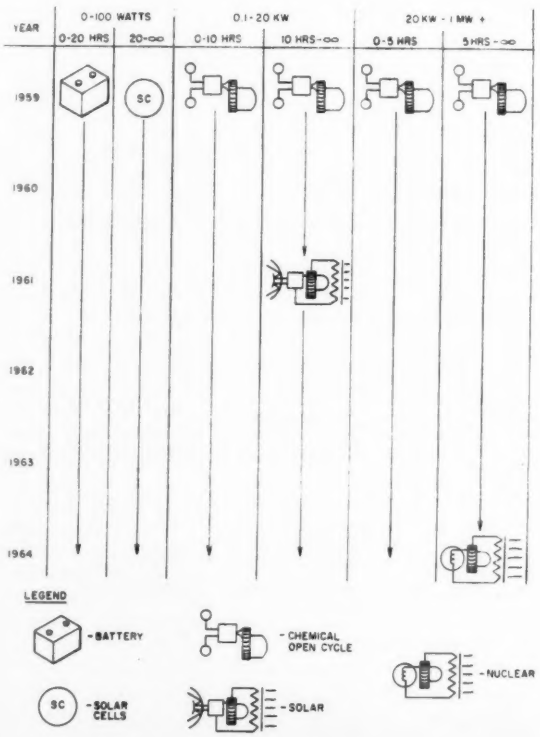

Fig. 17 Power level

proximately 20 kw. In addition to these crossover points, it is rather interesting to observe the specific weight values which these powerplants approach at high power levels. The solar cells, as indicated in Fig. 16, should achieve a specific weight of about 100 lb per kw at large power levels. Some of the more optimistic investigators in this area have estimated that they will achieve a 50-lb-per-kw specific weight for large power levels, but this state of the art advance is, to the best of our knowledge, not possible at the present time. The closed cycle solar powerplants should achieve a specific weight of approximately 10 lb per kw at large power levels; the closed cycle unshielded nuclear powerplants should achieve approximately 2 lb per kw at about a 1-megawatt rating.

Conclusions

The powerplant selection indicated by Figs. 15 and 16 is presented graphically in Fig. 17 together with an estimate as to when these powerplants will be available. An estimate of the crossover point between batteries and solar cells at low power levels has also been included for the sake of completeness. We see that below a power level of 100 w, batteries are optimum up to about 20-hr duration, at which point solar cells become the lightest available system. Both of these devices are currently available. From 100 w to 20 kw, chemical powerplants are optimum for relatively short durations, say up to 10 hr, whereas for the longer durations a solar closed cycle machine is optimum. As indicated in the graph, however, the solar powerplant is not presently available, although we estimate that a working machine would be available by approximately 1961. Chemical powerplants are the proper choice for interim applications.

For power levels in excess of 20 kw, chemical powerplants are suitable for short durations on the order of 5 hr or less, depending on power level, whereas nuclear powerplants, which should be available by 1964, are optimum for the longer duration application. Missions requiring 20 kw or more will use chemical powerplants until more advanced systems become available.

An important conclusion which we have reached as a result of the study presented here is indicated by Fig. 18. Here

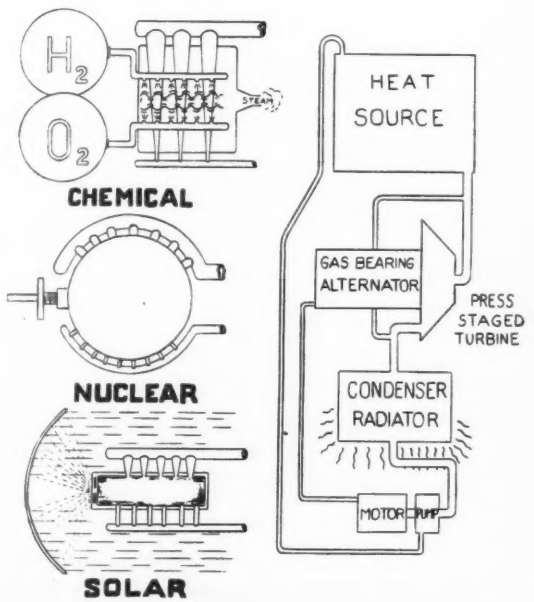

Fig. 18 Heat sources

we show a closed cycle powerplant which can derive its heat energy from either chemical, nuclear or solar means. Each of these powerplants is well suited to practical missions in space. The superiority of these powerplants over other means of power generation which have been considered stems largely from the high thermal efficiency which is achievable from Rankine cycle engines. In particular, at high power levels where total system weight is directly related to thermal efficiency, these closed cycle systems are clearly superior. Turbomachinery will find application in space vehicle power systems for a long time to come.

References

Balje, O. E. and Silvern, D. H., "A Study of High Energy Level, Low Power Output Turbines," American Machine & Foundry Turbo Division, TD no. 1196, April 1958.

Heidt, Lawrence J., "Converting Solar to Chemical Energy," Proc. of the World Symposium on Applied Solar Energy, Nov. 1958.

Jordan, Richard C. and Ibele, Warren E., "Mechanical Energy from Solar Energy," Proc. of the World Symposium on Applied Solar Energy, Nov. 1955.

Trombe, Felix, "High Temperature Furnaces," Proc. of the World Symposium on Applied Solar Energy, Nov. 1955.

Sandelman, S. L. and McJones, R. W., "Evaluating APU Systems for Spacecraft," *Space Aeronautics*, March 1959, p. 86.

"State of the Art: Accessories," *ibid.*, March 1959, p. 72.

Huth, J. M., "Power for Satellites," ASME paper 59-AV-3.

Callinan, Joseph P. and Berggren, Willard P., "Some Radiator Design Criteria for Space Vehicles," ASME paper 59-AV-29.

Fisher, James H. and Menetry, Walter R., "Problems Associated with Power Requirements for a Mars Mission," ASME paper 59-AV-18.

Proc. of a Seminar on "Advanced Energy Sources and Conversion Techniques," Pasadena, Calif., Nov. 3–7, 1958.

Hatsopoulas, G. N. and Kay, J., "Electrical Energy Conversion and Control," MIT Special Summer Program 6.529, 1958.

Blair, J., Lyden, H. A. and Rias, M., "Notes on Thermoelectric Energy Conversion," MIT Special Summer Program 6.529, 1958.

Sama, D. A., "Fuel Cells, Review," MIT Special Summer Program 6.529, 1958.

ARS 14th ANNUAL MEETING and ASTRONAUTICAL EXPOSITION

November 16-20

Sheraton-Park Hotel, Washington, D.C.

Guidance and Navigation
Missiles and Space Vehicles
Propellants and Combustion
Non Steady-State Phenomena
Far Space Communications Techniques
Man in Space
Space Law and Sociology
Ionic Propulsion
Instrumentation and Control
Solid Rockets Technology
Human Reliability and Instrumentation
Logistics and Operations
Physics of the Atmosphere and Space
Astrodynamics
Test Facilities and Support Equipment
Hydromagnetics
Space Communications Equipment
Near Space Effects on Materials
Power Systems
Nuclear Propulsion
Curricula in Astronautics
Safety and Reliability of Liquid Rockets

Honors night dinner, Wednesday, November 19: Main speaker, John A. McCone, Chairman, Atomic Energy Commission; subject, The Influence of Nuclear Technology on Rockets and Space.

Hotel reservations should be made directly to the Sheraton-Park Hotel no later than November 2, identifying the applicant as an Annual Meeting attendee, to take advantage of a special ARS block of hotel rooms.

Lockheed X-17 Rocket Test Vehicle and Its Applications

RONALD SMELT[1]

Lockheed Aircraft Corp.
Sunnyvale, Calif.

The Lockheed X-17 test vehicle was originally designed, in 1955, to permit experiments to be made in flight at the Mach numbers and Reynolds numbers appropriate to re-entry of ballistic missile nose cones. It consists of three stages of solid propellant rocket motors, and carries an instrumented model re-entry body. Although the model is much smaller in scale than the simulated re-entry body, full-scale Reynolds numbers at Mach numbers up to 15 are obtained by a flight program in which the second and third stages are fired on the downward part of the flight trajectory. Details of design and performance, and a description of the telemetering equipment developed for the vehicle are given in the report. No guidance equipment is carried; the X-17 depends upon aerodynamic stabilization for correct orientation, both during the ascent and in the re-entry phase. The resulting oscillations and dispersion have been analyzed in considerable detail, and the results of the analysis are summarized. Although most of the flights of the X-17 have been made to obtain re-entry data, some recent flights have utilized the vehicle in nuclear experiments at altitudes exceeding 400 miles. The vehicle then operates as a conventional sounding rocket, all three stages firing in rapid succession during ascent. The performance of the X-17 vehicle operating in this manner is included in the report, together with some discussion of the techniques adopted to stabilize at high altitude by spinning.

WHEN the Air Force began the development of the present generation of long range and intermediate range ballistic missiles, it was immediately apparent that one of the major problems to be solved was the design of the vehicle to withstand the conditions of re-entry into the Earth's atmosphere near the end of its flight. The aerodynamic characteristics of this phase of the flight were unprecedented: Mach number in the range from 15 to 20, air stagnation temperatures around 20,000 F, and excessive rates of heat transfer into the vehicle, indicated by theoretical work to rise to several thousand Btu per sec per ft^2 of surface. None of the conventional experimental aerodynamic facilities in the country could approach the simulation of these conditions, and although new types of facilities with extremely short flow durations, the shock tube and arc-heated wind tunnels, showed some promise of being able to duplicate re-entry conditions, they were in a very early stage of development. They had not yet passed the acid test of aerodynamic facilities, the attainment of some measure of agreement with aerodynamic data from free flight. The re-entry problem presented a particular difficulty here, since the critical quantity, the heat transfer rate, is greatly dependent upon the point of transition from laminar to turbulent flow, and even at lower speeds in wind tunnels factors, such as stream turbulence and model surface roughness make it very difficult to simulate free flight transition conditions with certainty.

The Lockheed X-17 hypersonic test vehicle was developed, at the request of the Air Force Ballistic Missile Division, to give design information on this critical problem. Propelled by solid fuel rockets, and much smaller in scale than the ballistic missiles whose re-entry it simulated, it could be put into operation much more cheaply and rapidly than the full-scale vehicle. Design of the X-17 vehicle began in February 1955, and in July 1956 it gave the first flight data on heat transfer rate at the Mach numbers and Reynolds numbers of typical re-entry. (The technique used to attain full-scale Reynolds numbers, in spite of the smaller scale of the X-17 vehicle, will be described.) Since that time, 26 X-17 vehicles have been launched on the Air Force re-entry program, and 20 of these have been successful in providing aerodynamic data.

Because of its unique features of hypersonic performance and excellent reliability, the X-17 test vehicle has been utilized on other programs subsequent to the Air Force re-entry investigation for which it was first developed. Some of these later vehicles have been operated as re-entry vehicles, following a flight path similar to those of the original program. The X-17 has also been utilized in the Argus program for nuclear research at extremely high altitude, taking advantage of the fact that a high speed vehicle of this type is necessarily also capable of flight to very great heights. More details of the performance of the X-17 in these alternative applications are given later.

Description of the X-17 Test Vehicle

Vehicle Configuration

The X-17, shown in Figs. 1, 2 and 3, is a three-stage tandem configuration, powered by solid propellant rocket motors. Separation of the second stage is achieved by an explosive charge usually fired by a pressure switch. Thrust from the third-stage rocket motor separates the third stage approximately 3 sec after second-stage separation.

The rocket motors for all three stages are manufactured by the Thiokol Chemical Corp. An XM-20 (Sergeant) motor is used for first-stage boost, a cluster of three XM-19 (Recruit) motors for the second stage, and an XM-19E1 motor for third stage. Powerplant characteristics are listed in Table 1, and typical static test thrust curves are presented in Figs. 4 and 5. The variation of weight during rocket motor burning is given for each stage in Fig. 6.

Presented at the ARS 13th Annual Meeting, New York, N. Y., Nov. 17–21, 1958.

[1] Manager, Satellite Systems, Missiles and Space Division. Member ARS.

Fig. 1a Lockheed X-17 on launching pad

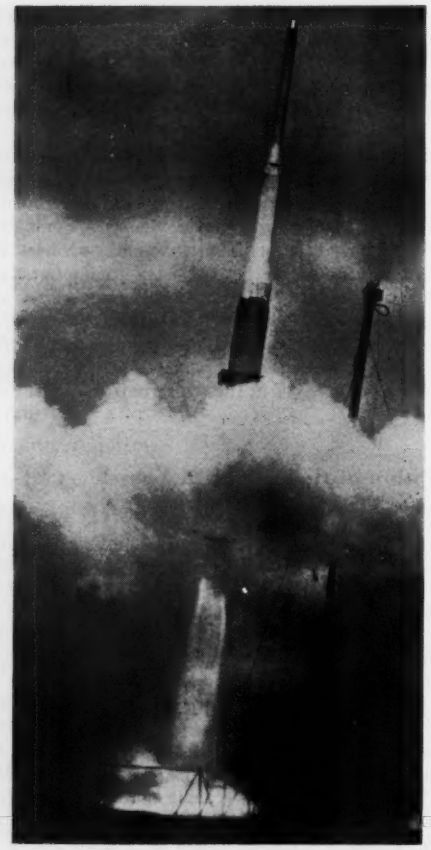

Fig. 1b Launching of Lockheed X-17

Two different methods of aerodynamic stabilization are used on this vehicle. The first stage is stabilized by lifting surfaces consisting of four straight, tapered fins, with a 4 per cent thick biconvex section, arranged in cruciform. The second and third stages are stabilized by conical skirts with approximately 10-deg semivertex angles.

In addition to aerodynamic stabilization, dispersion is minimized by spinning the first stage up to about 2 rps immediately upon leaving the ground, using two small spin rockets clamped to the outside of the case of the XM-20 rocket. These are jettisoned after operation, and in configurations designed for re-entry testing, the large first-stage fins then take over, gradually reducing the spin to zero. These first-stage fins are made large enough to provide rapid damping of the large amplitude oscillations in angle of attack which occur when the vehicle re-enters the atmosphere, so as to ensure that the second stage separates and fires when aligned along the re-entry flight path.

Table 1 Rocket motor characteristics

	XM-20	XM-19	XM-19E1
Performance, sea level			
web burning time, 70 F, sec	23.8	1.53	1.53
average thrust, 70 F, lb	50,000	34,861	35,950
total impulse, 70 F, lb-sec	1,344,000	57,024	58,800
total impulse/ initial weight, sec	164	164	169
specific impulse, sec	191	216	223
Weight, lb			
case	768	66.5	66.5
nozzle	295	15.6	15.6
liner	89	2.6	2.6
propellant	7033	264	264
total weight	8185	348.7	348.7

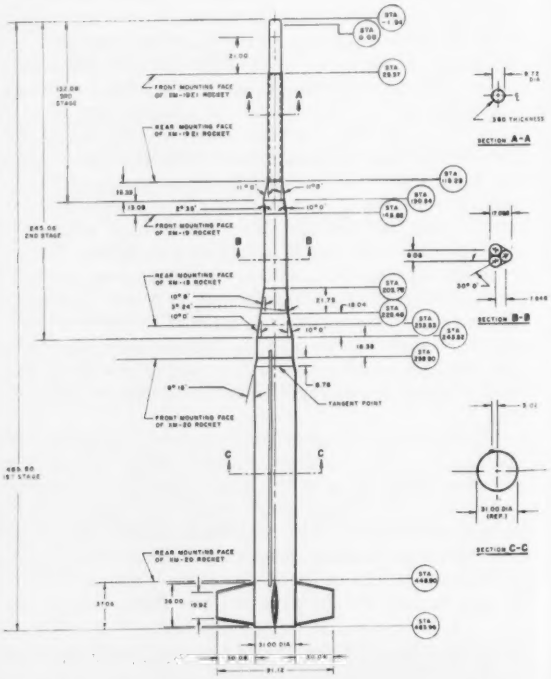

Fig. 2 Lockheed X-17 typical configuration

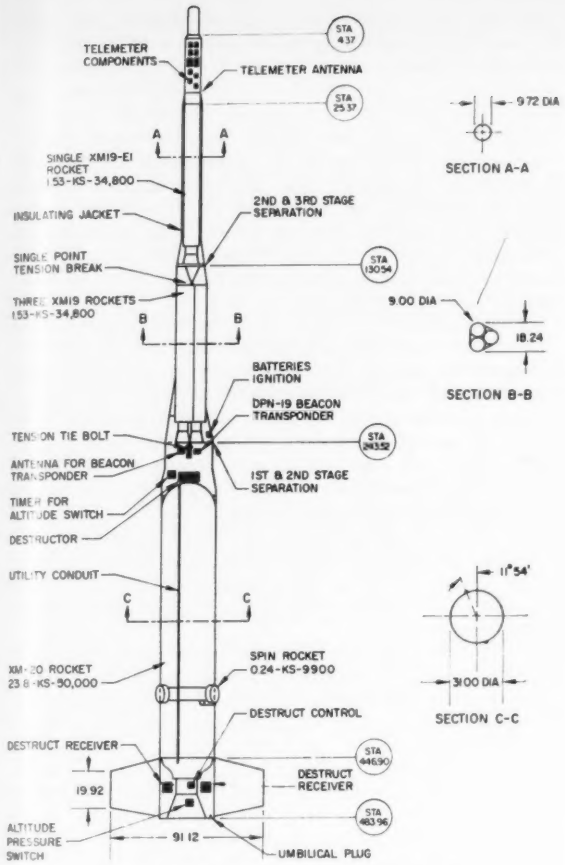

Fig. 3 Lockheed X-17 equipment location

In configurations intended for high altitude applications, dispersion due to misalignment of second- and third-stage motor thrust, or to upper atmosphere winds, is minimized by spinning the combined second and third stages immediately after separation from the first. This is achieved by the addition of small tabs at suitable points around the perimeter of the second-stage rocket nozzles, dimensioned to impart a spin rate of about 8 rps. A more detailed consideration of the whole problem of stabilization and dispersion is given in the Appendix.

Equipment

The majority of the flights of the X-17 vehicle have taken place from the Air Force missile range at Cape Canaveral, and the equipment normally provided in the first stage, as indicated in Fig. 3, is defined by the requirements of that range for missile tracking and destruction in the event of malfunction.

By far the most critical equipment item is the telemetering system carried in the final stage to transmit test data to ground. Evidently, since it is a major part of the third stage, its weight and bulk are of extreme importance. Further, it is required to withstand extremely severe acceleration conditions. These will be evident from the data given in Figs. 5 and 6, where it will be observed that during third-stage burning, a thrust of about 35,000 lb is acting upon a total mass which is decreasing from 500 to 230 lb, an acceleration of the order of 100 g. During re-entry experiments, conditions are still worse; as can be seen from a typical trajectory, such as

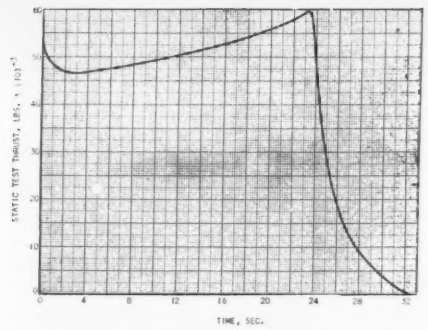

Fig. 4 Thrust characteristics of XM-20 rocket motor at 70 deg, sea level

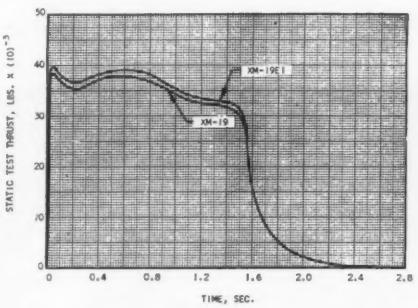

Fig. 5 Thrust characteristics of XM-19 rocket motor at 70 deg, sea level

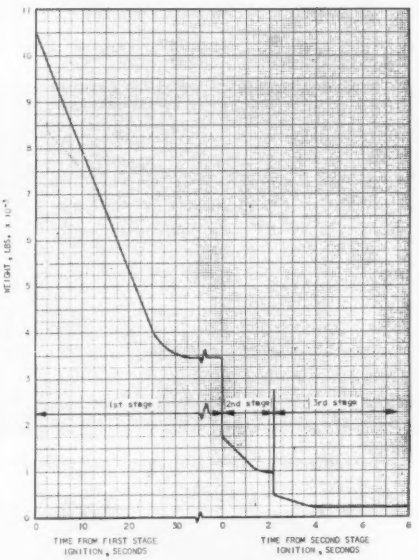

Fig. 6 Weight variation during burning

in Fig. 11, the high drag associated with re-entry appears toward the end of third-stage burning and imposes a deceleration of about 100 g immediately after an acceleration of the same order. When it is remembered that the thrust of the rocket motor is not completely steady, so that its variations represent considerable shaking superposed on the high steady acceleration, the severity of the environment will be apparent.

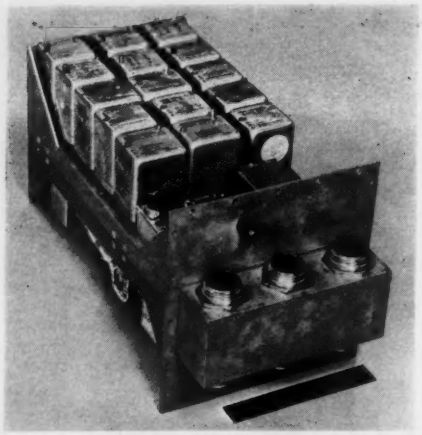

Fig. 7 Lockheed X-17 telemetering transmitter assembly, original form

Fig. 8a Nose cone and telemetering system after flight

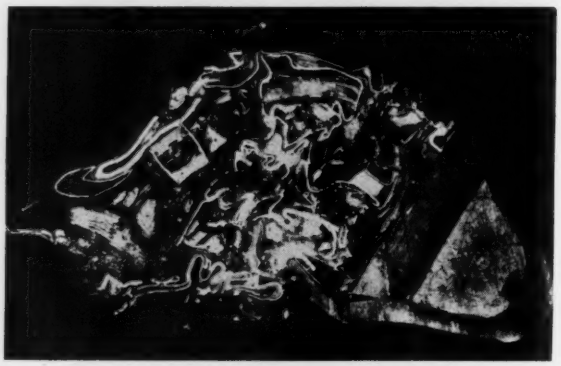

Fig. 8b Nose cone and telemetering system after flight (section)

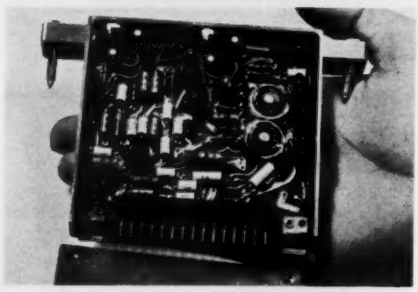

Fig. 9 Lockheed transistorized FM-FM telemetering system, typical component

To meet these conditions, Lockheed Missiles and Space Division found it necessary to develop its own special telemetering equipment. Fig. 7 shows the FM-FM system as used originally in the vehicle. It provides 16 continuous channels of information, coded in accordance with the standards set by the Inter-Range Instrumentation Group; one or two of the 16 channels are subcommutated, giving up to 48 channels of sampled data. Its total weight, including a 10-w RF section, is 44 lb. Before use, it is tested on the ground in a centrifuge, to assure that it can withstand the accelerations and decelerations discussed, and it is also subjected to shaking at accelerations up to 10 g, over a wide frequency range up to 2,000 cps.

In contrast to Fig. 7, a section of the nose cone recovered from the desert at Holloman Air Force Base is shown in Fig. 8. Evidently the telemetering equipment is not yet able to withstand the final decelerations upon impact after such a flight!

More recently, the steady improvement in transistor techniques has permitted the development of telemetering equipment which can meet even more severe environmental specifications than the original X-17 equipment, and is capable of being packaged into much smaller bulk and weight. Fig. 9 shows a typical component of the fully-transistorized telemetering equipment; it permits the same amount of information to be transmitted as the original system, with about 60 per cent of the total weight and a considerable saving in battery power.

It will be appreciated that all the instruments contained in the third stage of the vehicle—measuring pressures, temperatures, heat transfer rates and other quantities required to determine the aerodynamic characteristics—are subject to the same difficulties due to high accelerations. In addition, the instruments on the surface near the nose are subject to the excessive heating rates during re-entry; temperatures up to the melting point of copper have been recorded. Again, it was necessary to develop special end instruments for many of these measurements.

Performance of the X-17 Vehicle

Performance as a Re-Entry Vehicle

In the original application of the X-17 test vehicle to the aerodynamic problems of re-entry, the basic objective was to furnish information at Reynolds numbers appropriate to a full-scale re-entry body, although using a smaller scale model on the nose of the X-17 vehicle. Evidently this requirement can be met if the smaller scale of the X-17 model is compensated by making measurements at a lower altitude. The major difficulty is then to impart to the model, at this lower altitude, the hypersonic velocities anticipated in the full-scale re-entry body at its higher critical altitude; to achieve this in free fall would imply that the drag-to-weight ratio of the model must be much less than the full-scale object. Since this is extremely difficult to achieve in practice, the alternative expedient is employed of canceling the model drag by an applied thrust during re-entry.

To achieve this objective, the X-17 vehicle utilizes only the first stage to reach its maximum altitude, usually somewhat in excess of 500,000 ft when launched at an angle of 85 deg. The first-stage motor burns out at about 90,000 ft, when the velocity of the vehicle is slightly over 5,000 fps, and the vehicle coasts to apogee and into the descent. Typical trajectories during this phase of the flight are shown in Fig. 10. Separation of the spent first stage from the remainder of the vehicle is intentionally not initiated during this part of the flight so as to make use of the high stability margin of the complete configuration with its large fins to align the vehicle along the descending flight path before the air density is sufficient to produce high heating rates.

At a point on the descent defined by the setting of a timer, the first stage is separated, and the second stage fires, followed

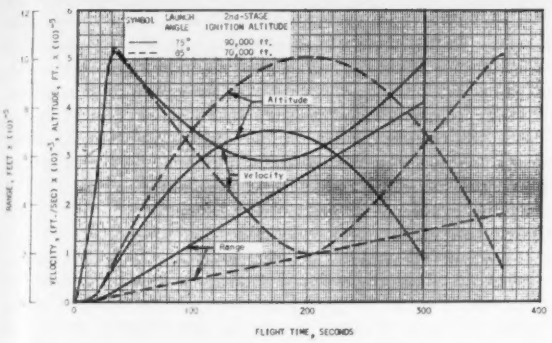

Fig. 10 X-17 trajectories, first stage

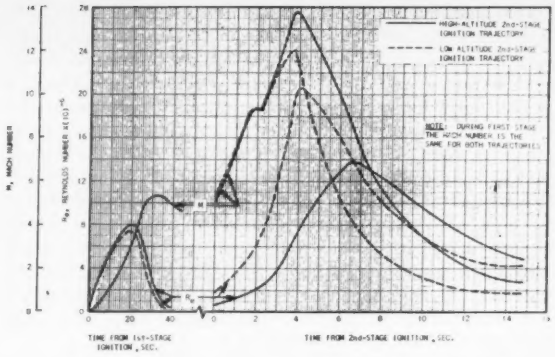
HIGH-ALTITUDE 2nd-STAGE IGNITION TRAJECTORY
LOW-ALTITUDE 2nd-STAGE IGNITION TRAJECTORY
NOTE: DURING FIRST STAGE THE MACH NUMBER IS THE SAME FOR BOTH TRAJECTORIES
TIME FROM 1st-STAGE IGNITION, SEC.
TIME FROM 2nd-STAGE IGNITION, SEC.

Fig. 11 Variations in Mach number and Reynolds number

in about 3 sec by the third stage. This drives the velocity rapidly up to hypersonic values. The maximum Mach number and maximum Reynolds number attained during this portion of the descent can be varied over quite a wide range by selection of the altitude at which second-stage ignition is initiated. Evidently, if ignition is deferred until a low altitude is reached, the resulting maximum Reynolds number can be very high, but the maximum Mach number is not so great as that given by ignition at high altitudes. Fig. 11 compares the performances which can be obtained by typical high altitude and low altitude second-stage ignition; the Reynolds number in this figure is a typical value utilizing the diameter of the nose of the vehicle as a characteristic length.

This technique, appropriately referred to as the "nail-driving" method, has proved to be very successful in providing data at extremely high Reynolds numbers. It will be observed from Fig. 11 that the maximum Reynolds number obtained can be as high as 20 million for a flight with delayed second-stage ignition, and is around 8 to 10 million at the highest Mach numbers in flights aimed specifically at achieving the highest speeds. Of course, the major importance of these high Reynolds numbers lies in the fact that they permit the test to cover the complete range of Reynolds number in which transition phenomena are normally expected to occur, so that the aerodynamics of both laminar and turbulent conditions can be studied.

Utilization of the X-17 Vehicle for Maximum Altitude

An alternative type of operation permits the X-17 test vehicle to be used as a sounding rocket attaining very high altitude, and a number of flights have been made in this manner. To obtain maximum altitude, the vehicle is again launched into an almost vertical flight path, but the second stage is now fired after burnout of the first stage, with the minimum possible delay to permit satisfactory separation. The third stage again fires as soon as possible after burnout of the second stage. The performance of the vehicle in this mode of operation, defined by the maximum altitude which can be reached, is of course entirely dependent upon the weight of instrumentation and equipment to be carried to the extreme altitude. Fig. 12 shows the calculated maximum height as a function of the total weight to be carried with the third stage, but excluding the weight of the third-stage rocket motor itself. The flights already made with the X-17 vehicle in this condition conform quite closely to the calculated curve on Fig. 12.

Applications

The large number of flights made in the X-17 re-entry research program have given aerodynamic information for a very wide variety of re-entry vehicle nose shapes, ranging from simple hemispheres to the more complex shapes selected in the ballistic missile programs. Pressure distributions measured on these shapes during X-17 flights, at Mach numbers up to 14 or 15, have shown excellent agreement with current hypersonic blunt body theories. Distribution of heat transfer coefficient over the surface of the same shapes, in both laminar and turbulent flow, has been obtained over the same Mach number range. This has permitted a selection to be made among the several alternative theoretical methods of calculating heating rates at re-entry conditions.

Probably the most valuable contribution of the X-17 re-entry flight data has been in the experimental determination of the criteria for transition from laminar to turbulent flow on a re-entering vehicle. As described earlier, a typical X-17 experiment covered the Reynolds number range at which transition is likely to occur, and the transition point could be quite accurately located from the measured distribution of surface temperature. The position of the transition point is of vital importance in the determination of re-entry heating on ballistic missiles, and much of the X-17 test program was therefore aimed at investigation of factors influencing transition. In addition to variations in nose cone shape, the tests included several alternative surface roughness conditions, with both distributed and local roughness elements.

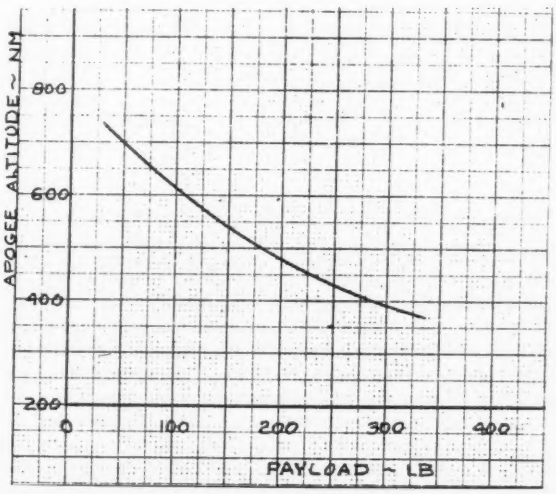

Fig. 12 Payload vs. height

The maximum Mach number attained in these flights, about 15, is adequate for direct application to intermediate range ballistic missiles, but is less than the Mach number at which high heating rates may be expected when re-entering from a satellite orbit or long range ballistic missile trajectory. In spite of this lower Mach number, heating rates encountered during the X-17 experiments were well in excess of the heating rates to be expected on these higher speed re-entering vehicles. In consequence, the X-17 served as a useful test vehicle for the nose cone materials to be used to withstand re-entry heating conditions. On several flights, the measured surface temperatures in critical areas reached the melting point of the material, but the nose cone generally maintained its structural integrity under these extreme conditions and gave early assurance that the re-entry problem could be solved.

To appreciate how the X-17 flights could produce heating rates exceeding ICBM or satellite re-entry conditions, although its Mach number was limited to a maximum of 15, it should be noted that the full-scale re-entry vehicle is generally several times larger than the model carried on the X-17. Since the special trajectory and firing program of the X-17 were designed to give full-scale Reynolds numbers at the critical high heat rate conditions, these occurred at lower altitude and at several times the atmospheric density appropriate to full-scale re-entry. The rate of convective heat transfe H to the surface is defined very generally by an expression

$$H = k_H C_p \rho V \Delta T \quad \text{per unit area}$$

where k_H depends primarily upon Reynolds number and is therefore roughly the same on the X-17 model and the full-scale vehicle, and the density ρ is several times larger on the X-17 model; C_p, V, ΔT, the specific heat, velocity and air-to-surface temperature difference, are dependent upon Mach number, the product varying roughly as (Mach number)^3.

In general, the Mach number of the X-17 test was sufficiently close to the corresponding full-scale value so that the influence of the small model scale predominated in this expression; the heating rate on the model, per unit area, was usually greater than the corresponding full-scale condition.

The X-17 re-entry test program has made an interesting contribution to the problem of radio transmission through the ionized boundary layer on a hypersonic vehicle. At the highest speeds, around Mach number 15, the transmitted telemetering signal from it invariably showed a dip in signal strength which could be correlated quite well with the actual speed from flight to flight. Evidently this resulted from the commencement of ionization of the air near the vehicle, and some work was done to identify the mechanism of signal loss from ionization, whether from antenna mismatch, antenna pattern change or direct absorption.

The most recent applications of the X-17, as a high altitude test vehicle in almost vertical flight, have contributed considerably to the study of the influence of the Earth's magnetic field on ionized gas flow at extreme altitudes. The general nature of these effects has recently been discussed in a number of articles in the technical press, and will therefore not be reviewed in this paper.

Appendix Stability and Dispersion Problems

One of the major factors contributing to the reliability of the X-17 vehicle is the absence of guidance equipment. Operation without guidance implies that the various errors which can modify the flight path—the errors in launch, the asymmetries of the missile itself, the misalignments in the thrust and the atmospheric disturbances—remain uncorrected during the flight and contribute to the final dispersion. To insure that the changes in trajectory due to these factors do not prevent attainment of the objectives of a particular flight, it has been necessary to undertake a comprehensive program of calculation of the actual flight paths, taking into account probable values of the major disturbances. Since it is necessary to include the changes in mass and moment of inertia of the vehicle as the fuel is expended, the aeroelastic distortions of the vehicle structure under the aerodynamic loads and the effects of roll on the missile dynamics, the calculation of the flight trajectory is fairly complex. The equations of motion including all these variables have been solved directly by the use of high speed digital computers; in addition, a method of separation of the overall flight trajectory from the local oscillation at a particular point has been utilized to permit graphical solution of the oscillatory motion on an analog computer.

In the present paper, it is not feasible to present the results of these calculations in detail. Instead, the following paragraphs will outline the most important general features which appear from the results. Evidently the critical question is the response of the vehicle to any disturbance; i.e., how quickly the disturbance will be damped out as a result of the aerodynamic damping. There are damping components due to the acceleration of the missile under the motor thrust, and also damping from the change in angular momentum with time as the rocket grain burns; these are added to the normal aerodynamic damping, which arises mainly from the large fins of the first stage. It appears from the results of our calculations, however, that the major effect contributing to the damping is the influence of varying air density, which changes the natural frequency of pitch oscillation as the vehicle transverses the atmosphere. It has been shown by Friedrich and Dore (1)[2] in a recent paper that the damping of a vehicle passing through a region of varying air density will depend upon the change of aerodynamic stability in accordance with the approximate equation

$$\frac{A_2}{A_1} = \sqrt{\frac{w_{n1}}{w_{n2}}}\, e^{-\frac{1}{2}\int_1^2 2\zeta w_n dt}$$

where

A = amplitude of the oscillation
w_n = frequency of pitch oscillation
ζ = damping factor

$$2\zeta w_n = \frac{C_{n\alpha} qS}{mV} - \frac{C_{m_\dot{\alpha}} d^2 qS}{2VI} + \frac{T - D}{mV} + \frac{\dot{I}_y}{I_y}$$

using conventional aerodynamic symbols.

The natural frequency of pitch oscillation w_n varies roughly in accordance with the dynamic pressure. At the beginning of the trajectory it increases steadily as speed is gained, up to an altitude of about 35,000 ft. It then drops rapidly due to the increase in air density. In accordance with the equation given above, the oscillations at launch and disturbances on the initial part of the trajectory are very rapidly damped, but above a height of 35,000 ft the damping ceases to be as effective, until at extremely high altitudes the motion becomes completely divergent. This is clearly illustrated in Figs. 13 and 14, which show the oscillations of a typical trajectory of the X-17 utilized in a re-entry test. It will be seen that the large angle of attack induced at launch dies out within about 7 sec, and that the subsequent variations in angle of attack are extremely small until a period of about 40 sec has elapsed. The oscillations then begin to build up to a complete divergence at the maximum altitude. On the return path to ground, the rapid increase in dynamic pressure again induces an extremely large effective damping, so that the large error in angle of attack which has been built up at high altitude is very rapidly reduced to zero.

The experimental data collected on flights of the X-17 vehicle to the present have generally confirmed these calculations on the nature of the disturbances in trajectory. Examining first the ascending part of the trajectory, it is evident from Fig. 13 that the disturbances occurring in the few seconds immediately after launch are large in magnitude, and although

[2] Numbers in parentheses indicate References at end of paper.

they are heavily damped, they can be expected to contribute considerably to the final dispersion of the vehicle. Experimentally it has been found that the greatest single cause of dispersion is the effect of prevailing winds on the vehicle during the initial part of the flight, and that this effect is felt for approximately 6 sec of flight time (to an altitude of about 1000 ft). For this reason, the prevailing winds are included in predictions of the flight path, and a final prediction is made on the basis of the wind determination approximately 15 min in advance of the flight. It is of interest to compare this prediction with the flight path deduced from the wind strength 3 min after the flight. As a typical example, the dispersion in a horizontal plane at an altitude of 200,000 ft has been determined, both from the calculations on the basis of these two wind determinations and also from the actual flight trajectory as determined by radar. Calculations based upon the wind strength 15 min before flight gave a dispersion at 200,000-ft altitude which averaged 17,400 ft from the actual determined position of the vehicle. When the wind determination 3 min after the flight was utilized, the mean error in the same 9 flights was only 13,400 ft.

In operation as a re-entry test vehicle, there is no further major disturbance on the ascending trajectory, and separation of the first stage followed by ignition of the second-stage rockets occurs in the damped part of the descending trajectory. Fairly large disturbances are therefore permissible without significant effect upon the resulting motion. Calculations show that a disturbance inducing an angle of attack of 20 deg in the second-stage rocket motor does not produce critical conditions. This is fortunate, since the second stage consists of three motors in parallel, and there is a possibility of delay of ignition of one of the motors relative to the other two. Extension of the calculations to include this delay shows that a delay of 0.02 sec does not produce seriously high angle of attack or critical loads. However, if one rocket should fail to ignite completely, the effect would be disastrous, since the moment produced is equivalent to a thrust misalignment of about 3 deg. There is no case yet during the flights of the X-17 where such an accident has occurred.

When the X-17 is used as a high altitude sounding rocket, conditions at separation of the first and second stage are much more critical than in the re-entry mode of operation, since these separation disturbances and thrust misalignments then occur during the phase of flight where the decreasing dynamic pressure is effectively reducing the vehicle damping. It is then necessary to resort to spinning of the vehicle to minimize the influence of misalignments. Calculations show that with a spin rate of 2.5 cps the second stage will develop a maximum angle of attack of approximately 1.9 deg, with an associated maximum change in flight path angle of 1.15 deg, if a thrust misalignment angle of 0.2 deg is assumed. The problem of the third stage during high altitude sounding rocket operation is even worse; the same thrust misalignment of 0.2 deg will produce a maximum angle of attack of 20 deg with the same spin rate of 2.5 cps and a corresponding change in flight path angle of about 6 deg at third-stage burnout. To reduce these large disturbances, it is necessary to resort to much higher rates of spin, approaching 10 rps. Fig. 15 shows the effect of the third-stage spin rate upon the maximum angle of attack at burnout, and illustrates the very powerful effects of high spin rate.

It is appropriate at this point to discuss generally the influence of spin upon the flight path as utilized in the X-17 vehicle. It is important to emphasize that in comparison with the spinning shell, the rates of spin are low, so that gyroscopic torques and Magnus effects are usually negligible. At extremely high altitudes the gyroscopic torques may be significant, when the aerodynamic moments are negligible and the rate of change of angle of attack is low, as is usually the case. The gyroscopic effects then convert a pure divergence into a precision motion, so that the deviations can be less than in nonspinning flights as shown in Fig. 14. At lower

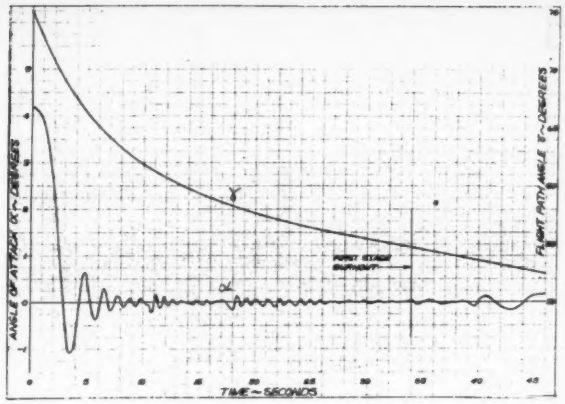

Fig. 13 Angle of attack oscillation in typical re-entry trajectory, ascent

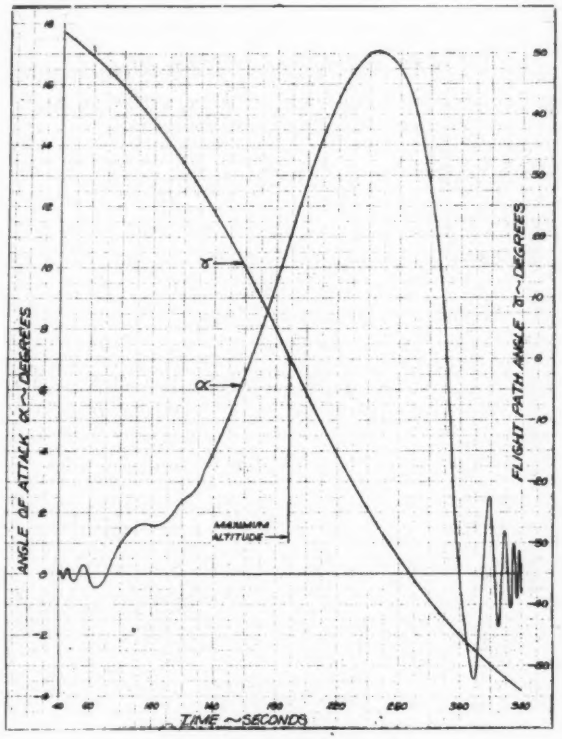

Fig. 14 Angle of attack oscillation in typical re-entry trajectory (continued), descending phase

altitudes, the spin is merely utilized to ensure that asymmetries in missile construction and in motor thrust do not build up a large change of angle of attack during the motion. Disturbances which do not rotate with the missile, such as wind shear or gusts, will have almost identical effects whether the missile is spinning or not. However, at high altitude, the wind effects are evidently small, so that the moments created by the missile itself due to fin or thrust misalignments are much more significant; in this case, spinning can be extremely valuable in minimizing the resulting disturbances, as is evident from Fig. 15. To illustrate its major effects, it is instructive to examine the trim characteristics of a missile as

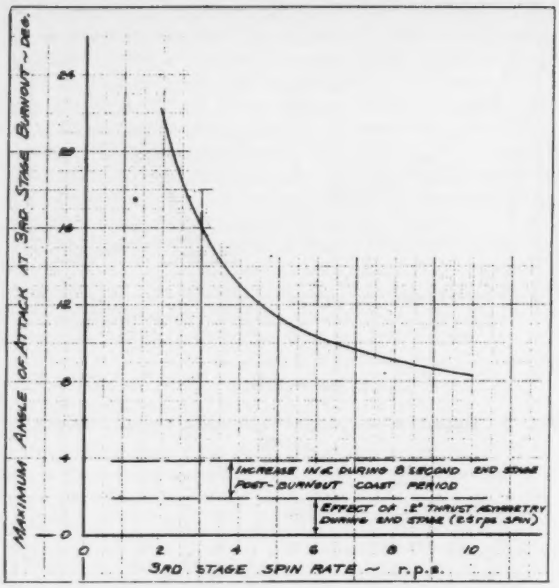

Fig. 15 Effect of third-stage spin rate on angle of attack, assuming 0.2-deg thrust misalignment

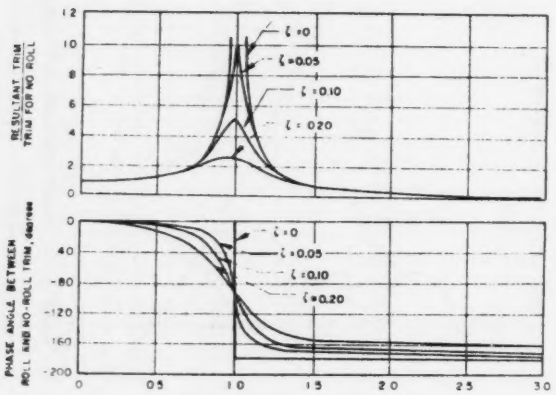

Fig. 16 Effect of roll on trim

the rate of roll is increased from zero. Fig. 16 shows both the magnitude of the resultant trim and the phase angle between the roll and no-roll conditions, as a function of the ratio of the roll frequency to the pitch frequency, the individual curves on each figure referring to changes in the damping factor as defined above. It will be seen from this figure that to produce a favorable effect upon the motion, it is necessary that the spin rate should be much more rapid than the pitch frequency.

When the ratio of the rolling frequency to the pitch frequency approaches unity, the effect known as "roll resonance" will occur. The disturbances then build up continuously with time, so that extremely high effective trims can be obtained if the damping is not high. At high altitudes, as discussed, the damping is usually extremely low, so that coincidence of rolling frequency and pitch frequency can be catastrophic in its effect upon the flight path. To avoid these effects, and also to take maximum advantage of the influence of high spin rates in reducing the effect of disturbances, the third stage of the X-17 is provided with jet tabs which spin it to the high rate of about 10 rps for high altitude sounding work. The missile passes through the resonance condition in reaching this spin rate, but the acceleration through resonance is sufficiently rapid to prohibit a significant buildup in oscillation.

The spinning of a large missile at such high rates presents some structural problems, and, indeed, the upper limit to which the missile can be spun is determined entirely by the structural characteristics. The structural problem involved is essentially the classical problem of shaft whirl, but there are a number of complicating features. The center of mass is not exactly along the axis of the missile, but has a distributed eccentricity. In addition, the spin rate is time varying, so that the problem of the whirling shaft must be generalized. A further effect which must be taken into account arises from the thrust and drag applied to the vehicle, making the problem analogous to that of a whirling shaft in compression (2).

Acknowledgment

In presenting this paper on the X-17 vehicle, the author is acting as a reporter only. The X-17 program was a team effort, and credit for successes in its various aspects must be given to the Air Force members of the team, at AFBMD and AFMTC; to the Navy groups who were active in some of its later programs, and to the engineers at Lockheed Missiles and Space Division who formed the X-17 project group. Acknowledgment should also be made to the Space Technology Laboratories of the Ramo-Wooldridge Corp.

References

1 Friedrich, H. R. and Dore, F. J., "The Dynamic Motion of a Missile Descending Through the Atmosphere," *J. Aeron. Sci.*, vol. 22, Sept. 1955, pp. 628–632.

2 Harvey, T. J., "Bending Dynamics of a Spinning Missile," JET PROPULSION, vol. 27, June 1957, pp. 669–672.

ARS SOLID PROPELLANTS CONFERENCE

January 28–29, 1960

Princeton University, Princeton, N. J.

Thrust and Vector Control
Unstable Burning
Grain Design

Combustion, Gas Kinetics and Ignition
Interrelations of Nozzle Geometry and Nozzle Performance

Abstracts should be submitted to Ivan Tuhy, Staff Engineer, Solid Propellants, The Martin Co., Baltimore 3, Md., by September 30.

Aerothermodynamic and Electrical Properties of Some Gas Mixtures to Mach 20

W. CHINITZ[1]
C. L. EISEN[2]
R. A. GROSS[3]

Fairchild Engine Division
Deer Park, N. Y.

Pressure, temperature, chemical composition and electrical conductivity data are presented for gas mixtures behind strong air shocks and detonations of hydrogen-air and acetylene-air mixtures up to Mach 20. A digital computer program has been developed which solves the simultaneous aerodynamic and chemical equilibrium equations. The latest thermodynamic and collision cross-section data are used. Data are also presented wherein the initial gas composition was varied to obtain the maximum electrical conductivity for a given shock or detonation strength.

SCIENTIFIC and engineering interest have been focused upon the properties of high temperature gas mixtures by the increasing effort being devoted to high speed gas dynamics. Dissociation and ionization affect the properties of the gas mixture and open up new opportunities for study and application to the chemist, physicist and engineer. For example, magnetohydrodynamics is critically dependent upon the concentration of ions present in a gas mixture.

One-dimensional steady flow equations of fluid mechanics, together with the concept of thermodynamic equilibrium and the basic thermochemical data are the foundations upon which such studies rest. The basic equations are presented in the next section, and the sources of thermochemical data which we used are listed in the Appendix. The problem is reduced to the simultaneous solution of a large number of nonlinear algebraic equations. In our particular case, where we consider chemical systems with hydrogen, oxygen, nitrogen, carbon and argon atoms, the number of equations is 15. A digital electronic computer (IBM 650) was used to solve this system of equations.

Knowing the thermodynamic state of a gas mixture, i.e., pressure, temperature and chemical composition, permits the calculation of the electrical conductivity of the mixture if the electron-atom collision cross sections are known. Such calculation has been carried out here for several important cases of air shocks and strong hydrogen- and acetylene-air detonations. Finally, we have explored the effect of initial chemical composition to find what mixtures will yield maximum electrical conductivity in the product gases of a given strength shock or detonation.

Fundamental Equations

Consider the one-dimensional steady flow of a homogeneous, chemically metastable, gaseous mixture. The thermodynamic and physical properties and composition of this reactant mixture are assumed known. We seek to determine the thermodynamic and physical properties and equilibrium composition of the product mixture. Specifically we treat the class of reactions

$$\alpha_0 C_x H_y + \alpha_1 O_2 + \alpha_2 N_2 + \alpha_3 A \rightarrow \beta_1 CO_2 + \beta_2 H_2O + \beta_3 N_2 + \beta_4 O_2 + \beta_5 CO + \beta_6 OH + \beta_7 N + \beta_8 O + \beta_9 H + \beta_{10} NO + \beta_{11} H_2 + \beta_{12} A + \beta_{13} C + \beta_{14} O_3 + \beta_{15} NO_2 + \beta_{16} NO^+ \quad [1]$$

where x and y determine the particular hydrocarbon fuel entering the reaction, and α_0, α_1, α_2, α_3, V_1, T_1 and p_1 are known. The last three quantities are the velocity, temperature and pressure of the reactant gas, respectively. The final four species treated in Equation [1] are present only in relatively small amounts, their concentrations being about 10^{-4} times those of the major product gas constituents. As a result, these species are treated as a perturbation to the main problem, to determine the 15 quantities: β_i, $i = 1, 2, \ldots, 12$, V_2, T_2 and p_2 of the product gas. From the solution, other properties of the product gas can be calculated.

To determine the 15 unknowns, we require 15 relations between them. These are provided by the various conservation laws and the chemical equilibrium equations.

For one-dimensional steady flow, conservation of momentum is expressed by

$$p_1 + \rho_1 V_1^2 = p_2 + \rho_2 V_2^2 \quad [2]$$

Conservation of mass is expressed by

$$\rho_1 V_1 = \rho_2 V_2 \quad [3]$$

The fact that the total number of atoms of each atomic species entering the reaction given by Equation [1] remains constant is expressed by

$$\begin{aligned} x &= \beta_1 + \beta_5 \\ y &= 2\beta_2 + \beta_6 + \beta_9 + 2\beta_{11} \\ \alpha_1 &= \beta_1 + \frac{1}{2}\beta_2 + \beta_4 + \frac{1}{2}\beta_5 + \frac{1}{2}\beta_6 + \frac{1}{2}\beta_8 + \frac{1}{2}\beta_{10} \\ \alpha_2 &= \beta_3 + \frac{1}{2}\beta_7 + \frac{1}{2}\beta_{10} \\ \alpha_3 &= \beta_{12} \end{aligned} \quad [4]$$

where we have set $\alpha_0 = 1$.

For one-dimensional steady flow of a homogeneous mixture

Presented at the ARS 13th Annual Meeting, New York, N. Y., Nov. 17–21, 1958.

[1] Research Engineer; now Senior Scientific Research Engineer, Republic Aviation Corp., Farmingdale, N. Y. Member ARS.

[2] Senior Analyst; now Principal Scientific Research Engineer, Republic Aviation Corp., Farmingdale, N. Y.

[3] Chief Research Engineer; now National Science Foundation Fellow, Physics Dept., Univ. of Calif., Berkeley. Member ARS.

of gases, the conservation of energy is expressed by

$$\frac{1}{2}(\Sigma\alpha_i m_i)V_1^2 + \Sigma\alpha_i h_i(T_1) = \frac{1}{2}(\Sigma\beta_i m_i)V_2^2 + \Sigma\beta_i h_i(T_2) \qquad [5]$$

where h_i is the specific enthalpy of the ith species.

For the reaction expressed by Equation [1], chemical equilibrium of the products requires that the following set of equations be satisfied

$$K_{N_2}(T_2) = \frac{\beta_2\Sigma\beta_i}{\beta_1^2 p_2} \qquad N_2 \rightleftarrows 2N$$

$$K_{H_2O}(T_2) = \frac{\beta_2(\Sigma\beta_i)^2}{\beta_9^2\beta_8 p_2^2} \qquad H_2O \rightleftarrows 2H + O$$

$$K_{O_2}(T_2) = \frac{\beta_4\Sigma\beta_i}{\beta_8^2 p_2} \qquad O_2 \rightleftarrows 2O$$

$$K_{OH}(T_2) = \frac{\beta_6\Sigma\beta_i}{\beta_8\beta_9 p_2} \qquad OH \rightleftarrows O + H$$

$$K_{H_2}(T_2) = \frac{\beta_{11}\Sigma\beta_i}{\beta_9^2 p_2} \qquad H_2 \rightleftarrows 2H$$

$$K_{NO}(T_2) = \frac{\beta_{10}\Sigma\beta_i}{\beta_7\beta_8 p_2} \qquad NO \rightleftarrows N + O$$

$$K_{CO_2}(T_2) = \frac{\beta_1^2\Sigma\beta_f}{\beta_3^2\beta_4 p_2} \qquad 2CO_2 \rightleftarrows 2CO + O_2$$

..... [6]

In Equations [5 and 6] $\Delta h_i(T)$ and $K_i(T)$ are known functions of the temperature (see Appendix A). Equations [2 through 6] then constitute 15 nonlinear algebraic equations in the 15 unknowns: β_i, $i = 1, 2, \ldots, 12$ and V_2, T_2 and p_2. This set of simultaneous equations has been solved by means of the Newton-Raphson method using a digital computer (IBM 650). The details of the solution are given in (1).[4]

The concentrations of the four rare species C, O_3, NO_2 and NO^+ are then computed from the equilibrium equations

$$\beta_C = \frac{\beta_2\Sigma\beta_i}{\beta_8 p_2 K_C(T_2)} \qquad CO \rightleftarrows C + O$$

$$\beta_{O_3} = \frac{\beta_8^3 p_2 K_{O_3}(T_2)}{(\Sigma\beta_i)^2} \qquad O_3 \rightleftarrows 3O$$

$$\beta_{NO_2} = \left[\frac{\beta_3\beta_4^2 p_2 K_{NO_2}(T_2)}{\Sigma\beta_i}\right]^{1/2} \qquad 2NO_2 \rightleftarrows N_2 + 2O_2$$

$$\beta_{NO^+} = \left[\frac{\beta_{10}\Sigma\beta_i}{p_2 K_{NO^+}(T_2)}\right]^{1/2} \qquad NO \rightleftarrows NO^+ + e^-$$

..... [7]

The conductivity of the product is computed by using the equation proposed by Chapman and Cowling (2) for slightly ionized gases consisting of rigid elastic spherical molecules

$$\sigma = \frac{n_e\epsilon^2}{kT} D_{12} = \frac{n_e\epsilon^2}{kT}\left\{\frac{3}{8n_f r_{12}^2}\left[\frac{kT(m_1 + m_2)}{2\pi m_1 m_2}\right]^{1/2}\right\} \qquad [8]$$

We introduce the collision cross section Q defined by

$$Q = \pi r_{12}^2$$

and assume that the mass of the electron is negligible compared to that of the molecule. We obtain finally

$$\sigma = \frac{0.532\, y_{NO^+}\epsilon^2}{(m_e kT)^{1/2}}\cdot\frac{1}{Q}\cdot 10^9$$

or

$$\sigma = 5.16 \times 10^{-10}\frac{y_{NO^+}}{\sqrt{T}}\cdot\frac{1}{Q}\ \frac{\text{mhos}}{\text{cm}} \qquad [9]$$

[4] Numbers in parentheses indicate References at end of paper.

where T = temperature, R, and Q = collision cross section, cm^2.

The value of the collision cross section Q to be used in Equation [9] is the sum of the Maxwell-averaged collision cross sections of the neutral molecules and the ions, each weighted with the number density. That is

$$Q = \frac{\sum_n n_n\bar{Q}_n + \sum_i n_i\bar{Q}_i}{\sum_j n_j}$$

where

n_n = number density of neutrals
n_i = number density of ions
$\bar{Q}_n$ = electron collision cross section of neutrals
$\bar{Q}_i$ = electron collision cross section of ions
$\sum_j n_j$ = total number density of particles

In the temperature range considered here, the number density of ions is much less than that of the neutrals. Therefore, the contribution of the ions to the total collision cross section may be neglected. Thus

$$Q = \frac{\sum_n n_n\bar{Q}_n}{\sum_j n_j} \qquad [10]$$

For the gas mixtures considered here, the major product gas constituents are N_2, N, O_2, O, CO and H. Therefore, Equation [10] may be written

$$Q = \frac{n_{N_2}}{\Sigma n}\bar{Q}_{N_2} + \frac{n_N}{\Sigma n}\bar{Q}_N + \frac{n_{O_2}}{\Sigma n}\bar{Q}_{O_2} + \frac{n_O}{\Sigma n}\bar{Q}_O + \frac{n_{CO}}{\Sigma n}\bar{Q}_{CO} + \frac{n_H}{\Sigma n}\bar{Q}_H$$

or

$$Q = y_{N_2}\bar{Q}_{N_2} + y_N\bar{Q}_N + y_{O_2}\bar{Q}_{O_2} + y_O\bar{Q}_O + y_{CO}\bar{Q}_{CO} + y_H\bar{Q}_H \qquad [11]$$

The values of the collision cross sections for atomic oxygen and nitrogen are not known with certainty. Reference (3) presents values of this parameter for O and N. The cross section for H in this temperature range is unknown. A value of 1.5×10^{-15} cm^2 has been assumed, however, since this is of the same order of magnitude as the cross section for H at higher temperatures (4). In addition, cross-section values for the atomic species O and N are of this magnitude in the temperature range of interest. Fig. 1 shows the electron collision cross sections for several interesting species. The values for the molecular species were obtained experimentally by the Townsend method and are taken from (4).

Results

The basic equations were solved for the case of air shocks. The results of the computations are shown in Figs. 2, 3 and 4. The temperature vs. the shock Mach number curve is shown for three different initial pressures: 10^{-6}, 10^{-3} and 1 atm. The lower temperatures obtained at the lower initial pressures result from the increase in dissociation as the pressure is decreased. In addition, the waviness in the curves results from the various dissociation processes which are occurring. The dissociation which occurs in the product gas as the Mach number is increased is shown in Fig. 3. Of particular interest is the appearance of ionized nitric oxide in appreciable quantities at the higher Mach numbers. The product gas pressure as a function of Mach number is shown in Fig. 4 for an initial pressure of 10^{-3} atm.

Figs. 5 and 6 show the results of solving the basic equations for the fuels hydrogen and acetylene, respectively, burning in air. On the curve of temperature vs. Mach number is indicated the subsonic and supersonic Chapman-Jouguet points. The steady-state system of equations is not solvable in the Mach number range between these two points. The curve of

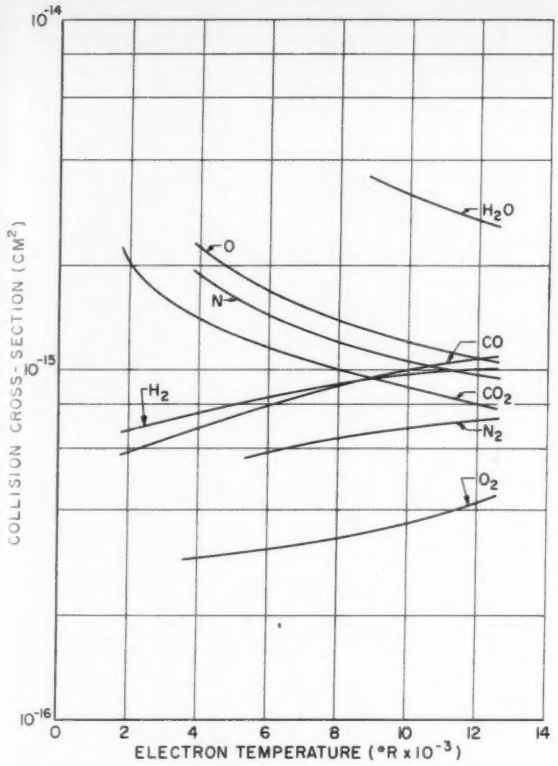

Fig. 1 Collision cross sections for slow electrons

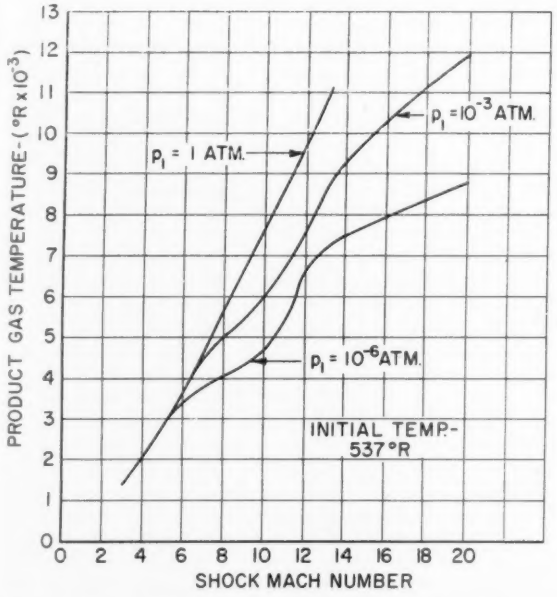

Fig. 2 Effect of initial pressure on the product gas temperature behind air shocks

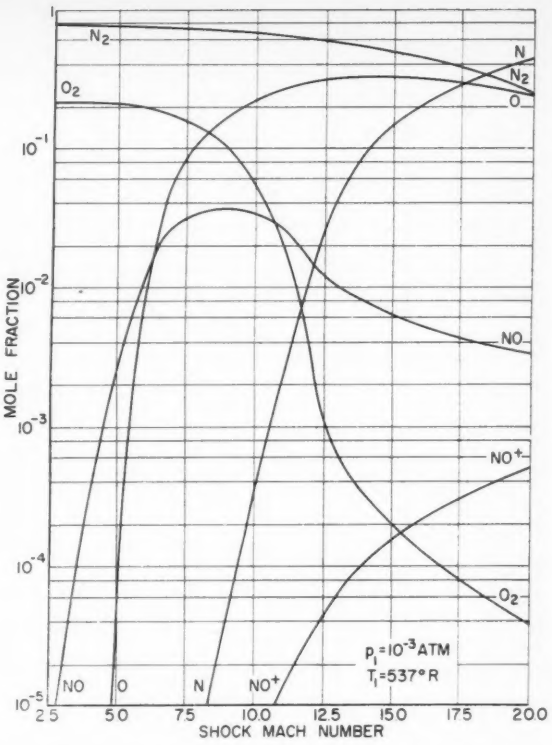

Fig. 3 Constituents of the product gas behind air shocks vs. shock Mach number

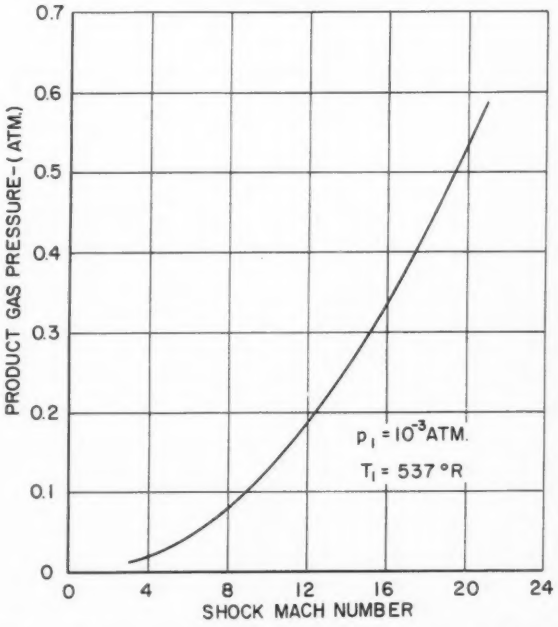

Fig. 4 Product gas pressure vs. shock Mach number behind air shocks

pressure vs. Mach number for both fuels was found to be virtually coincident with the same curve for air shown in Fig. 4. The effect on the dissociation of the combustion products of acetylene of increasing the initial Mach number (hence the final temperature) is shown in Fig. 6. Again, the rise in the quantity of ionized nitric oxide at the higher Mach numbers should be noted.

In performing magnetohydrodynamic experiments in a shock tube, it is desirable to use reactant gases which will yield the highest quantity of ionized constituents. This is a consequence of Equation [9] which indicates that the electrical conductivity of a gas is directly proportional to the mole fraction of ionized species. In the range of temperatures considered here, only ionized nitric oxide (NO^+) ap-

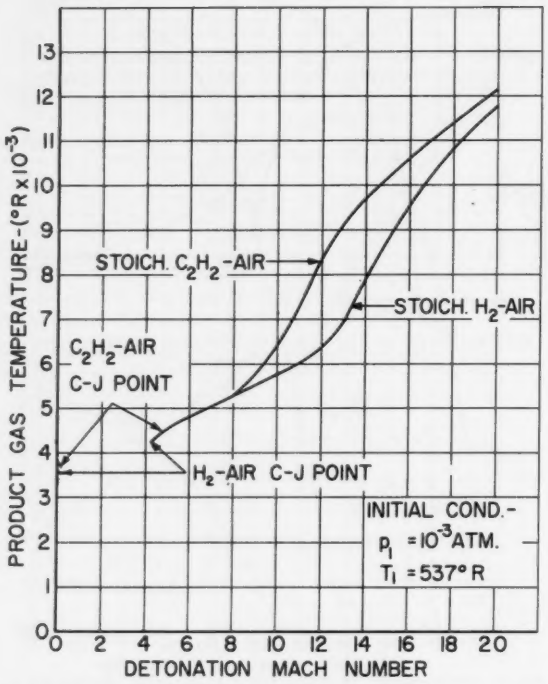

Fig. 5 Product gas temperature vs. Mach number for fuel-air detonations

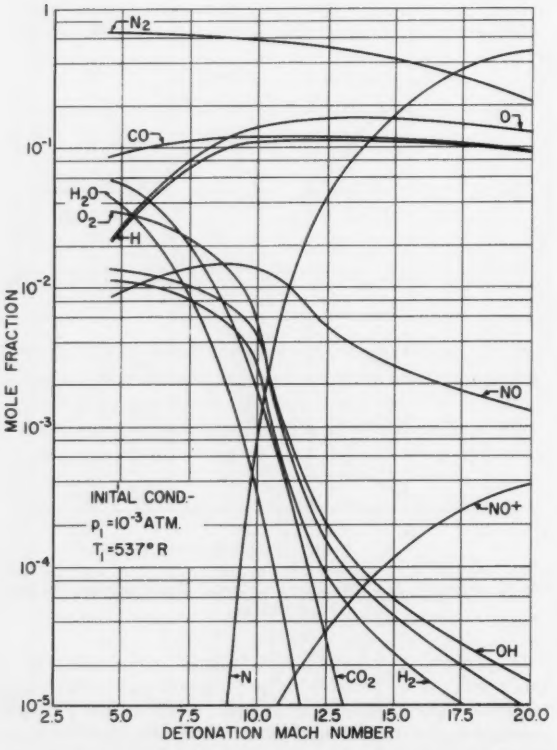

Fig. 6 Constituents of the product gas for a stoichiometric acetylene-air detonation vs. detonation Mach number

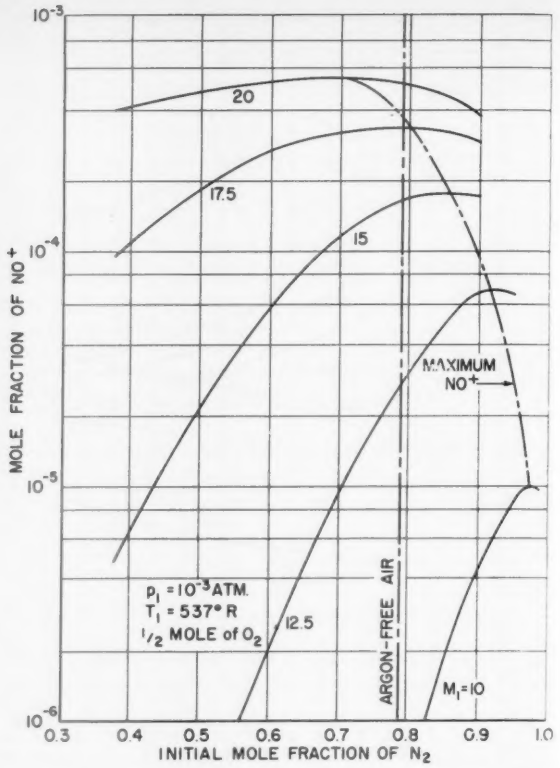

Fig. 7 Effect of nitrogen concentration on the quantity of ionized nitric oxide in the product gas of mixtures initially O_2 and N_2

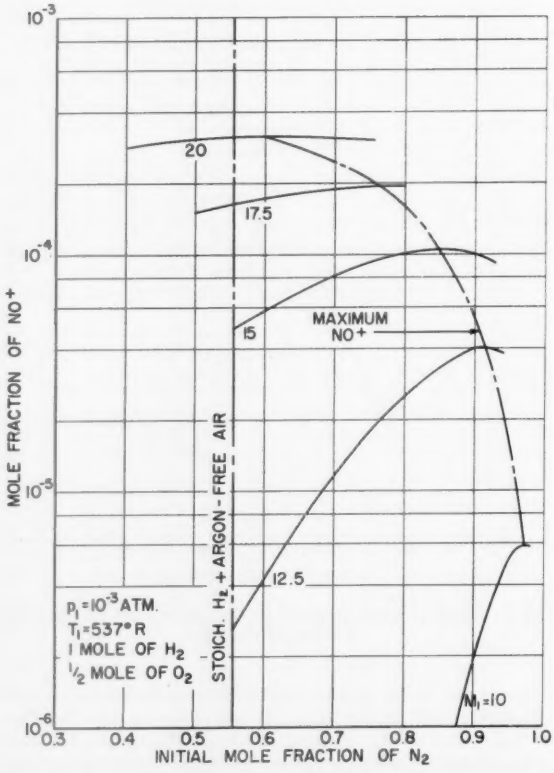

Fig. 8 Effect of nitrogen concentration on the quantity of ionized nitric oxide in the product gas of mixtures initially H_2, O_2 and N_2

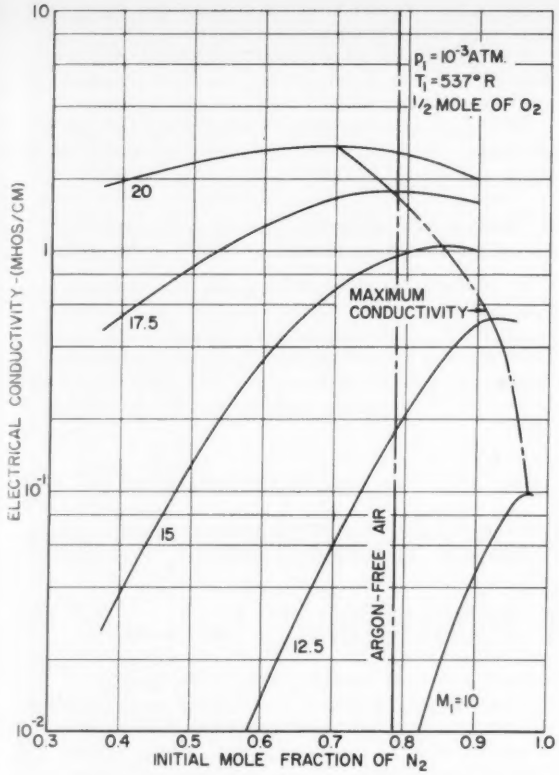

Fig. 9 **Effect of nitrogen concentration on the electrical conductivity of mixtures initially O_2 and N_2**

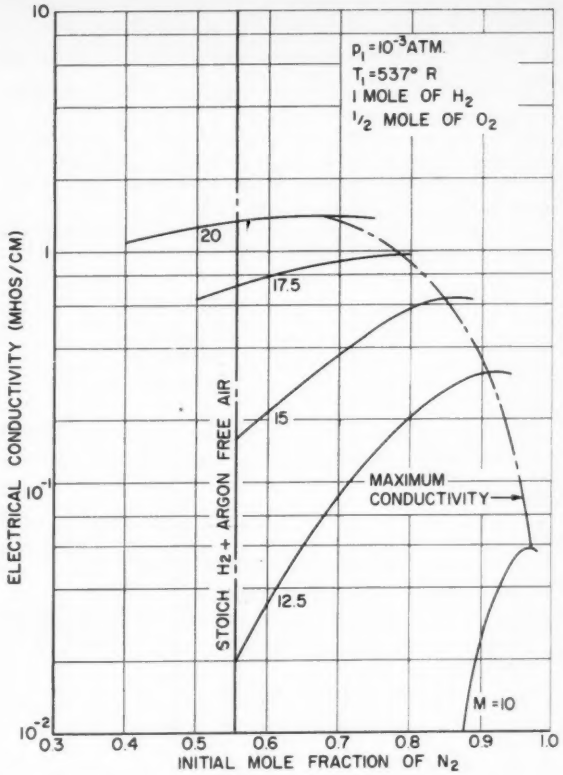

Fig. 10 **Effect of nitrogen concentration on the electrical conductivity of mixtures initially H_2, O_2 and N_2**

pears in appreciable quantities due to its relatively low ionization potential (9.5 ev).

Figs. 7 and 8 indicate the effect of varying the quantity of nitrogen in O_2-N_2 and H_2-O_2-N_2 mixtures such that the largest amount of NO^+ will be yielded for Mach numbers ranging up to 20. The corresponding curves of electrical conductivity vs. the quantity of nitrogen in the reactant gas are shown in Figs. 9 and 10. Only at a Mach number of about 17.5 for the O_2-N_2 mixtures and a Mach number greater than 20 for the H_2-O_2-N_2 mixtures does the optimum composition coincide with that of air. At the lower Mach numbers, a larger amount of nitrogen than is present in air is required to obtain the maximum conductivity.

Fig. 11 is a compilation of electrical conductivity computations for acetylene-air and hydrogen-air detonations and air shocks. It is seen that in the Mach number range considered, the electrical conductivity behind air shocks exceeds the conductivity of the product gases resulting from H_2-air or C_2H_2-air detonations.

In an effort to attain higher electrical conductivities than are possible by using air or optimizing the quantity of nitrogen, the technique exists of "seeding" a gas mixture with a substance that ionizes easily. The alkali elements have low ionization potentials and might be used to increase the electrical conductivity. The computation of the equilibrium constants for three of the alkali metals (cesium, potassium and sodium), using the Saha equation, is shown in the Appendix. Fig. 11 indicates the large increase in electrical conductivity which may be achieved using cesium to "seed" air. The quantities of cesium shown are 0.001 and 0.01 per cent by volume, that is, one mole of cesium to 10^5 and 10^4 moles of mixture, respectively.

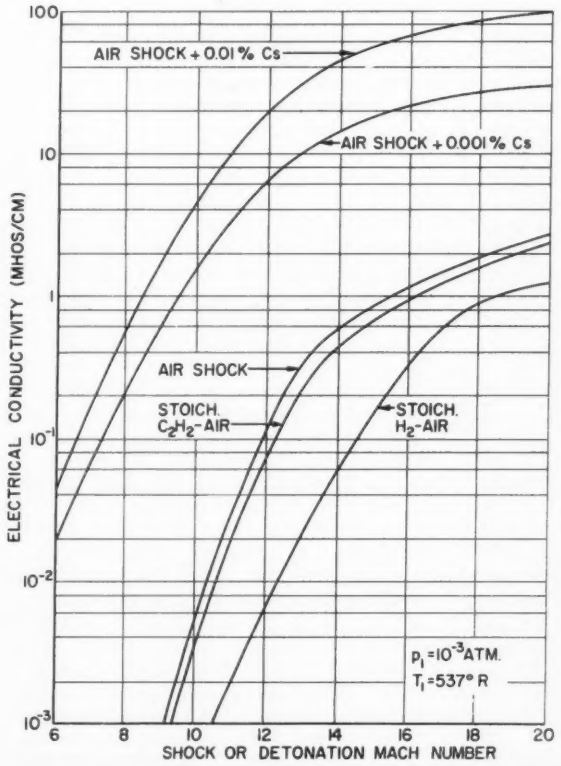

Fig. 11 **Electrical conductivity vs. shock or detonation Mach number**

Appendix

A Sources of Thermochemical Data

The major sources of thermochemical data were tables compiled by the National Bureau of Standards (6, 7). In some cases, where NBS data were not available, sources which were believed to contain the most accurate, modern data were employed. Table 1 lists the heats of formation used in the computation and the various data sources.

For purposes of computation, the composition of air at standard conditions was taken as

Molecule	Mole fraction
N_2	0.780881
O_2	0.209795
A	0.009324

We have compared the results obtained from our computer program with the data in (9 and 11) for the case of air shocks.

Table 1 Thermochemical data

Gas	Heat of formation, ΔH_f, at zero deg K Kcal/mole	Source (Ref. no.)
O_2	0	(6)
O	58.586	(6)
H_2	0	(6)
H	51.620	(6)
N_2	0	(9)
N	112.535	(9)
OH	10.0	(6)
NO	21.477	(6)
H_2O	−57.107	(6)
CO_2	−93.9686	(6)
CO	−27.2019	(6)
C (solid)	0	(6)
C (gas)	170.39	(6)

Gas	Free-energy function or Equilibrium Constant (Ref. no.)	Enthalpy (Ref. no.)
N_2	(7)	(7)
N	(7)	(7)
O_2	(7)	(7)
O	(7)	(7)
H_2	(7)	(7)
H	(7)	(7)
OH	(10)	(8)
NO	(9)	(8)
H_2O	(10)	(7)
CO_2	(7)	(7)
CO	(7)	(7)
C	(9)	(8)

Table 2 Equilibrium constants for the alkali metals

Metal	Na	K	Cs
Ionization potential, ev	5.14	4.33	3.87
Temperature, K		$\log_{10}K(T)$	
1000	−24.901	−20.818	−18.499
2000	−11.193	−9.151	−7.992
3000	−6.434	−5.073	−4.300
4000	−3.963	−2.942	−2.362
5000	−2.425	−1.608	−1.145
6000	−1.363	−0.682	−0.296
7000	−0.578	0.004	0.336
8000	0.029	0.539	0.829
9000	0.517	0.970	1.228

Equilibrium composition of the product gas was found to agree very well with both references.

A comparison of our electrical conductivity data with the data in (5) for the case of air shocks indicates excellent agreement over the entire Mach number range considered.

In (1), the heat of formation of nitrogen was taken as 85.120 kcal/mole. The value presently accepted is 112.535 kcal/mole which, as indicated in Table 1, was used in the present report.

B Computation of the Equilibrium Constants for Ionization Reactions Involving the Alkali Elements

To compute the thermal ionization of a monatomic gas, Saha has applied the Nernst equation for the equilibrium constant. By neglecting the contribution of the upper electronic states of the neutral atom to the specific heat, and considering the atom, ionized atom and electron to be ideal gases, he derived the following equation for the equilibrium constant

$$\log K(T) = -\frac{U}{4.573T} + \frac{5}{2}\log T - 6.491 + \log \frac{g_{A^+} \cdot g_e}{g_A} \qquad [B\text{-}1]$$

For the electron, $g_e = 2$. In the case of the alkali metals, $g_A = 2$ and $g_{A^+} = 1$. In addition, $U = 23{,}053\,I$. Substitution into Equation [B-1] gives

$$\log K(T) = -5041\,\frac{I}{T} + \frac{5}{2}\log T - 6.491 \qquad [B\text{-}2]$$

where I is in electron volts, and T is in deg Kelvin.

Equation [B-2] has been used to solve for the equilibrium constants of the three alkali metals, sodium, potassium and cesium, in the temperature range from 1000 to 9000 K. Table 2 indicates the results.

It should be noted that these results in Table 2 assume the occurrence of singular ionization only, according to the reaction equation

$$A = A^+ + e^-$$

where A is the neutral atom, A^+ the ionized atom, and e^- the electron. The equilibrium constant is defined by

$$\log K(T) = \log \left[\frac{y_{A^+} \cdot y_e}{y_A}\, p \right]$$

where

y_n = mole fraction of the nth constituent in the equilibrium mixture
p = pressure of the mixture

Nomenclature

D_{12} = diffusion coefficient
g = statistical weight
h = specific enthalpy
I = ionization potential, ev
k = Boltzmann constant
$K(T)$ = equilibrium constant
m = molecular weight (see Eq. 5); mass
m_e = electronic mass
n_e = number density of electrons
n_j = number density of particles
p = pressure
Q = electron-particle collision cross section
r_{12} = distance between particle centers at collision
T = temperature
U = ionization potential, cal per mole
V = velocity
x = number of carbon atoms
y = number of hydrogen atoms; mole fraction
α = moles of reactants
β = moles of products
ϵ = electronic charge
ρ = density
σ = electrical conductivity

References

1 Eisen, C. L., Gross, R. A. and Rivlin, T. J., "Theoretical Calculations in Gaseous Detonation," Fairchild Engine Division, AFOSR TN-58-326, March 15, 1958.

2 Chapman, S. and Cowling, T. G., "The Mathematical Theory of Non-Uniform Gases," Cambridge University Press, 1952, 2nd ed., pp. 321, 245.

3 Hammerling, P., Shine, W. W. and Kivel, B., "Low-Energy Elastic Scattering of Electrons by Oxygen and Nitrogen," *J. Appl. Phys.*, vol. 28, no. 7, July 1957, pp. 760–764.

4 Massey, H. S. W. and Burhop, E. H. S., "Electronic and Ionic Impact Phenomena," Oxford University Press, London, 1952, pp. 12, 206–208.

5 Lamb, L. and Lin, S. C., "Electrical Conductivity of Thermally Ionized Air Produced in a Shock Tube," *J. Appl. Phys.*, vol. 28, no. 7, July 1957, pp. 754–759.

6 Rossini, F. D. et al., "Selected Values of Chemical Thermodynamic Properties," Nat. Bur. Standards Circular 500, Feb. 1, 1952.

7 Hilsenrath, J. et al., "Tables of Thermal Properties of Gases," Nat. Bur. Standards Circular 564, Nov. 1, 1955.

8 Rossini, F. D. et al., "Selected Values of Physical and Thermodynamic Properties of Hydrocarbons and Related Compounds," American Petroleum Institute Research Project 44, Carnegie Press, Pittsburgh, 1953.

9 Gilmore, F. R., "Equilibrium Composition and Thermodynamic Properties of Air to 24,000°K," The Rand Corp., RM-1543, Aug. 24, 1955.

10 Huff, V. N., Gordon, S. and Morrell, V. E., "General Method and Thermodynamic Tables for Computation of Equilibrium Composition and Temperature of Chemical Reactions," NACA Rep. 1037, 1951.

11 Logan, J. G., Jr. and Treanor, C. E., "Tables of Thermodynamic Properties of Air from 3000°K to 10,000°K at Intervals of 100°K," Cornell Aeronautical Laboratory Rep. no. BE-1007-A-3, Jan. 1957.

Meteoric Ablation Through Interfacial Instability[1]

SIN-I CHENG[2]

Princeton University
Princeton, N. J.

The interfacial instability of the Taylor-type of the molten layer on the surface of a meteoric body is analyzed when the representative situation on the surface of a blunt nosed body is taken into consideration. The presence of a component of the effective gravity field tangent to the gas-liquid interface considerably increases the seriousness of the instability, especially in the region of the transonic shoulder. In the transonic region, the logarithmic increment per second of the most critical component of initial disturbance is likely to be significantly larger than that in the stagnation region where the normal component alone acts. In view of this result, the recovered meteorite, with smooth nose but ablated downstream, as illustrated in Fig. 2B, can be understood from the ablation mechanism through interfacial instability. The value of the logarithmic increment per second at a given location is inversely proportional to the local value of the kinematic viscosity of the liquid at the interface. The contribution from the normal component of the gravity field is proportional to $R^{1/2}$ (where R is the radius of curvature of the body, a linear scale representing geometrically similar bodies), but is rather insensitive to the thickness h of the liquid film. The contribution from the tangential component is insensitive to the body scale R, but is linearly proportional to the local thickness h of the liquid film. The total logarithmic increment per second of the combined excitation over the blunt nose region will, therefore, increase with the linear scale of the body and with the thickness of the molten layer, but not so seriously as $\sim R^{1/2}$ and $\sim h$.

THE VELOCITY of meteoric objects entering the atmosphere is usually so great that the impact of the atmospheric particles will "melt" the surface material of the body. The surface of the meteoric object will be covered by a layer of the molten material when the collisions are sufficiently frequent. The stability of the molten layer, therefore, becomes of interest. An energy approach (1)[3] has been developed to treat such stability problems. It is shown that the presence of an effective gravitational field normal to the liquid-gas interface and directed toward the gas side is important (1). In addition, it has been shown that the interface in the stagnation region is always unstable, and the instability is predominantly of the Taylor type, possibly leading to mass ablation from the body (2). A method of determining the amplification rate based upon the energy approach is also presented in (2) and illustrated with sample results. It is found that the interfacial instability can be quite vigorous, and it is, therefore, considered necessary to determine the amplification rate more carefully by taking into account several factors which were ignored in (1): The effect of the tangential componenent of the gravitational field along the local liquid-gas interface, and the effect of the variation of the viscosity coefficient of the liquid, etc. For this purpose, the energy equation must be modified slightly. The analysis of the instability condition of the molten layer on different portions of the meteoric surface, from the stagnation point downstream, leads to several conclusions of practical importance.

It is found that the tangential component of the gravity field is always destabilizing over the nose region, and by its action alone, the transonic region over the blunt nose may be

Received Nov. 2, 1958.

[1] This paper was written for the Research and Development Division, Avco Manufacturing Corp.

[2] Associate Professor, Aeronautical Engineering Dept.; also Consultant, Rad, Avco Manufacturing Corp. Member ARS.

[3] Numbers in parentheses indicate References at end of paper.

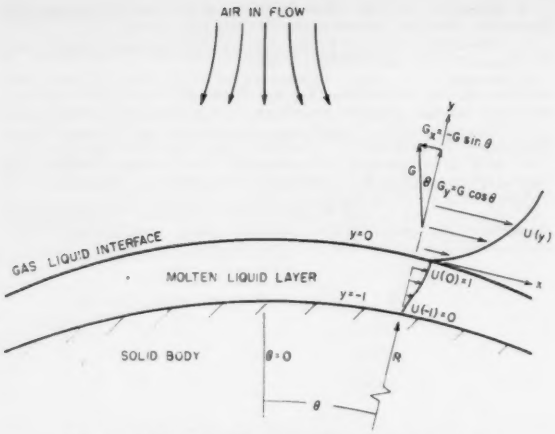

Fig. 1 Schematic diagram of coordinate system

more vigorously unstable than the stagnation point region. The destabilizing action of the normal component of the gravity field increases with the linear scale of the nose dimension. Simple formulas are given for estimating the logarithmic increment per second (L.I./sec) over this subsonic and transonic nose region. The conditions in the region downstream of the transonic region cannot be determined without detailed numerical work for specific instances.

Energy Equation for Disturbance Motion

When a small segment of the body surface is considered, it will be assumed that the mean or the undisturbed flow of the liquid layer and the gas stream is essentially a locally parallel flow. The undisturbed position of the gas-liquid interface will be chosen as the x-axis ($y = 0$) with the solid-liquid interface located at $y = -1$. Following (1), the linear scale is here nondimensionalized by using the local thickness of the liquid film h(cm) as the reference length. The mean flow properties are necessarily the local values. Since the film thickness h is small compared with other linear dimensions of the body, the variations of the mean flow properties along the surface, within a length equal to h are small, and the assumption of nearly parallel flow is then justifiable.

The object under consideration is moving at a very great velocity with respect to the surrounding atmosphere. The deceleration, large as it may be, will not change the relative velocity percentagewise to any appreciable extent during a period of, say, 1 sec. Nevertheless, the actual displacement of the object during 1 sec may be of the order of 10 or more miles with consequent variation of the atmospheric environment due to altitude change. In order that a quasi-steady mean flow may be assumed, the results of (1) clearly indicate that the two characteristic times h/U_0 and ν_l/Gh should be sufficiently small. Here U_0 is the mass velocity of the liquid-gas interface, G the magnitude of the deceleration and ν_l the kinematic viscosity of the liquid in consistent dimensional units. Representative conditions are such that this quasi-steady-state assumption is well justified.

The mean pressure p will be taken as constant across the liquid layer, but the mean temperature T must vary significantly. At the gas-liquid interface, the liquid temperature will be rather close to the stagnation temperature of the gas; while at the liquid-solid interface, the liquid must be at the melting temperature, which is much lower than that of the gas-liquid interface. The absence of a sharp melting temperature for an amorphous solid is not of great significance as later results indicate. The large temperature gradient produces a high heat transfer rate Q into the solid to melt further the solid surface. The density of the liquid may be taken as constant if the thermal expansion is neglected—an assumption easily justified. The large temperature variation across the liquid layer will, however, lead to a large variation of the viscosity coefficient $\mu(T)$. It is not expected that the variation of viscosity coefficient will result in any change in the qualitative stability behavior of the liquid layer, but it may equally well be asserted that any variation will change the amplification rate quantitatively.

The deceleration G (cm/sec²) of the body, and also the effective gravity field when referred to body frame of reference will, in general, be inclined to the normal of the local liquid-gas interface (the y-axis) at an angle θ. The component of the gravity field normal to the interface will then be $G_y = G \cos\theta$, and that tangential to the interface will be $G_x = -G \sin\theta$. The gravitational potential may then be written as $\Omega = yG_y + xG_x$ where both G_y and G_x will be taken as positive if directed in the positive y- and positive x-directions, respectively. The positive x-direction is defined as the direction of the flow velocity U_0 (cm/sec) of the interfacial mass. This velocity will be taken as the reference velocity so that $U(y = 0) = 1$ (Fig. 1). The tangential component of the gravity field G_x tends to modify the boundary layer flow so that the mean velocity profile $U(y)$ will be different according to whether the G_x field is present or not. The tangential field G_x will exchange energy with the disturbance motion if it involves net mass displacement in the direction of the field G_x. The tangential field should, therefore, appear directly in the equation of energy balance of the disturbance motion.

Let us consider only the two-dimensional disturbances, propagating in the direction of the mean flow (x-direction) defined by the disturbance stream function

$$\psi(x, y, t) = \Re\{\varphi(y) \exp [i\alpha(x - ct)]\} \qquad [1]$$

with

$$u = \psi_y = \Re\{\varphi'(y) \exp [i\alpha(x - ct)]\}$$
$$v = -\psi_x = \Re\{-i\alpha\varphi(y) \exp [i\alpha(x - ct)]\}$$
$$c = c_r + ic_i$$

and the instantaneous position of the disturbed interface

$$y_0 = \Re\{\eta_0 \exp [i\alpha(x - ct)]\} \qquad [2]$$

where

- $\Re$ = real part of the terms following
- α = angular wave number = 2π times the number of complete waves in a distance equal to h in the x-direction
- c_r = wave velocity in the units of U_0
- αc_i = amplification rate in the unit time h/U_0

The stream function is used because the density of the media (liquid as well as gas in the vicinity of the liquid-gas interface) is assumed to be constant. Take the scalar product of the disturbance velocity vector (u, v) with the equation of motion and integrate over the control volume V defined by $-1 \leq y \leq \infty$ and $0 \leq x \leq \lambda = 2\pi/\alpha$, i.e., a strip bounded by the solid and open on the gas end, and extending over a wave length λ in the x-direction, as in (1). The following expression for the rate of change of the disturbance energy of all the fluid elements occupying the control volume V at any instant t is obtained after neglecting terms which are of third order or higher in disturbance quantities

$$\frac{\partial}{\partial t}\int \rho \frac{u^2 + v^2}{2} dV = \int \rho(-uw) \frac{dU}{dy} dV - \frac{1}{R_e}\left\{\int \mu \left(\frac{\partial v}{\partial x} - \frac{\partial u}{\partial y}\right)^2 dV - 2\int \left(u \frac{\partial u}{\partial x} + v \frac{\partial v}{\partial y}\right) \frac{d\mu}{dy} dV + \right.$$
$$\left. \int_{x=0,\ y=y_0}^{x=\lambda} \Delta \left[\mu \cdot v \left(\frac{\partial v}{\partial x} - \frac{\partial u}{\partial y}\right)\right] dx \right\} + \int_{x=0}^{x=\lambda} \left[v_0 \left(y_0 \frac{\Delta\rho}{F_y} - \Delta p\right) - u_0 \frac{\partial y_0}{\partial x} \frac{\Delta\rho}{F_x}\right] dx \qquad [3]$$

where Δ indicates the discontinuity of the following quantity across the liquid-gas interface, i.e., the difference of the quantity evaluated at $y = 0_-$ less that at $y = 0_+$. $F_y = U_0^2/G_y h$, $F_x = U_0^2/G_x h$ represent the component Froude numbers with proper sign associated with G_y and G_x. The first term on the right-hand side is the Reynolds stress excitation. The following group of terms is the direct viscous contribution, which vanishes as the Reynolds number $R_e = \rho_l U_0 h/\mu_{l0}$ approaches infinity. Here μ is nondimensional, expressed in terms of the liquid viscosity coefficient μ_{l0} just below the liquid-gas interface, i.e., $\mu(y = 0_-) = 1$. The first integral in this group is the ordinary viscous dissipation term, proportional to the square of the vorticity. The second integral is due to the variation of the viscosity coefficient in each layer, and the third term is the contribution from interfacial discontinuities. The last integral over the wave length λ is due entirely to the interfacial discontinuities of fluid density and of static pressure in the presence of surface tension. Only two terms in Equation [3] involving $d\mu/dy$ and F_x are new when compared with the corresponding equation in (1).

Following exactly the procedure as described in (1), replace u and v from Equation [1], y_0 from Equation [2] and Δp by $(1/W)(\partial^2 y_0/\partial x^2)$ with W designating the Weber number, $W = \rho_l U_0^2 h/\tau$ (τ stands for surface tension, dynes/cm), and carry out the integration with respect to x in Equation [3]. Then divide the whole expression by

$$\frac{\pi}{\alpha}\eta_0\eta_0^* c_i \exp[2\alpha c_i t] = \frac{\pi}{\alpha}\varphi_0\varphi_0^* c_i \exp[2\alpha c_i t]/[(1 - c_r)^2 + c_i^2]$$

The last equality is due to the assumption that the liquid-gas interface is a streamline at all times. Here (*) indicates the complex conjugate of the quantity. The final expression is then

$$\alpha^2[(1 - c_r)^2 + c_i^2]\frac{M}{2} = \Lambda' + \frac{\alpha^2}{\alpha c_i}[(1 - c_r)^2 + c_i^2](E - D) \qquad [4]$$

where

$$\frac{M}{2} = \int_{-1}^{\infty} \rho \frac{\alpha^2\varphi\varphi^* + \varphi'\varphi'^*}{\alpha^2\varphi_0\varphi_0^*}\, dy$$

$$E = -\Re\int_{-1}^{\infty} \rho \frac{i\alpha\varphi'\varphi^*}{\alpha^2\varphi_0\varphi_0^*}\frac{dU}{dy}\cdot dy$$

$$D = \frac{2}{R_{el}}(1 - \mu_{g0})\Re(\varphi'/\varphi)_{y=0} + \frac{1}{R_{el}}\int_{-1}^{\infty}\mu\frac{(\alpha^2\varphi - \varphi'')(\alpha^2\varphi^* - \varphi''^*)}{\alpha^2\varphi_0\varphi_0^*}\, dy - \frac{4}{R_{el}}\int_{-1}^{\infty}\frac{d\mu}{dy}\Re\left[\frac{\varphi'\varphi^*}{\varphi_0\varphi_0^*}\right] dy \qquad [5]$$

$$\Lambda' = \left[(1 - \rho_{g0})\frac{1}{F_y} - \frac{\alpha^2}{W}\right] + \frac{1 - \rho_{g0}}{F_x}\frac{\pi}{c_i}\Re\left[-\frac{i(1 - c)\varphi'}{\varphi}\right]_{y=0} - \frac{1}{2F_x}\frac{1}{c_i}\Re[i(1 - c^*)\alpha\varphi'/\varphi^*]_{y=0}\sin(2\alpha c_r t) + \frac{1}{F_x}\frac{1}{c_i}\Re[(1 - c^*)\alpha\varphi'/\varphi^*]_{y=0}[\sin^2(\alpha c_r t) - \tfrac{1}{2}] \qquad [6]$$

Comparison with the corresponding results in (1) shows that both the apparent mass M and the Reynolds stress excitation remain unchanged in form. The viscous dissipation term D is augmented by a new term proportional to $d\mu/dy$. The interfacial excitation term given as Equation [6] is greatly complicated especially because part of the contributions of $G_x \sim 1/F_x$ are time dependent. The situation may be simplified if one agrees to consider the energy balance not at any instant t but during a period of oscillation of the disturbance $2\pi/\alpha c_r$ (in fact, half a period would suffice). This will be conceptually acceptable if $2\pi/\alpha c_r$ is not so large that the actual time $2\pi h/\alpha c_r U_0$ would still be small enough to admit the quasi-steady mean flow.

By applying the timewise average over the period $2\pi/\alpha c_r$, the time independent terms M, E and D remain unchanged as given by Equation [2], but the interfacial excitation Λ' becomes

$$\Lambda = \left[(1 - \rho_{g0})\frac{1}{F_y} - \frac{\alpha^2}{W}\right] + \frac{1 - \rho_{g0}}{F_x}\frac{\pi}{c_i}\Re\left[-\frac{i(1 - c)\varphi'}{\varphi}\right]_{y=0} \qquad [7]$$

and the disturbance energy balance over a wave length $\lambda = 2\pi/\alpha$ and over a period $2\pi/\alpha c_r$ is

$$\alpha^2[(1 - c_r)^2 + c_i^2]\frac{M}{2} = \Lambda + \frac{\alpha^2}{\alpha c_i}[(1 - c_r)^2 + c_i^2](E - D) \qquad [8]$$

This equation is identical in form to the corresponding equation in (1), but the definitions of Λ and D are slightly different. The presence of the tangential component gravity field G_x or $1/F_x$ in dimensionless form greatly increases the complexities of the problem, even qualitatively. This is due primarily to the fact that Λ the interfacial excitation term can no longer be reduced to a form independent of the disturbance motion. This dependence is extremely important. The contribution to the disturbance energy of the tangential component gravity field may add to, or subtract from, that of the normal component, depending upon the mean flow condition. The simultaneous presence of a tangential component of the gravity field and a normal component of the gravity field directed toward the less dense medium, will not necessarily result in the Taylor-type instability of the interface. Moreover, it is no longer clear that the waves, nearly stationary with respect to the mean interfacial mass motion, are the most unstable. Although the normal gravity field does not participate in determining the stability boundary of the waves not stationary with respect to the mean mass motion at the interface ($c_r \neq 1$), the tangential component does. That the contribution of the tangential component of the gravity field may or may not add to that of the normal component, depending on the fluid mechanical situation, can be visualized directly from the following discussion.

The normal component of the gravity field is operative in energy exchange with the y-component mass velocity of oscillations, whereas the tangential component is operative with the x-component. The velocity oscillation of the interfacial mass will clearly depend on the many variables of fluid mechanical nature, of which one is the mean shear flow, that govern the disturbance motion of the flow field. It is, therefore, imperative to have an estimate of $(\varphi'/\varphi)_{y=0}$ before the contribution of the tangential component gravity field may be discussed any further.

Effect of the Tangential Component of the Gravity Field

The linearized equation of motion for small disturbances in an incompressible medium but with varying viscosity co-

efficient is slightly different from the Orr-Sommerfeld equation. Two terms associated with $d\mu/dy$ and $d^2\mu/dy^2$ need be added, but they do not appear to complicate the analytic nature of the disturbance equation which is obtained by direct substitution of Equation [1] into the linearized equation of motion after the elimination of the pressure disturbances

$$[\varphi^{iv} - 2\alpha^2\varphi'' + \alpha^4\varphi] + \frac{2}{\mu}\frac{d\mu}{dy}[\varphi''' + \alpha^2\varphi'] + \frac{1}{\mu}\frac{d^2\mu}{dy^2}[\varphi'' + \alpha^2\varphi] = i\alpha R_{el}\left[\frac{U(y) - c}{\mu(y)}(\varphi'' - \alpha^2\varphi) - \frac{U''(y)}{\mu(y)}\varphi\right] \quad [9a]$$

$$[\varphi^{iv} - 2\alpha^2\varphi'' + \alpha^4\varphi] = i\alpha R_{eg}[(U(y) - c) \times (\varphi'' - \alpha^2\varphi) - U''(y)\varphi] \quad [9b]$$

for the liquid and the gas streams, respectively. Here $R_{el} = \rho_l U_0 h/\mu_{l0}$ with μ_{l0} designating the liquid viscosity coefficient at the interface. $\mu(y)$ is the liquid viscosity coefficient in terms of μ_{l0} so that $\mu(y = 0_-) = 1$. The gas Reynolds number is defined as $R_{eg} = \rho_g U_0 h/\mu_{g0}$ with ρ_{g0} and μ_{g0} taken to be constant throughout. The inviscid approximation to this equation, obtained by dropping terms of $0(R_e^{-1})$ compared with terms of $0(1)$ naturally remains the same as the one with constant viscosity

$$[U(y) - c](\varphi'' - \alpha^2\varphi) - U''(y)\varphi = 0 \quad [10]$$

This is the equation that governs the bulk of the gaseous flow ($y > 0$), when R_{eg} is sufficiently large. For the viscous correction near the critical layer, where $U(y_c) = c_r$, the substitution into Equations [9] of the expansion of

$$\varphi(y) = 1 + \epsilon\frac{U''_c}{U'_c}F(\eta) + \ldots \quad [11]$$

with

$$\eta = (y - y_c)/\epsilon \qquad \epsilon = (\alpha R_{eg}U'_c)^{-1/3} \quad [12]$$

leads to the following equation for the viscous correction $F(\eta)$

$$i\frac{d^4}{d\eta^4}F(\eta) + \eta\frac{d^2}{d\eta^2}F(\eta) = 1 \quad [13]$$

This equation is again identical with the one for constant viscosity. Accordingly, the argument, identical with the one given in (1) based upon well-known mathematical results (3) leads to the following condition at the critical layer

$$\left(-\frac{\varphi'}{\varphi}\right)_{y=y_c} = \left(-\frac{U''_c}{U'_c}\right)\left[\frac{1}{3}\ln(\alpha R_{eg}U'_c)\right] - i\int_{y_{c+}}^{\infty}\frac{U''(y)c_i}{[U(y) - c_r]^2 + c_i^2}dy \quad [14a]$$

or in the limit of $c_i \to 0$

$$\left(\frac{\varphi'}{\varphi}\right)_{y=y_c} = \left(-\frac{U''_c}{U'_c}\right)\left[\frac{1}{3}\ln(\alpha R_{eg}U'_c) + i\frac{\pi}{2}\right] \quad [14b]$$

where it is understood that the principal value of the natural logarithm will be taken. These relations (Eqs. [14]) will be valid approximations so long as the critical layer does not lie in the interior of the liquid layer, and the value of $\alpha R_{eg}U'_c$ is sufficiently large.

For the "stationary disturbances," resulting in Taylor-type instability, the critical viscous layer overlaps, at least in part, the boundary viscous layer so that

$$(\varphi'/\varphi)_{y=0} = (\varphi'/\varphi)_{y=y_c} \quad [15]$$

Substitution of Equations [14 and 15] into Equation [7] gives

$$\Lambda = \left[\frac{1 - \rho_{g0}}{F_y} - \frac{\alpha^2}{W}\right] + \frac{1 - \rho_{g0}}{F_x}\left(\frac{U''_{0+}}{U'_{0+}}\right)\frac{\pi}{3}\ln(\alpha R_{eg}U'_{0+}) \quad [16]$$

Under these circumstances, whether the tangential gravity field is exciting or damping the disturbance motion depends only on the product $(-1/F_x)\cdot(-U''_{0+}/U'_{0+}) \gtrless 0$. Thus, if $F_x < 0$, as it is on the surface of a decelerating body, the tangential gravity field tends to excite interfacial instability if $(-U''_{0+}/U'_{0+}) > 0$. The simplicity of this relation is deceiving however, because the component gravity field tangent to the interfacial flow partly determines U''_{0+}/U'_{0+} of the mean flow.

It may be shown that the instability of the propagating disturbances ($c_r \neq 1$) remains of the Helmholtz type, and can be completely suppressed by a sufficiently large increase of the viscosity of the medium despite the excitation of the tangential gravity field. The Taylor-type instability of the stationary disturbances which may be excited simultaneously by the normal and the tangential components of the gravity field cannot, on the contrary, be completely eliminated, no matter how large the medium viscosity may be. The instability of the stationary disturbances is of more serious concern to the engineer and will now be discussed.

Logarithmic Increment

In order to discuss the stability behavior of the liquid film on the surface of a decelerating object in any general terms with the hope of extracting some important qualitative information, it will be necessary to look into the method of determination of the amplification rate αc_i from Equations [8, 7 and 5], with all the steady-state properties known. By considering representative configurations, we hope to simplify the expression of the key quantity of practical interest. From this, qualitative information may be obtained without extensive numerical work. As concluded in a previous section, only the stationary disturbances ($c_r \cong 1$), will be considered, for which the energy balance Equation [8] becomes

$$(\alpha c_i)^2\frac{M}{2} = \Lambda + \alpha c_i(E - D) \quad [17]$$

with Λ given by Equation [16] and E and D by Equations [5]. It is assumed that $\Lambda > 0$, so that the Taylor-type instability will prevail for the cases being considered. αc_i is the amplification rate expressed in terms of the characteristic time h/U_0, which is very small, $0(10^{-3}$ sec). Therefore, αc_i will remain numerically small even for vigorously unstable disturbances with the logarithmic increment of the order of 10 to 100 per sec. As indicated by the sample calculations reported in (1) and those for other representative conditions, the inertia terms $(\alpha c_i)^2 M/2$ and the Reynolds stress terms E may be ignored as small quantities compared with D, at least at small R_{el}, primarily because of the small h and large ν_l of interest. Thus the simplified formula

$$\alpha c_i \cong \frac{\Lambda}{D} = \frac{\Lambda R_{el}}{D_i + D_T + D_d/\alpha^2} \quad [18]$$

may serve as a convenient basis for qualitative discussions concerning the effect of individual parameters if R_{el} remains

0(1) or smaller. Here

$$D_i = 2(1 - \mu_{\varphi 0})\left(-\frac{1}{3}\frac{U''_{c+}}{U'_{c+}}\right)\ln(\alpha R_{e_0} U'_{0+})$$

$$D_d/\alpha^2 = \int_{-1}^{0} \mu \frac{(\varphi'' - \alpha^2\varphi)(\varphi''^* - \alpha^2\varphi^*)}{\alpha^2\varphi_0\varphi_0^*}\, dy$$

$$D_T = -4\int_{-1}^{0} \frac{d\mu}{dy}\, \Re\left[\frac{\varphi'\varphi^*}{\varphi_0\varphi_0^*}\right] dy \qquad [19]$$

are the viscous dissipation contributions:

D_i due to interfacial discontinuity
D_d due to distributed vorticity
D_T due to variation of the liquid viscosity coefficient under nonuniform thermal field

The contributions of the gaseous layer to D_d and D_T have been neglected on account of its relatively small viscosity.

If the viscosity coefficient μ of the liquid is taken to be a function of temperature only, and if the temperature field across the thin liquid layer may be evaluated by considering only the conduction process, D_T may be written as

$$D_T = 2\beta_0\left(\frac{\dot{Q}_0 h}{\lambda_0 T_0}\right) = 2\beta_0 Nu_0 \qquad [20]$$

where

β_0 = representative average value of the ratio of $d\mu/dT$ to the heat conductivity coefficient λ
Nu_0 = Nusselt number corresponding to the heat transfer rate $\dot{Q}_0$ across the interface under the fictitious temperature gradient T_0/h

If both the viscosity coefficient μ and the heat conductivity coefficient λ are assumed to vary $\sim\exp[-\beta_0 T/T_0]$ where T/T_0 represents the temperature, then β_0 in Equation [20] would precisely be the same β_0 in this exponent. For practical molten materials, this is unlikely. Nevertheless, the upper bound of $(d\mu/dT)/\lambda$ will be of the order of unity. It is thus apparent that, for most of the molten materials under consideration, D_T (being of the order of Nu) will be considerably less than unity, and may be neglected when compared with $D_i + D_d/\alpha^2$.

The relative magnitudes of D_i and D_d/α^2 depend to some extent on the value of the wave number α. Since the magnitudes of $R_{e_0}U'_{0+}$ for practical systems are very large, the logarithm of $\alpha R_{e_0}U'_{0+}$ remains large compared with unity even with α as small as 10^{-1}, 10^{-2}. On the other hand, D_d is of the order of 10^{-1} and is rather insensitive to the variation of α, as shown by the results of sample computations. The variation of viscosity in the liquid layer results in some modification of the disturbance Equation [9A] of $\varphi(y)$. This disturbance amplitude function $\varphi(y)$ may, nevertheless, be determined in essentially the same manner as in (1). The basic behavior of $\varphi(y)$ and D_d will be expected to remain unchanged. Therefore, for α of 0(1) and when $(-U''_{0+}/U'_{0+})$ remains positive and of 0(1), D_i will certainly predominate. But for small α, say $0(10^{-1})$ or smaller, D_d/α^2 will predominate, and the amplification rate αc_i will vanish as α^2. Thus, for the practical problem of obtaining an estimate of the maximum amplification rate of the most critical disturbance, the region of small α is relatively unimportant. The amplification rates of disturbances of different wave numbers α may be calculated numerically in the same manner as in (1). It appears, nevertheless, that useful qualitative information about the effect of the tangential gravity field and the variation of the stability behavior along the surface of meteorlike bodies may be obtained by ignoring D_d/α^2 compared with D_i. This approximation will, in fact, give quite satisfactory quantitative results if W/F is fairly large and $(-U''_{0+}/U'_{0+})$ is positive and not too small. The situation with $U''_{0+}/U'_{0+} > 0$ requires much more careful investigation.

The amplification rate of the most critical disturbances will then be estimated after equating the gas density to zero by

$$\frac{1}{10}\Gamma = \frac{F}{R_{el}}(\alpha c_i)_{\max} \cong \frac{\cos\theta - \alpha^2 F/W}{\left(-\frac{2}{3}\frac{U''_{c+}}{U'_{0+}}\right)\ln(\alpha R_{e_0}U'_{c+})} + \frac{\sin\theta}{2} \qquad [21]$$

where θ is the inclination of the gravity field G (and therefore F) to the outward normal of the local surface. In this form, the effect of the tangential gravitational field as represented by the x-component Froude number $F_x = -F\sin\theta$ becomes deceptively simple. It merely serves to add a constant shift of $(1/10)\Gamma = F(\alpha c_i)_{\max}/R_{el}$ of the amount $(1/2) \times \sin\theta$ to the contribution of the normal component. In terms of the dimensionless group $\Gamma = (10F/R_{el})(\alpha c_i)_{\max}$ as used in (1), the logarithmic increment per second of initial disturbances may be written as

$$\text{L.I./sec} = (Gh/10\nu)(\Gamma_y\cos\theta + 5\sin\theta) \qquad [22]$$

where Γ_y may be read from curves similar to those given in (1). The simplicity of the results of Equations [21 and 22] is deceiving, because the presence of a tangential gravity field will not only introduce the second term $5\sin\theta$ in Equation [22], but will also modify the values of the interfacial mass velocity U_0 of the mean flow and of U''_{0+}/U'_{0+} of the mean flow velocity profile. The second quantity U''_{0+}/U'_{0+} alone is important in determining the logarithmic increment per second of the initial disturbances. For very thin liquid layers of large viscosity, a fair estimate of $-U''_{0+}/U'_{0+}$ may be made from the local streamwise pressure gradient $\partial p/\partial x$ and the body force field from

$$-\frac{U''_{0+}}{U_{0+}} = \frac{1}{\mu}\left(-\frac{\partial p}{\partial x} + \rho G_x\right)$$

on which Γ_y critically depends. Thus, the effect of the presence of a tangential gravity field is far from being merely additive to the result when the tangential field is absent. The simplicity exists only in the dimensionless parameters chosen in the present investigation.

For the practical application of a decelerating meteorlike body, the deceleration G is related to the pressure on the body nose. The pressure gradient of the nose is overwhelmingly large, so that the associated deceleration has little consequence in altering the steady-state value of $-U''_{0+}/U'_{0+}$ on the gas side. It is because of this fortunate circumstance that many important qualitative conclusions may be obtained.

Effect of Scale and Position on the Surface of a Meteoric Body

The logarithmic increment per second of the most critical disturbance corresponding to the local steady-state conditions will be considered as a measure of the seriousness of the instability of the molten layer over that part of the surface of a meteoric body. Accordingly, Equation [22] will serve as the foundation of the ensuing discussion. G is the deceleration of the body, a constant for all parts of the surface. The variation of the inclination θ of the equivalent gravitational field to the local normal is accounted for by the expression $\Gamma = \Gamma_y\cos\theta + 5\sin\theta$. Γ_y will be taken as inversely proportional to $(-U''_{0+}/U'_{0+})$ from the mean velocity profile on the gas side of the interface. The quantities of primary importance that vary along the surface of the body are $(-U''_{0+}/U'_{0+})$, h and ν_l. It will be assumed that the body under consideration is blunt with a sphere-like nose, decelerating along the axis of symmetry. The front stagnation point corresponds to $\theta = 0$. An accurate determination of any of these three quantities is an extremely complicated matter. It is hoped that the following simple estimate will yield the correct qualitative results suitable for our purposes.

The variation of (U''_{0+}/U'_{0+}) as a function of θ will be considered first. Its effect is pronounced only in the evaluation of $\Gamma_y \sim (-U''_{0+}/U'_{0+})^{-1}$; i.e., it modifies the contribution of

the normal component of the gravity field only. It will be assumed that the liquid film is very thin compared with the characteristic geometrical scale of the body (as is the nose radius R with $h/R \ll 1$) and that the liquid is very viscous. The inertia force is then negligible. Thus, the ratio of $(d^2U/dy^2)_{y=0+}$ to $(dU/dy)_{y=0+}$ at the interface is roughly the same as that at the solid wall in the absence of the molten layer, and may be given by

$$\left(\frac{\mu d^2U/dy^2}{\mu dU/dy}\right)_{y=0+} = \frac{(dp/dx) - \rho_b G_x}{S} \qquad [23]$$

Here, the inviscid pressure gradient along the surface may be expressed roughly in terms of the modified Newtonian approximation as

$$-\frac{\gamma M_\infty{}^2 p_\infty}{2R} \cdot C_{p\,\max} \sin 2\theta$$

This approximation is essentially correct upstream of the sonic point, ($\sin 2\theta \lesssim 1$). Here

$\gamma M_\infty{}^2 p_\infty/2$ = dynamic head of the incoming stream
$C_{p\,\max}$ = pressure coefficient at the stagnation point
R = characteristic radius of curvature of the nose

The tangential component of the deceleration $G_x = -G \sin \theta$ may be expressed as

$$G_x \cong -\frac{\gamma M_\infty{}^2 p_\infty}{2} \frac{C_{p\,\max} \cdot A}{\rho_b A \cdot L} \sin\theta \cdot f(\gamma) \qquad f(\gamma) = 0(1) \qquad [24]$$

where

A = the frontal area
ρ_b = average density of the body
L = effective length of the body defined by
$\rho_b A \cdot L$ = the total mass of the decelerating body
$f(\gamma)$ = 0(1) is a shape factor of body nose

The shear stress S at the liquid-gas interface will be replaced by the skin friction coefficient of the gas stream over the solid surface in the absence of the liquid layer as

$$S \cong (\gamma M_\infty{}^2 p_\infty/2) \cdot C_D$$

Thus, when all the quantities are reduced to the present dimensionless forms

$$-\frac{U''_{0+}}{U'_{0+}} \cong \frac{h/R}{C_D}\left[\sin 2\theta - \sin\theta \left(\frac{\rho_b}{\rho_g} \cdot \frac{L}{R}\right)^{-1}\right] \qquad [25]$$

Several aspects may be noted from this expression. Firstly, ρ_b/ρ_g the ratio of the average density of the body to that of the surrounding atmosphere is very large $\sim 0(10^3)$. The ratio L/R may be expected to be no less than 0(1). Therefore, throughout the region of validity of the Newtonian approximation around the nose ($\sin 2\theta \lesssim 1$), which may be roughly interpreted as the entire subsonic region, the ratio $-U''_{0+}/U'_{0+}$ is essentially determined by the pressure gradient

$$-\frac{U''_{0+}}{U'_{0+}} \cong \frac{h/R}{C_D} \sin 2\theta > 0 \qquad [26]$$

which is always positive. Both h/R and C_D are of the order of 10^{-3} sufficiently far away from the stagnation region. Thus, the value of $-U''_{0+}/U'_{0+}$ may be expected to be of order unity. When the stagnation point is approached, C_D also tends to vanish as θ, with $-U''_{0+}/U'_{0+}$ approaching a finite positive limit. The limiting value at the stagnation point may be estimated independently as

$$\left(-\frac{U''_{0+}}{U'_{0+}}\right)_{stag} \cong 0.66\left[\frac{h^2 U_{ex}}{\nu_g}\right]^{1/2}_{stag}$$
$$= 0.66\left[\frac{4(\gamma-1)}{(\gamma+1)^2}\right]^{1/4}\left[\frac{h^2 U_\infty}{R\nu_g}\right]^{1/2} \qquad [27]$$

in the present dimensionless form, where

$$\frac{h^2 U_{ex}}{\nu_g} \sim \frac{h^2 U_\infty}{R\nu_s}$$

is the Reynolds number characterizing the stagnation point gas flow, and U_{ex} is the tangential velocity gradient of the inviscid axisymmetric stagnation flow field (compressibility and dissociation ignored in this stagnation point analysis).

The value of $U_{ex\,stag}$ has been estimated from the Newtonian pressure distribution over the blunt nose, and the normal shock relation over the stagnation region of the nose as

$$U_{ex\,stag} = \frac{U_\infty}{R}\left(\frac{4}{\gamma+1}\right)^{1/2}\left(\frac{\rho_\infty}{\rho e}\right)^{1/2} = \frac{U_\infty}{R}\left[\frac{4(\gamma-1)}{(\gamma+1)^2}\right]^{1/2}$$

where γ is the average specific heat ratio of the gas over the nose region. If we take the following representative values:

$h \cong 10^{-1}$ cm
$U_\infty \sim 10$ km/sec
$R \sim 1$ m

ν_g of the hot air over the nose ~ 1 cm^2/sec, the stagnation point value of $-U''_{0+}/U'_{0+}$ may be as big as 5. Thus, it appears likely that $-U''_{0+}/U'_{0+}$ will decrease from the stagnation point downstream but remain 0(1) throughout the subsonic nose region. This is then the region where the simplified results (Eq. [22]) of the previous analysis will apply.

By substituting Equations [26 and 27] into [22], one obtains:

1 For small θ, i.e., in the immediate vicinity of the stagnation point region

$$\frac{\text{L.I.}}{\text{sec}} = \frac{G}{\nu_l}\left\{\frac{\Gamma_1}{4.2}\left[\frac{R\nu_g}{U_\infty}\right]^{1/2} + \frac{h\theta}{2}\right\} \qquad [28]$$

where Γ_1 is the value of $\Gamma = [10(\alpha c_i)F/R_{el}]_{\max}$ as shown in Fig. 8 of (1) when $-U''_{0+}/U'_{0+}$ is taken to be unity. ν_g is the kinematic viscosity coefficient of the gas at the interface.

2 For θ not too small, i.e., away from the stagnation region

$$\frac{\text{L.I.}}{\text{sec}} = \frac{G}{\nu_l}\left(\frac{\Gamma_1}{20} \cdot \frac{RC_D}{\sin\theta} + \frac{h}{2}\sin\theta\right) \qquad [29]$$

where

R = representative radius of curvature of the body nose
C_D = the gaseous skin friction coefficient referred to the undisturbed dynamic head, $\gamma M_\infty{}^2 p_\infty/2$, of the incoming stream

The result of Equation [28] at the stagnation point is in sharp contrast with the result of (1), in that the stabilizing effect of decreasing h (the liquid film thickness) is far less significant in the present result [28] where it is only through the slight dependence of Γ_1 on $W/F = \rho G h^2/\tau$, $R_{el} = \rho_l U_0 h/\mu_l$, etc., that h exerts its influence. This unexpected result originates physically from the fact that viscous dissipation depends very much on the shear flow condition at the interface, being nearly proportional to $-U''_{0+}/U'_{0+}$ and, therefore, to h as indicated by Equation [27]. The linear dependence of U_{ex} on the linear scale R at the stagnation point over a blunt body may be recognized alternatively on a purely intuitive basis in that the sonic velocity will be reached roughly over a distance $R \cdot \pi/4$ from the axis. By holding $-U''_{0+}/U'_{0+}$ constant in the flat plate calculation as in (1), the estimate of the viscous dissipation contribution fails to simulate the stagnation point condition. The present result in Equation [28] indicates the importance of the overall linear scale of the body nose instead of the local film thickness h. Equation [28] indicates that, for geometrically similar

noses with corresponding physical properties

$$\text{L.I./sec} \sim R^{1/2} \qquad [30]$$

i.e., a large linear scale of the body implies a more serious instability condition of the interface at the stagnation point.

Equation [29] reveals additional aspects in line with this scale effect away from the stagnation point region. Firstly, the contribution of the normal component gravity field, (G/ν_l) $(\Gamma_1/20)$ $(RC_D/\sin\theta)$, similar to the situation in the stagnation region, is relatively insensitive to changes in film thickness h (so long as it remains small), but the contribution increases with the body linear scale R roughly as $R^{1/2}$. This is because C_D, which is proportional to the square root of the local Reynolds number, introduces a $R^{-1/2}$ dependence. Secondly, the contribution of the tangential gravity field (G/ν_l) $(h/2)$ $\times$ $\sin\theta$ is linearly proportional to the local film thickness h, but is independent of the linear scale R of the body.

It may, therefore, be concluded that geometrically similar scaling to larger sizes will, in general, aggravate the instability conditions over the subsonic nose region. Doubling the diameter of the nose will possibly increase the logarithmic increment per second by 20 to 40 per cent. An increase from 10 to 13 would mean an increase of linear increment from $10^{4.3}$ to $10^{5.6}$, a matter of some concern. A laboratory test of a model of 1 cm diameter may be apparently stable with an L.I. per sec, say 3 or 4. But on a full-scale object of 10^2 cm diameter, the L.I./sec would be 10 to 30, if scaled according to $R^{1/4}$ to $R^{1/2}$. The instability on the full-scale model is intolerable, despite the apparent stability of the small-scale test in the laboratory. The inference from the small-scale test results concerning the interfacial instability should, therefore, be very cautiously made.

From Equation [29], the relative importance of the tangential vs. the normal field in exciting instability may also be visualized. The tangential field will contribute more to the logarithmic increment per second than the normal field if

$$\sin^2\theta > \frac{\Gamma_1}{10}\frac{RC_D}{h} \qquad [31]$$

For order-of-magnitude purposes, Γ_1 will be taken as 1 and h as 10^{-1} cm. Let the local flow Reynolds number be of the order of 10^6 per ft (per 30 cm); let C_D be written as $f\cdot R^{-1/2}\times 10^{-3}$ where f is expected to be 0(1). Then with R expressed in centimeters

$$\theta > \theta_t \cong \left[\frac{fR^{1/2}}{10h}\times 10^{-3}\right]^{2/5} \sim \left(\frac{Rf^2}{10}\right)^{1/5}\cdot 10^{-1} \qquad [32]$$

defines the downstream region in which the tangential field is more important. For $Rf^2 = 10^2$, 10 and 1 cm, the values of θ_t are 0.16, 0.1, 0.06 rad (i.e., 9, 6 and 4 deg), respectively. It can now be visualized that over almost the entire subsonic nose region, except for a very small area around the stagnation point, the destabilizing effect of the tangential field is even more important than that of the normal field.

The logarithmic increment per second at the point θ_t will be roughly equal to twice the value for either the tangential or the normal component of the gravity field acting alone. The closeness of the position θ_t to the stagnation point $\theta = 0$ and the symmetry of the mean properties about the $\theta = 0$ axis tend to indicate that the excitation contribution due to the normal component of the gravity field cannot vary substantially from the stagnation region to θ_t. The decrease of the normal field excitation, if any, would be of the order of θ_t^2, which is negligible compared with the 100 per cent augmentation from the excitation of the tangential field. Therefore, unless the kinematic viscosity coefficient ν_l of the liquid is more than doubled in the region 5 to 10 deg downstream, the L.I./sec is likely to increase, or at least remain substantially the same, from the stagnation point downstream toward θ_t. The local investigation in the stagnation region fails to yield any decisive conclusion whether the L.I./sec will increase monotonically from the stagnation point downstream. It is, at least, a local minimum. Accordingly, under ordinary circumstances, the L.I./sec and, therefore, the seriousness of the instability will, in contradiction to one's intuition, increase from the stagnation point downstream.

The variation of the seriousness of the instability conditions over the blunt nose may be further clarified by comparing the local conditions at the sonic point and the stagnation point. A lower bound of the logarithmic increment per second at the sonic region may be obtained from Equation [29] by simply ignoring the contribution from the normal component of the gravity field which is always positive in the subsonic nose region. Assuming that the sonic point lies in the immediate vicinity of $\theta \cong \pi/4$ then

$$(\text{L.I./sec})_{\text{sonic}} \cong 0.35\, Gh_{\text{sonic}}/\nu_{\text{sonic}} \qquad [33]$$

By comparing the estimate of Equation [33] with that at the stagnation point [28], it is found that the logarithmic increment per second in the sonic region will be larger than that at the stagnation point so long as

$$\frac{\nu_{l\text{sonic}}}{\nu_{l\text{stag}}} < 2.3\left[\frac{h^2_{\text{sonic}}U_{sx\ \text{stag}}}{\nu_{g\ \text{stag}}}\right]^{1/2} \cong 1.5\left[\frac{h^2_{\text{sonic}}\,U_\infty}{R\,\nu_{g\ \text{stag}}}\right]^{1/2} \qquad [34]$$

Here, the value of $U_{sx\ \text{stag}}$ has again been estimated from the Newtonian pressure distribution over the blunt nose and the normal shock relation with γ taken as $1.25 \sim 1.15$. If the kinematic viscosity coefficient of the gas at the high temperature under consideration is taken as 1 cm^2/sec and U_∞ as 10 km/sec $\sim 10^6$ cm/sec and the nose radius as 1 m or 10^2 cm, then this critical ratio as calculated from Equation [34] will be 15 or 1.5 if h_{sonic} is 10^{-1} cm or 3×10^{-2} cm. The corresponding figures when the nose radius is taken as 10 cm will be 45 and 4.5, respectively. Thus, if the kinematic viscosity coefficient of the liquid at the gas-liquid interface at the sonic point is no more than four to five times that at the stagnation point, the interfacial instability at the sonic region, as expressed by the logarithmic increment of the initial disturbances per second, will be more serious than that in the stagnation region under most of the circumstances. Suppose some silicone-based amorphous material, like pyrex glass as reported in (4), is considered with an interface temperature at the stagnation point roughly 2800 K; the kinematic viscosity coefficient will not then increase more than four times when the temperature drops to 2200 K. Such a large temperature drop of the interfacial liquid mass to the sonic point cannot be considered impossible. Even so, the sonic region may still be more unstable than the stagnation region under practical conditions. The situation clearly depends greatly on the fluid properties, the scale and the geometry of the body nose of the specific problem under consideration, as indicated by Equation [34].

By combining the information deduced from the local investigation in the stagnation point region concerning the relative seriousness of the instability at the stagnation point and its immediate surroundings, one cannot but draw the following conclusion: From the point of view of estimating mass ablation through this instability mechanism, it appears hardly justifiable to derive satisfaction from the "tolerable instability" in the stagnation region. Nor does it appear plausible to lay confidence on the "apparent stability" as may be observed from the laboratory tests without any consideration of the effect of scale and of the effect of the tangential field. It should, furthermore, be borne in mind that the relative area of the unstable region involved in the sonic region is much larger than that associated with the stagnation point and, therefore, should receive more careful attention.

So far, little has been said concerning the situation downstream of the sonic region. This is not because it is relatively unimportant, but rather because little could be done to an-

alyze it. The analysis of the nose region, as given previously, clearly demonstrates the importance of the aerodynamic situation in determining viscous dissipation and the logarithmic increment per second. The Newtonian pressure distribution is of dubious value too far downstream of the sonic region. The change of pressure along the surface in the downstream region is of the order of the undisturbed free stream pressure p_∞, and its detailed variation depends greatly on the geometry of the body under consideration. It is not possible to make any general statements for $(-U''_{0+}/U'_{0+})$ as was done with Equation [25] for the subsonic nose region. It is not possible to claim that $(-U''_{0+}/U'_{0+})$ will be 0(1) or even remain positive. Thus, the simplification from Equations [18 to 21] cannot be made. Furthermore, compared with the nose region, very little is known about the interface temperature and, therefore, the kinematic viscosity coefficient of the liquid ν_l.

Any discussion of the situation in the downstream region must necessarily be made with detailed calculations for specific instances. The crucial criterion restricting the range of validity of the previous qualitative discussions is the validity of the modified Newtonian approximation for the static pressure distribution over the nose, which may, under certain circumstances, be a good approximation well downstream into the lower supersonic region. Whether the inviscid free stream is supersonic or subsonic makes little difference in the present investigation. The "sonic region" is referred to as the downstream limit of the present investigation primarily for convenience and, secondarily, because the Newtonian pressure distribution often fails to be good farther downstream.

Observed Phenomena

Fig. 2 shows four photographs of meteorites from the collection of the Chicago Museum of Natural History, representing different categories of meteorites insofar as the extent of ablation is concerned. The Shelburne is stony ($10 \times 5\frac{1}{2} \times 3$ in.) with a smooth surface (accompanied by a similar but slightly larger piece). The Long Island is also stony, but much larger (34×20 in. cone) smooth over the nose, but ablated downstream. The South Bend is stony-iron ($5\frac{1}{2} \times 5 \times 3\frac{1}{2}$ in.) with a heavily ablated surface. The Williamette is a much larger iron meteorite, heavily eroded. The relative ablation intensities of these examples may be understood through interfacial instability in the light of results from the present analysis.

The kinematic viscosity of the molten iron is much smaller than that of the silicone-based material of a stony meteorite. The smaller kinematic viscosity as well as the larger size tend to indicate the relative seriousness of interfacial instability in mass ablation in the case of the Williamette meteorite, even if it is assumed that the history of deceleration $G(t)$ is essentially the same for all meteorites under comparison. It is here emphasized, however, that the present analysis concerns only the initial phase of instability, and not the fully developed phase of shedding droplets from spikes and the last phase of etching into the depth of the surfaces. Accordingly, the inference in this case is not much more than a plausible conjecture. Actually, the deceleration encountered by different meteorites will vary considerably as the square of their entering velocities.

The different surface conditions exhibited by the relatively smooth Shelburne and the ablated Long Island meteorites, both of stony nature, may be explained by their difference in size, if the entering velocity is again assumed to be the same.

The most crucial, and by far the most interesting, aspect is illustrated by the Long Island meteorite (Fig. 2B) and is probably the most convincing. The Long Island meteorite exhibits a smooth nose of relatively small extent, followed by an extended but not seriously ablated region. Firstly, the

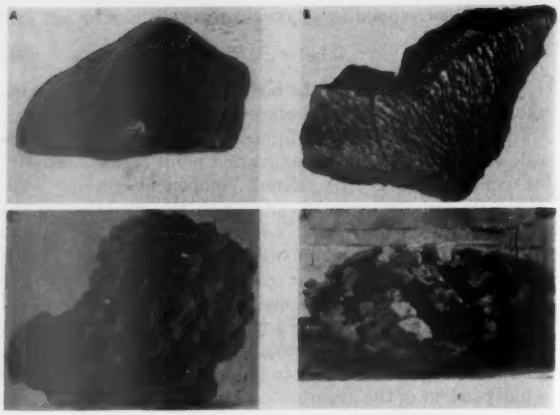

Fig. 2 Photograghs of typical recovered meteorites. A: Shelburne, stony. B: Long Island, stony. C: South Bend, stony-iron, 80–20. D: Williamette, iron

appearance of the ablated surface, resembling wavy ripples, tends to suggest that the ablation be related to some instability phenomenon of surface waves, at least in the early stages of development. Because the liquid layer is very thin and the temperature difference across it is large, the wavy shape of the liquid-gas interface tends to produce a similar wavy appearance of the solid-liquid interface. Secondly, the relatively smooth nose region and the wavy appearance in the downstream region tend to indicate that the interfacial instability becomes increasingly more serious as one moves farther downstream. This last observation is in agreement with the prediction made earlier when the effect of the tangential component of the gravity field was taken into account. According to the conclusions of the present analysis, the stagnation point over the nose is, in fact, the point of minimum instability locally, and the seriousness of the instability is, most likely, increasing toward the downstream region; the sonic shoulder is likely to be much more seriously affected. As a result, the mass ablation rate over the sonic shoulder of a body will be larger than that over the nose. This tends to flatten out the shoulder and to reduce the nose radius of the body. This latter effect, in turn, reduces the seriousness of instability over the nose. The shape and the ablation pattern exhibited by the Long Island meteorite are shared by many others. These characteristics of the recovered large stony meteorite need not necessarily be attributed to the incidental geometry and composition of the meteoric body. It may also be noted that the waves in Fig. 2B exhibit a three-dimensional character with important azimuthal component. It is indicated in (1) that three-dimensionality of the waves has no fundamental importance.

From the comparison of the analytical predictions and the "post-mortem" observation of the meteorites, it is fair to assert the plausibility of the proposed mechanism of mass ablation through interfacial instability, leading to loss of liquid mass directly from the liquid-gas interface. The logarithmic increment per second calculated from the simple formulas in this report, may well serve as a relative measure of the seriousness of the mass ablation rate through this interfacial instability mechanism.

It may also appear pertinent to remark on the spectacular phenomena of the last phase of Sputnik II plunging into the dense atmosphere over the Caribbean Sea as reported by many incidental observers (5). The process of disintegration was accompanied by the breaking off of "fragments" or "large particles" from the main object, and these remained distinct after the passing of the tail. This implies that fragments or larger particles must have been "projected away" to some

distance from the body, under some mechanism like that of the interfacial instability as described in (2). The possibility of laminar separation of the liquid layer from the body cannot alone be accepted as the primary mass ablation mechanism. Any particles or object breaking away from the body with a small velocity component normal to the body surface would simply be swept downstream along the body surface and could not possibly appear as distinctly brilliant sparks away from the main body brilliance, especially when viewed from great distances.

It should be pointed out, in addition, that the excessive mass ablation over the sonic shoulder of the blunt nose may locally weaken the structural strength to such an extent as to cause the actual mechanical failure or breaking up of the body into large solid pieces. The phenomena are, indeed, very much involved. It is not suggested that interfacial instability alone will account for every detail of the observed phenomena. The primary purpose of the present investigation is to indicate the plausibility and the likelihood of the proposed mechanism of mass ablation, which has, so far, led to predictions in no way contradicting observations.

Conclusions

The presence of the tangential component of the equivalent gravitational force field and of the variation of the fluid dynamical situation of the shear flow on the surface of a blunt nosed body flying at hypersonic speed, considerably modify the relative importance of the physical variables affecting the seriousness of the interfacial Taylor-type instability as a mechanism of mass ablation. The main results of significant practical importance are qualitatively:

1 The seriousness of the interfacial instability, as expressed by the logarithmic increment of the most critical component of the initial disturbances, increases with the linear scale R of the geometrically similar body nose, everything else being the same.

2 The stagnation region over the nose need not be the region most seriously affected by interfacial instability. It is more likely to be much less seriously affected than the sonic region downstream. The situation depends greatly on the temperature sensitivity of the kinematic viscosity coefficient of the liquid at the gas-liquid interface. It appears that the temperature sensitivity of the viscosity coefficient of the liquid should be considerably larger than that of the silicone-based ordinary amorphous solids, in order that the stagnation region may be more critical on bodies of practical scales.

Quantitatively, the logarithmic increment may be split into two parts, one due to the normal component and the other due to the tangential component of the gravity field (Eqs. [28 and 29]):

1 That due to the normal component is proportional to $R^{1/2}$ and essentially independent of the film thickness h.

2 That due to the tangential component is independent of the linear scale R but linearly proportional to the film thickness h.

3 The tangential field contributes more than the normal field in exciting instability in the region with $\theta > \theta_t$, which is of the order of 0.1 radian from the stagnation point, as given by Equation [32].

4 The sonic region is more seriously affected by interfacial instability than the stagnation region if the ratio of the kinematic viscosity coefficients of the liquid is less than the quantity proportional to a Reynolds number as specified in Equation [34].

Although the normal component of the gravity field does not modify the stability boundary of the "propagating disturbances" $c_r \neq 1$ for the instability of the Helmholtz type, the tangential component does.

On the surface of the far downstream region of the body, where the Newtonian pressure distribution fails to be a fair approximation, the situation of the interfacial instability will have to be determined by detailed calculations under specific geometry and environment conditions.

Examination of the surfaces of the recovered meteorites and the reports from the incidental observers who witnessed the last phase of Sputnik II plunging into the lower atmosphere, tend to substantiate the plausibility and the likelihood of the proposed mass ablation mechanism through interfacial instability.

References

1 Cheng, S. I., "An Energy Approach to Interfacial Instability With Application to Meteoric Ablation," submitted to Rad. Avco Mfg. Corp., Mass., June 1958.

2 Cheng, S. I., "On the Mechanisms of Atmospheric Ablation," submitted to Rad, Avco Mfg. Corp., May 1958; *also* Princeton University Rep. 427; Proc. of the IAS Congress, Springer-Verlag, Aug. 1958.

3 Lin, C. C., "Theory of Hydrodynamic Stability," Cambridge Monograph on Mechanics and Applied Mathematics, Cambridge, University Press, 1953.

4 Scala, S. M. and Sutton, G. W., "Two Phase Hypersonic Laminar Boundary Layer—A Study of Surface Melting," preprints, Heat Transfer and Fluid Mechanics Institute Meeting at University of California, Berkeley, Calif., June 1958.

5 Miczaika, G. R. and Wahl, E. W., "The Orbital Motion of the Earth Satellite 1957β from 1 April 1958 to Its Decay 14 April 1958," AFCRC TN 58-445, Project Space Track, Air Force Cambridge Research Center, ARDC, USAF.

ARS—NORTHWESTERN UNIVERSITY GAS DYNAMICS SYMPOSIUM

"Dynamics of Conducting Fluids"

August 24–26, 1959, Northwestern University, Evanston, Illinois

Technical Notes

Graphical Computation of Shock and Detonation Waves in Real Gases[1]

GEORGE H. MARKSTEIN[2]

Cornell Aeronautical Laboratory, Inc., Buffalo, N. Y.

The conservation relations across a shock or detonation wave are represented in the form of a graph applicable to real gases of arbitrary composition. Computation of shock waves reflected from a closed end is performed by means of another universally applicable graph.

METHODS for computing the state of a real gas behind a shock wave or detonation wave have been discussed extensively in the literature, and comprehensive reviews of the subject have been published recently (1,2).[3] The numerical methods usually employed require time-consuming iteration. The present graphical procedure, similar to that described by Evans (3), avoids this drawback and, moreover, may be applied to gases of arbitrary composition.

Transformation of the shock relations to a form that is independent of the individual properties of the gas is achieved by introducing the following dimensionless variables, which apparently were first used by Skinner and Squire (4)

$$r = \rho/\rho_1 \qquad [1a]$$

$$P = p/p_1 \qquad [1b]$$

$$\theta = \frac{\mu_1}{\mu}\frac{T}{T_1} \qquad [1c]$$

$$U = \left(\frac{\rho_1}{p_1}\right)^{1/2} u = \left(\frac{\mu_1}{RT_1}\right)^{1/2} u = \gamma_1^{1/2}\frac{u}{a_1} \qquad [1d]$$

$$\chi = \left(\frac{\rho_1}{p_1}\right)(h - h_1) = \frac{1}{RT_1}\left(\frac{\mu_1}{\mu}H - H_1\right) \qquad [1e]$$

Note that in order to eliminate γ_1 from the shock relations, the definition of dimensionless velocity differs from the usual formulation in terms of Mach number. (It is normally not necessary to consider deviations of the compressibility factor $Z = \mu p/\rho RT$ from unity, but this may be done readily by incorporating a factor Z/Z_1 in Eq. [1c].)

Incident Shock

In terms of the variables [1a–1e] and with the notation indicated in Fig. 1, the equations of conservation of mass, momentum and energy and the equation of state for the incident shock assume the form

$$r_2(U_i - U_2) = U_i \qquad [2a]$$

$$P_2 - 1 = U_1U_2 \qquad [2b]$$

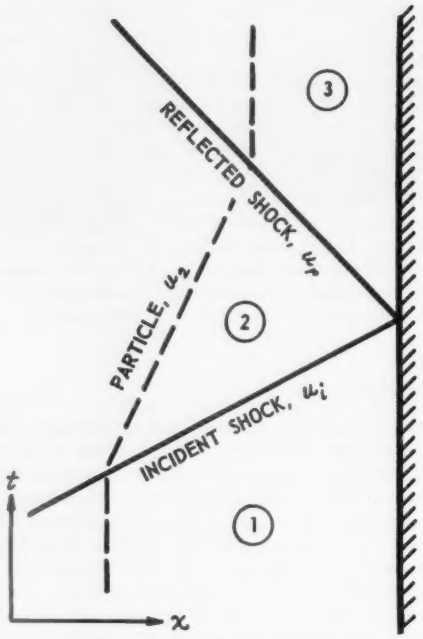

Fig. 1 Notation for shock reflection from a wall

$$\chi_2 = U_2[U_i - (1/2)U_2] \qquad [2c]$$

$$P_2 = r_2\theta_2 \qquad [2d]$$

The additional information required is the relation between enthalpy and temperature $\chi = \chi(\theta)$. This is the only relation that depends specifically on the composition of the gas. It is therefore convenient to represent the relations [2a–2d] graphically in the θ_2-χ_2 plane, in the form of families of curves that correspond to constant values of any one of the other variables. The P_2 = const. and r_2 = const. curves are straight lines; the U_i = const. curves are parabolas, and the U_2 = const. lines are hyperbolas. A plot of the two families U_i = const. and P_2 = const., that are usually of primary interest, is shown[4] in Fig. 2.

Shock computation is carried out by determining the $\chi(\theta)$ curve for a given gas mixture and initial conditions from thermodynamic tables. One may then obtain the state of the gas behind a shock wave of velocity U_i or pressure ratio P_2, from the intersection of the $\chi(\theta)$ curve and the respective curve of Fig. 2, using Equations [2] for computing the variables not contained explicitly in the graph, and Equations [1] for converting the results into dimensional values.

For perfect gases, the $\chi(\theta)$ curves are straight lines through the point $\theta = 1$, $\chi = 0$ of slope $\gamma/(\gamma - 1)$, i.e., 2.5 for a monatomic gas, 3.5 for a diatomic gas, etc. For real gases undergoing relaxation reactions behind a shock of velocity

Received May 8, 1959.

[1] This work was initially supported by the Monsanto Chemical Company and later continued under the auspices of Project Squid which is supported by the Office of Naval Research under Contract Nonr 1858(25). Reproduction in full or in part is permitted for any use of the United States Government.

[2] Principal Physicist, Aerodynamic Research Department. Member ARS.

[3] Numbers in parentheses indicate References at end of paper.

[4] Sets of graphs for incident and reflected shocks drawn to a scale suitable for computation may be obtained from the author.

EDITOR'S NOTE: The Technical Notes and Technical Comments sections of ARS JOURNAL are open to short manuscripts describing new developments or offering comments on papers previously published. Such manuscripts are published without editorial review, usually within two months of the date of receipt. Requirements as to style are the same as for regular contributions (see masthead page).

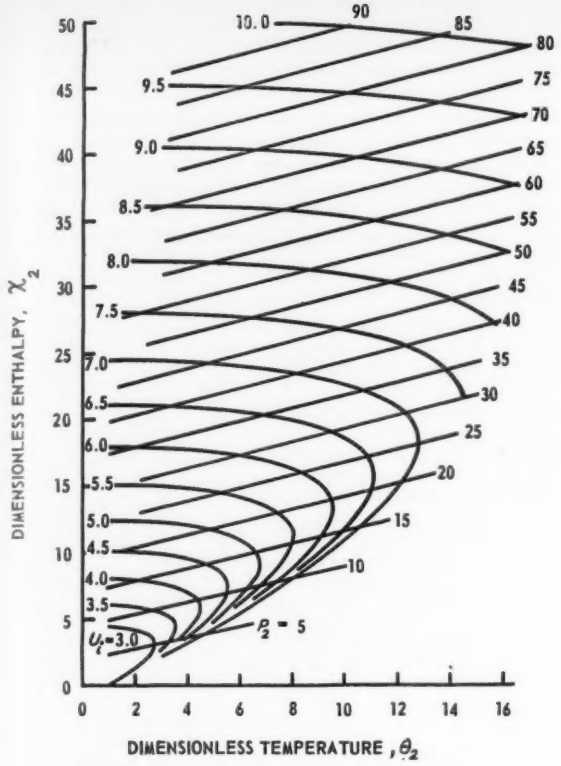

Fig. 2 Graph for incident shock computation

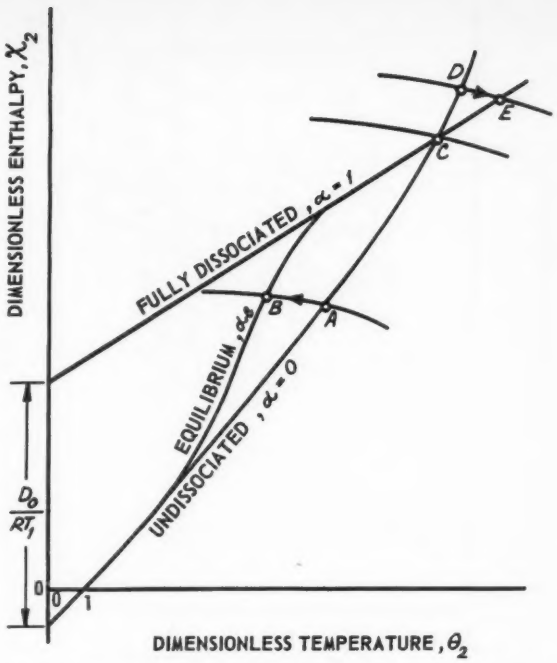

Fig. 3 Application of the graph shown in Fig. 2 to computation of a shock wave in dissociating diatomic gas

U_i, the conservation relations apply not only to the "frozen" state immediately behind the shock but also to any subsequent state in the relaxation zone, if the flow may be regarded as steady in shock coordinates. Therefore, the curves U_i = const. determine the reaction path in the θ_2-χ_2 plane (3).

Dissociation Behind a Shock

As an example of the application of the method to a real gas, the case of a diatomic dissociating gas is shown in Fig. 3. For this case, the relations [1c and 1e] become (3)

$$\theta = (1 + \alpha)\frac{T}{T_1} \qquad [3a]$$

$$\chi = \frac{1}{RT_1}[H_M - H_{M1} + \alpha(D_0 + 2H_A - H_M)] \qquad [3b]$$

Typical enthalpy curves for undissociated gas, $\alpha = 0$, fully dissociated gas, $\alpha = 1$, and equilibrium composition at constant pressure, $\alpha = \alpha_e(T, p)$, are shown in Fig. 3. Since the fully dissociated gas is monatomic, the corresponding $\chi(\theta)$ curve must be a straight line of slope 2.5. The curve for the undissociated gas always has a larger and gradually increasing slope, and therefore the two must intersect at some point C that normally lies at very high temperature. As a consequence, as discussed by various authors (1,3), dissociation relaxation at shock velocities below the value corresponding to point C is accompanied by increases of pressure and density, as from A to B, whereas at values above that critical velocity, as from D to E, the pressure and density decrease. At the point C the only effect of dissociation is a temperature drop by a factor $1/(1 + \alpha) = \frac{1}{2}$.

Detonation

The application of Fig. 2 to detonation is shown in Fig. 4. Since for an exothermic reaction, the $\chi(\theta)$ curve of the products at eqilibrium must lie below that of the reactants, the U_i = const. curves for U_i smaller than a critical value U_D do not intersect the enthalpy curve of the products. (Note on Fig. 2 that all the U_i = const. curves go through the point $\theta_2 = 1$, $\chi_2 = 0$.) For $U_i = U_D$, the enthalpy curve is tangential to the U_i = const. curve, whereas for $U_i > U_D$ there are two intersection points. Differentiation of Equations [2a and 2b] shows that along the U_i = const. curves the relation

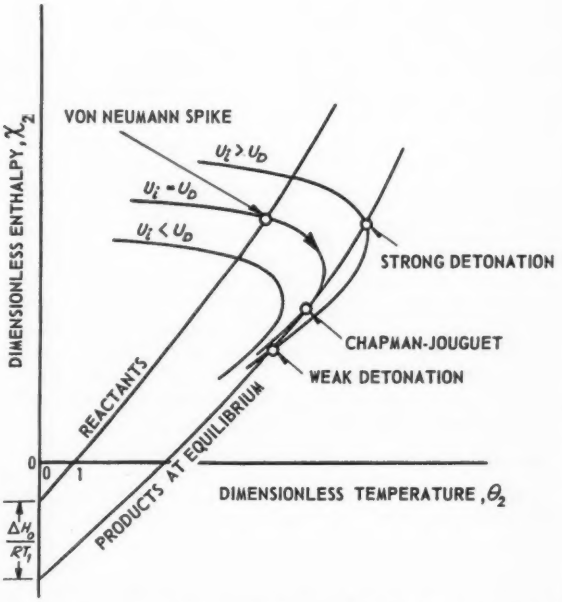

Fig. 4 Application of the graph shown in Fig. 2 to computation of a detonation wave

$$(\partial p_2/\partial \rho_2)_{U_i} = (u_i - u_2)^2 \qquad [4]$$

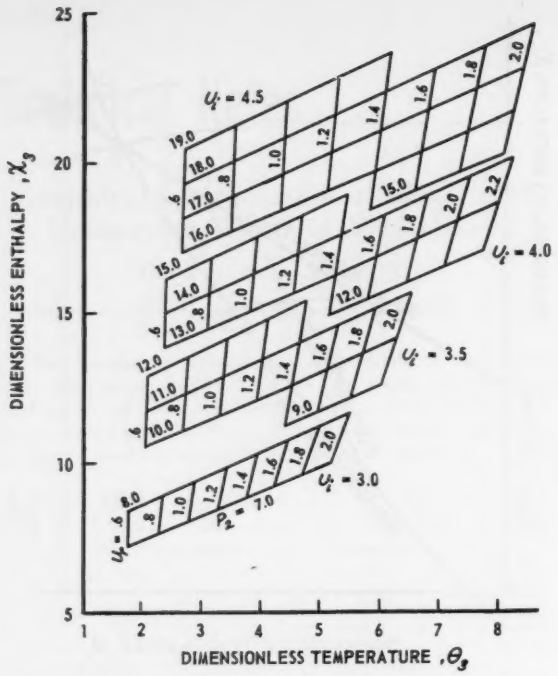

Fig. 5 Graph for reflected shock computation

is satisfied. Since along the $\chi(\theta)$ curve of the products the gas remains in thermodynamic equilibrium, the value of $(\partial p_2/\partial \rho_2)_{v_i}$ at the point of tangency must be equal to the square of the equilibrium speed of sound. This point therefore satisfies the Chapman-Jouguet condition, and the velocity U_D is the detonation velocity. The "von Neumann spike" corresponds to the state of the reactants behind the shock wave of velocity U_D, as indicated in Fig. 4. The two intersection points of curve U_i = const. > U_D with the $\chi(\theta)$ curve of the products correspond to so-called weak and strong detonation. The present method requires only the plotting of the $\chi(\theta)$ curve of the products on the graph, Fig. 2, and yields the Chapman-Jouguet condition automatically without computation of the equilibrium sound speed. It should therefore provide a considerable saving of labor compared with conventional numerical methods (2). However, for accurate computations, a graph with much smaller steps in U_i than shown in Fig. 2 would be required.

Reflected Shock Wave

In terms of the variables [1a–1e], the relations for the reflected shock, Fig. 1, become

$$\begin{aligned} r_3 U_r &= r_2(U_r + U_2) \\ P_3 &= P_2 + (U_r + U_2) r_2 U_2 \\ \chi_3 &= U_2(U_i + U_r) \\ P_3 &= r_3 \theta_3 \end{aligned} \qquad \ldots\ldots\ldots\ldots\ldots\ldots\ldots\ldots\ldots\ldots [5]$$

These relations cannot be represented as simply as those for the incident shock, because r_2 and U_2 are uniquely determined only if a pair of values U_i, P_2 is given. Thus, to each incident shock velocity U_i corresponds not a single curve but a two-dimensional region in the θ_3-χ_3 plane, in which a family of curves P_2 = const. may be plotted. Fig. 5 shows a portion of this graph. For a gas of given $\chi(\theta)$, the incident shock computation yields the values of P_2 corresponding to each U_i. The state behind the reflected shock is then found as the intersection between the (interpolated) P_2 = const. curve and the $\chi(\theta)$ curve, plotted in Fig. 5.

If relaxation reactions occur behind the reflected shock, the choice of the $\chi(\theta)$ curve to be used for computation depends, of course, on the rate of the reactions. If relaxation is so fast that the gas in region 3 may be regarded essentially as being at equilibrium, the equilibrium curve must be used. Conversely, the "frozen" composition curve must be used if the reactions are slow, as required, for instance, in the single-pulse chemical shock tube (5). The paths of relaxation reactions behind the reflected shock are given by the condition $U_r + U_2$ = const. Families of these curves may be plotted in the regions of interest on the θ_3-χ_3 plane for each U_i = const., if needed.

Nomenclature

a	=	speed of sound
D_0	=	heat of dissociation at T = zero K
h	=	enthalpy per unit mass
H	=	molar enthalpy
ΔH_0	=	heat of reaction at T = zero K
p	=	pressure
P	=	dimensionless pressure, p/p_1
R	=	universal gas constant
r	=	dimensionless density, ρ/ρ_1
T	=	absolute temperature
u	=	velocity
U	=	dimensionless velocity, $(\rho_1/p_1)^{1/2}u$
Z	=	compressibility factor
α	=	degree of dissociation
γ	=	ratio of specific heats
χ	=	dimensionless enthalpy, $(\rho_1/p_1)(h - h_1)$
μ	=	molecular weight
θ	=	dimensionless temperature, $(\mu_1/\mu)(T/T_1)$
ρ	=	density

Subscripts

1	=	initial state
2	=	state behind incident shock
3	=	state behind reflected shock
i	=	incident shock
r	=	reflected shock
A	=	atom
M	=	molecule
D	=	detonation
e	=	equilibrium

References

1 Glass, I. I., "Shock Tubes. Part 1, Theory and Performance of Simple Shock Tubes," University of Toronto, Institute of Aerophysics, UTIA Review no. 12, Part 1, May 1958.

2 Gross, R. A. and Oppenheim, A. K., "Recent Advances in Gaseous Detonation," ARS JOURNAL, vol. 29, no. 3, 1959, pp. 173–179.

3 Evans, J. S., "Methods for Calculating Effects of Dissociation on Flow Variables in the Relaxation Zone Behind Normal Shock Waves," NACA TN 3860, Dec. 1956.

4 Skinner, G. B., Unpublished Memorandum, Cornell Aeronautical Laboratory, Inc., Aug. 1956; Squire, W., unpublished work.

5 Glick, H. S., Squire, W. and Hertzberg, A., "A New Shock Tube Technique for the Study of High Temperature Gas Phase Reactions," in "Fifth Symposium (International) on Combustion," Reinhold Publishing Co., N. Y., 1955, p. 393.

Magnetic Boundary Layers

H. F. LUDLOFF[1]

New York University, New York, N. Y.

THE SUPERSONIC motion of a conductive fluid of magnetic Reynolds number $m = 2\pi\sigma Uc$ and Mach number M^o, about a thin airfoil contour $h(x)$, carrying a relatively weak magnetic field H_x, H_y, is determined by the equations

$$(M^{o2} - 1)q_{xx} - q_{yy} = G_r(H_x, H_y) \qquad [1]$$

Received May 25, 1959.

[1] Professor of Aeronautical Engineering.

where

q = disturbance velocity vector (u, v) due to the presence of H as well as $h(x)$

G_2 = polynomial of second degree in the derivatives of H_x, H_y

The magnetic flux satisfies

$$\Delta H - 2m \cdot \frac{\partial H}{\partial x} = 0 \qquad [2]$$

All distances are dimensionless, measured in units of chord length c.

After introducing characteristic coordinates $\xi, \eta = x \pm \beta \cdot y$ into Equation [1], and fulfilling the boundary conditions at $y = 0$, $v = U \cdot h'(x)$ and at $\xi = -\infty$, $q = 0$, we obtain as solution of Equation [1] in the upper half plane

$$v = \bar{G}(\xi, \eta) - \bar{G}(\eta, \eta) + h'(\eta) \qquad [3]$$

where

$$\bar{G}(\xi,\eta) = \int_{-\infty}^{\xi} d\xi \int_{-\infty}^{\eta} d\eta \cdot G_2(\xi, \eta)$$

This process is the same for u, and for the lower half plane. $\bar{G}$ can be computed after H has been determined from Equation [2].

If we require as boundary condition for Equation [2] that H vanish at infinity, and behave like the field of a current-carrying wire, near the wire, then we obtain by use of a vector potential A_z

$$H_x = -m \cdot e^{mx} \cdot (y/r) \cdot K_1(mr)$$

$$H_y = -m \cdot e^{mx} \cdot K_0(mr) + m \cdot e^{mx} \cdot (x/r) \cdot K_1(mr)$$

$$\ldots\ldots\ldots\ldots\ldots\ldots\ldots\ldots\ldots\ldots\ldots\ldots\ldots\ldots\ldots\ldots\ldots\ldots [4]$$

where K_ν is the modified Hankel function.

For small mr

$$H_x = -\frac{\sin\theta}{r} \qquad H_y = +\frac{\cos\theta}{r} \qquad [5]$$

This means the magnetic lines of force are circles around the origin (wire) for vanishing magnetic Reynolds number (i.e., without wind).

For large mr

$$H_x \sim -m \cdot e^{-m(r-x)} \cdot \sin\theta \cdot \sqrt{\pi/2mr} + \ldots$$

$$H_y \sim -m \cdot e^{-m(r-x)} \cdot (1 - \cos\theta) \cdot \sqrt{\pi/2mr} + \ldots$$

$$\ldots\ldots\ldots\ldots\ldots\ldots\ldots\ldots\ldots\ldots\ldots\ldots\ldots\ldots\ldots\ldots\ldots\ldots [6]$$

In this case, the magnetic lines of force are given by

$$A_z = e^{mx} \cdot K_0(mr) = c$$

They are, in approximation, narrow parabolae about the x-axis: $r - x =$ constant. The magnetic field, which was originally axisymmetric, is now "blown downstream" by the relative wind and forms a thin "magnetic boundary layer" along the x-axis. The H-lines are closed curves, also on the downstream end (see Fig. 1). Within such an egg-shaped curve lies the essential strength of the field; the outside field is negligible. From Equation [6], it follows that the field strength H has fallen off to less than 1 per cent of its value in the vicinity of the chord, within approximately 25 chord lengths along the x-axis on the downstream side; on the upstream side, its extension is practically zero. The width of the field in the cross-direction is indicated by

$$H^2 \sim \theta^2 \cdot e^{-mr\theta^2}$$

which means that the magnetic "boundary layer thickness" is

$$\theta \sim 1/\sqrt{mr}$$

a relation which is similar to that in viscous layers. The field profile inside the layer is shown in Fig. 2; there are other varieties.

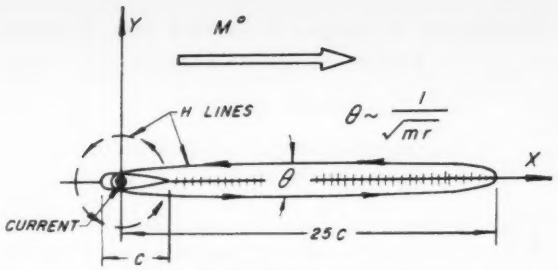

Fig. 1 Illustration of nomenclature

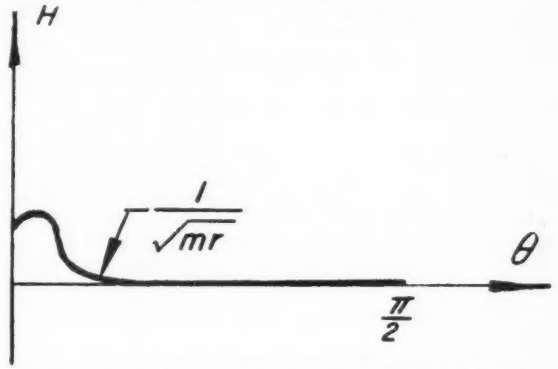

Fig. 2 Field profile inside magnetic boundary layer

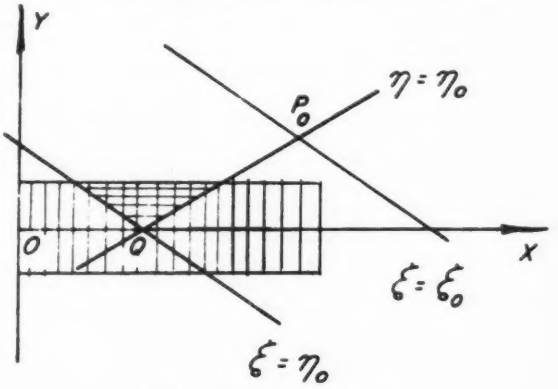

Fig. 3 Velocity disturbances

The influence of the magnetic field on the velocity profile can be deduced from Equation [1]. Clearly, due to the non-homogeneity of the wave Equation [1], the velocity disturbances are not only caused by the magnetic field along the same characteristic, as in ordinary gasdynamics, but are a cumulative effect of the whole field, extending upstream between the characteristics $\xi = \eta_0$ and $\xi = \xi_0$, which in some cases may be considerable. (See Fig. 3.)

By use of the preceding analytic expressions, the transformation of an originally axisymmetric field into a thin, long, magnetic boundary layer, due to the action of a strong relative wind, can be described in all details; this insight may be regarded as supplemental illustration to the often-quoted theorem that in a conducting fluid, the magnetic flux is partly carried with the fluid and partly dissipated through it. Note that these magnetic layers exist also in a free stream, if no disturbing body contour is present. The resulting velocity profiles are qualitatively different from those in ordinary gasdynamics in that the disturbances are zero on the symmetry line and increase toward the outside and in the downstream direction, as seen from Fig. 3.

A more general study of magnetic boundary layers is to be based on the nonlinear equations of motion.

Maximum Ejection Velocity for Return From Satellite Orbits

HARRY ESSES[1]

General Applied Science Laboratories, Inc., Hempstead, N. Y.

THE PROBLEM considered concerns the minimum velocity increment required to transfer an Earth satellite from its initial orbit into an orbit which intersects the Earth. This velocity increment will be referred to as the ejection velocity. In particular, it will be proved that the ejection velocity has an upper bound $v_{ej} = 4930$ fps at an altitude of 19,325 statute miles or about 4.88 Earth radii.

The interesting feature of this result is that the maximum occurs at a finite distance from the surface of the Earth, so that the ejection velocity first increases with altitude, reaches a maximum, and then decreases with altitude. At first glance, this result may be surprising, since one might expect the ejection velocity to increase monotonically with altitude, where a greater ejection velocity would be required for a satellite at an altitude of 50,000 statute miles, for example, than for one at an altitude of 25,000 statute miles. A simple calculation shows, however, that the ejection velocity for the 50,000-mile satellite is less than that for the 25,000-mile satellite.

The strangeness of this result vanishes, however, as soon as one notes that the velocity required to establish a circular orbit decreases monotonically with altitude, from about 26,000 fps at the surface of the Earth to zero "at infinity." It then becomes apparent that there exist altitudes for which the circular orbital velocity itself is less than the ejection velocities required for certain lower altitude orbits. Insofar as it is not necessary to remove the entire orbital velocity to cause a given orbit to intersect the Earth, it is at least intuitively clear that there exists a turning value for ejection velocity which occurs at a finite distance from the Earth's surface. A formal proof of this statement follows, which is based upon orbital motion about a spherical Earth, in the absence of the atmospheric envelope and all other perturbating forces.

The apogee velocity for a satellite traversing an elliptical orbit is well-known to be

$$v_a = \sqrt{\frac{\mu}{a}\left(\frac{1-e}{1+e}\right)} \qquad \mu \equiv g_0 R_0^2 \qquad [1]$$

where

a = semimajor axis
e = eccentricity
g_0 = acceleration due to gravity at the surface of the Earth
R_0 = radius of the Earth

The ratio of perigee radius r_p to apogee radius r_a is

$$\frac{r_p}{r_a} = \left(\frac{1-e}{1+e}\right) \qquad [2]$$

and the semimajor axis is

$$a = \frac{r_p + r_a}{2} \qquad [3]$$

The mathematical requirement for an elliptical orbit to intersect the Earth is that the perigee radius be equal to the radius of the Earth. Inserting Equations [2 and 3] in Equation [1] with $r_p = R_0$ gives

$$v_a = \sqrt{\frac{2\mu R_0}{r_a(r_a + R_0)}} \qquad [4]$$

Received May 20, 1959.

[1] Senior Scientist.

The circular velocity for a satellite at an altitude $h = r_a - R_0$ is

$$v_c = \sqrt{\frac{\mu}{r_a}} \qquad [5]$$

Clearly, the difference $(v_c - v_a)$ is the ejection velocity, or the velocity decrement required to reduce a given circular orbit into an elliptical orbit which intersects the Earth. Moreover, insofar as any elliptical orbit can be inscribed in a circular orbit with a radius equal to the apogee radius of the ellipse, the ejection velocity for any orbit will never exceed

$$v_{ej} = (v_c - v_a) = \sqrt{\frac{\mu}{r_a}}\left(1 - \sqrt{\frac{2R_0}{R_0 + r_a}}\right) \qquad [6]$$

The altitude at which the ejection velocity assumes its maximum value is obtained in the usual way by setting the derivative of Equation [6] with respect to r_a, equal to zero. This results in a cubic equation for r_a, given by

$$r_a^3 - 5R_0 r_a^2 - 5R_0^2 r_a - R_0^3 = 0 \qquad r_a \geqq R_0$$

or, with $r_a = KR_0$

$$K^3 - 5K^2 - 5K - 1 = 0 \qquad K \geqq 1 \qquad [7]$$

Equation [7] has one real root, $K = 5.88$, so that the maximum value for v_{ej} occurs at 23,285 statute miles from the center of the Earth or at 19,325 statute miles from the surface of the Earth. It then follows from Equation [6] that the minimum ejection velocity required for any satellite orbit never exceeds 4930 fps.

These numerical values agree with similar results reported without analysis in a Rand Corp. report[2] which, incidently, gives a very fine treatment, in lay terms, of almost the entire field of space technology.

[2] "Space Handbook: Astronautics and Its Applications," Staff report of the Select Committee on Astronautics and Space Exploration, prepared by the Rand Corp., Santa Monica, Calif.

Achieving Satellite Rendezvous

RICHARD J. WEBER[1] and WERNER M. PAUSON[2]

Lewis Research Center, NASA, Cleveland, Ohio

MANY proposed space missions will require achieving rendezvous of two bodies in an orbit about a planet. For example, an interplanetary transport vehicle may wish to transfer passengers to an orbiting space station. It is generally most efficient to control the spaceship during its approach to the final orbit altitude in such fashion that rendezvous is accomplished immediately upon entering orbit. (Methods of transferring between dissimilar orbits with simultaneous rendezvous are discussed in (1 and 2).[3]) However, as a result of guidance errors, unaccounted-for perturbative forces, etc., it is unlikely that perfect rendezvous will be achieved in this fashion. The situation may then be envisioned where the spaceship has established itself in the desired orbit (assumed to be circular), but is separated from the target body by some angle.

Several procedures are conceivable for correcting this angular error. With high thrust engines, it is possible for the spaceship to be transferred by means of an impulsive thrust to an elliptical trajectory that returns to the circular orbit at

Received May 21, 1959.

[1] Aeronautical Research Scientist. Member ARS.
[2] Aeronautical Research Scientist. Member ARS.
[3] Numbers in parentheses indicate References at end of paper.

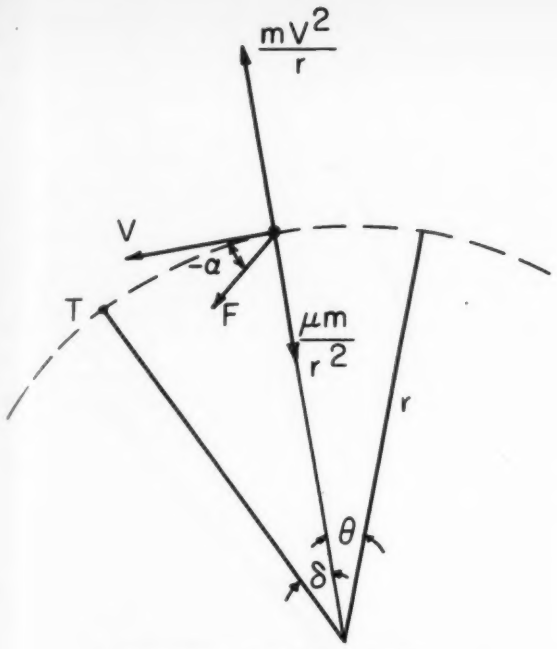

Fig. 1 Forces acting on spaceship

the proper instant for rendezvous (2). With low thrust engines (such as ion or plasma rockets), however, thrust must be applied continuously during an appreciable time interval in order to change the velocity or path of the spaceship. One expedient is to continuously direct the thrust in a more or less circumferential direction in order to spiral some distance away from the circle. The distance is chosen such that, upon spiraling back to the circle, rendezvous is achieved.

In this note an alternative method is considered in which the spaceship remains in the circular orbit while it accomplishes rendezvous with the target. The velocity increments and times required for this method are compared with those for the techniques mentioned above.

Analysis

The initial thrust applied to the spaceship is directed circumferentially. As the velocity of the spaceship changes, the thrust vector must be rotated so that its radial component compensates for the resulting imbalance between the centrifugal and gravitational forces in order to maintain the spaceship in the circular orbit (Fig. 1).

If it is assumed that the thrust-to-weight ratio of the spaceship is constant during the rendezvous maneuver, the differential equations of motion may be solved explicitly for this method of flight, yielding the relations

$$\alpha = \alpha_0 - 2\theta \qquad [1]$$

$$\Delta t = \frac{r^{3/2}}{\sqrt{\mu}} \int_0^{\theta} \frac{d\theta}{\sqrt{1 \pm (F/W) \sin 2\theta}} \qquad [2]$$

Initially, α is zero deg if the target is ahead of the spaceship (180 deg if the target is behind). Equation [1] shows that the thrust angle varies linearly with the distance traveled. Note that upon completion of 45 deg of spaceship travel, the full thrust vector is oriented radially in order to hold the spaceship in the circular orbit, and the vehicle can no longer be accelerated.

Equation [2] can be transformed into an elliptic integral of the first kind and evaluated with the use of tables. In the period of time Δt, the spaceship and the target travel through

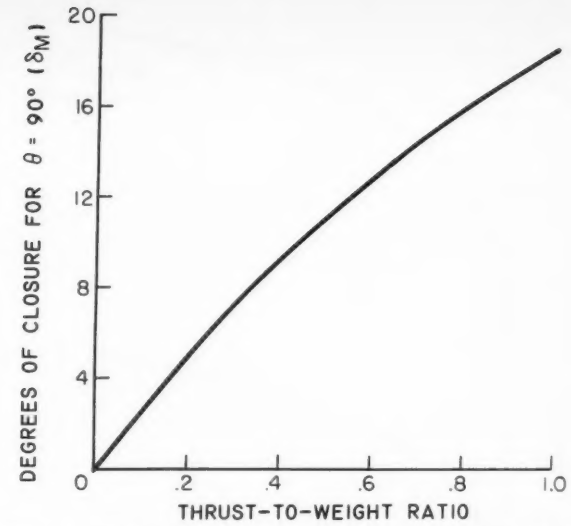

Fig. 2 Maximum possible decrease in angular separation during acceleration and deceleration phases as a function of thrust-to-weight ratio

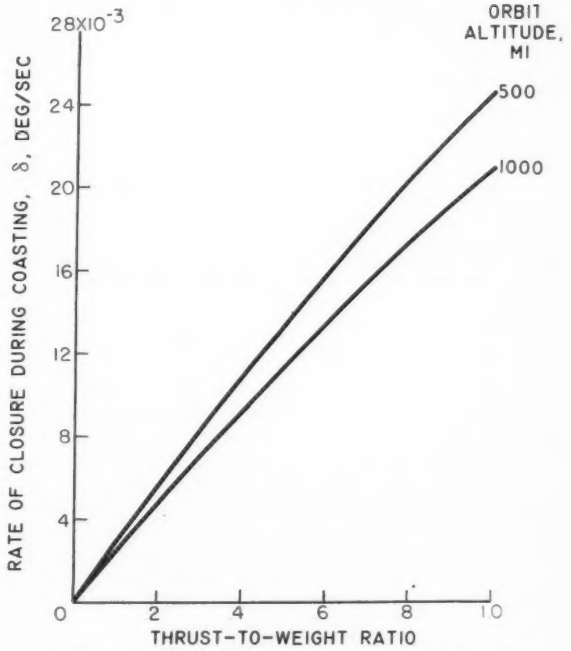

Fig. 3 Rate of closure during coasting as a function of thrust-to-weight ratio for two orbit altitudes

the angular distances θ and $v_c \Delta t/r$, respectively. The difference between these displacements is the amount by which the initial angular separation δ_0 is reduced. The thrust vector at time Δt is at an angle α_1 with the circumferential direction. To restore the spaceship to the circular orbit velocity, the thrust vector is reversed (mirrorwise) to an angle of $180 - \alpha_1$ deg and then rotated back to a circumferential position, ending, however, opposite to the initial thrust direction. The further reduction in angular separation during this deceleration phase is equal to the reduction accomplished during the initial acceleration period; also, each phase of the maneuver takes time Δt. The maximum amount δ_m by

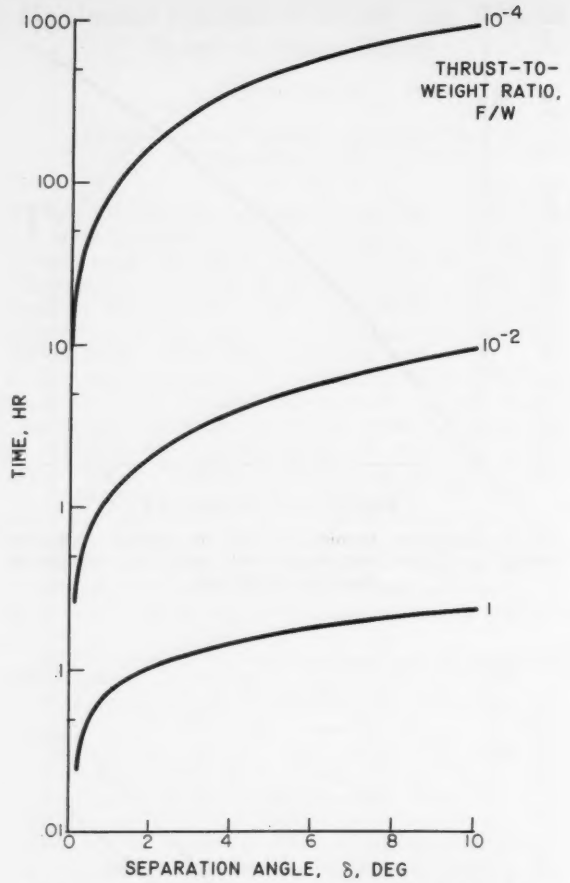

Fig. 4 Rendezvous time as a function of separation angle for several values of F/W. Altitude = 500 miles

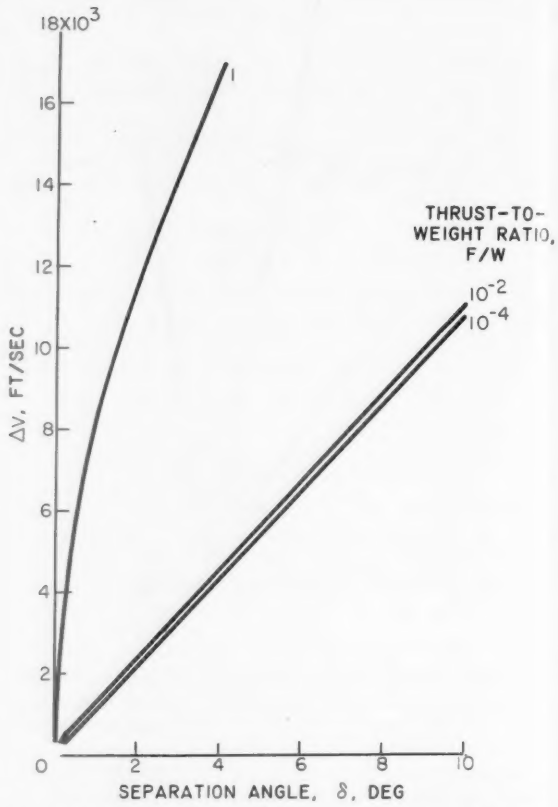

Fig. 5 Velocity increment required for rendezvous as a function of separation angle for several values of F/W. Altitude = 500 miles

which the initial angular separation δ_0 may be reduced during the acceleration period plus a similar deceleration period is shown in Fig. 2.

If the initial angular separation is greater than the value shown in Fig. 2, the thrust may be held in the intermediate radial position and the spaceship allowed to "coast" at constant velocity for a long enough period of time to make up the difference between δ_0 and δ_m. The rate of closure during the coasting phase is given by Equation [3] and plotted in Fig. 3

$$\dot{\delta} = \frac{180}{\pi}\frac{v_c}{r}\left(\sqrt{1+\frac{F}{W}}-1\right) \qquad [3]$$

As a measure of the fuel expenditure necessary to carry out a rocket mission, it is convenient to consider the characteristic velocity increment that would be achieved by the vehicle in linear gravitation-free flight. This velocity increment may be calculated for the constant radius rendezvous maneuver from Equation [4]

$$\Delta V = \int_0^{t_{\text{total}}} \frac{F}{m}\,dt = \left(\frac{F}{m}\right) t_{\text{total}} \qquad [4]$$

where $t_{\text{total}} = 2\Delta t + t_{\text{coast}}$.

The times and velocity increments required to correct for various angular separations are shown in Figs. 4 and 5. Note that both of these quantities are quite large for all but the smallest values of δ_0 in the range of thrust-to-weight ratios anticipated for continuous thrust propulsion systems.

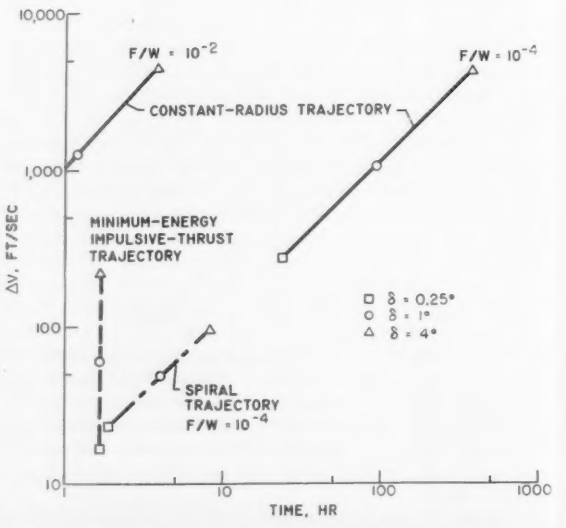

Fig. 6 Velocity increments required for rendezvous as a function of rendezvous time. Altitude = 500 miles

Discussion

A comparison among the various methods described for attaining rendezvous is made in Fig. 6 for several separation angles. (The velocity increments and times shown are for separation angles in which the target leads the spaceship.) The constant radius technique is definitely inferior to the other methods in terms of both the time and the velocity increment required for rendezvous. For a separation of 0.25 deg (which is only about 20 miles at an altitude of 500 miles) a ΔV of nearly 300 fps is necessary for a thrust-to-weight ratio of 10^{-4}. With sufficiently high values of specific impulse, the value of ΔV needed for rendezvous may not correspond to a very large fuel consumption; however, the spaceship crew would not care to take the indicated time of 24 hr to complete the last 20 miles of their journey.

The constant radius method of achieving final rendezvous does not, therefore, appear desirable unless available thrust-to-weight ratios are much higher than 10^{-4}, and then only if further study indicates some advantage (e.g., guidance) over the spiral trajectory method.

Nomenclature

F = engine thrust
m = spaceship mass
r = distance from center of Earth
t = elapsed time
v_c = circular orbit velocity
W = weight of spaceship
α = angle between thrust and velocity vectors
δ = angular separation between the target and spaceship
θ = angular distance traveled
μ = gravitational force constant for Earth

References

1 Paiewonsky, B. H., "Transfer Between Vehicles in Circular Orbits," WADC Rep. TN 57-267, Aug. 1957.

2 Brunk, W. E. and Flaherty, R. J., "Methods and Velocity Requirements for the Rendezvous of Satellites in Circumplanetary Orbits," unpublished NASA data.

Stability of a Globular Cluster in the Oblate Earth's Equatorial Plane

MARVIN H. HEWITT[1]

The Martin Company, Denver, Colo.

An expression is obtained for the stability of a globular cluster whose center of gravity describes a circle in the oblate Earth's equatorial plane. It is found that the stability criterion is not significantly changed if a spherical Earth is assumed.

THE CENTER of gravity of an aggregation of particles describes a circle in the equatorial plane of the oblate Earth. Let C denote this center, and let E be any element of the cluster. Also, r and θ will denote the equatorial polar coordinates of C referred to the Earth center 0, and ξ, η are the coordinates of E referred to C as origin, the axis of ξ being the prolongation of $0C$. Let M be the mass of the Earth. Neglect the Earth's atmosphere and assume that the cluster, as a first approximation, is homogeneous and spherical.

The magnitude of the globe's attraction at an internal point is given as

$$\mu z = -Cmz/b^3 \qquad [1]$$

where

m, b = mass and radius of the globe, respectively
z = CE

We obtain[2]

$$\mu = -Gm/b^3 \qquad [2]$$

The approximate potential function for the gravitational attraction of a solid homogeneous oblate Earth upon a distant particle in the equatorial plane may be given as[2]

$$U = -\frac{M}{x} - \frac{M(a^2 - c^2)}{10x^3} \qquad [3]$$

where

a = semimajor axis of the Earth
c = semiminor axis of the Earth
x = distance from the Earth's center to distant particle

The corresponding acceleration g is then given by the expression

$$g = -GM\left[\frac{1}{x^2} + \frac{3(a^2 - c^2)}{10x^4}\right] \qquad [4]$$

It is seen that this acceleration represents a central non-Newtonian force.

The equations of motion are given now as

$$\frac{d^2(r+\xi)}{dt^2} - (r+\xi)\left(\frac{d\theta}{dt}\right)^2 - \frac{1}{\eta}\frac{d}{dt}\left(\eta^2\frac{d\theta}{dt}\right) = -GM\left[\frac{1}{(r+\xi)^2} + \frac{3(a^2-c^2)}{(r+\xi)^4}\right] + \mu\xi \qquad [5]$$

$$\frac{d^2\eta}{dt^2} - \eta\left(\frac{d\theta}{dt}\right)^2 + \frac{1}{(r+\xi)}\frac{d}{dt}\left[(r+\xi)^2\frac{d\theta}{dt}\right] = -GM\left[\frac{\eta}{(r+\xi)^3} + \frac{3\eta(a^2-c^2)}{10(r+\xi)^5}\right] + \mu\eta \qquad [6]$$

These equations also hold for the motion of a cluster element at C, where $\xi = 0$, $\eta = 0$. Consequently, when Equations [5 and 6] are expanded in powers of ξ and η, all the terms independent of ξ and η must cancel. We obtain

$$\frac{d^2\xi}{dt^2} - 2\frac{d\eta}{dt}\frac{d\theta}{dt} - \eta\frac{d^2\theta}{dt^2} - \xi\left(\frac{d\theta}{dt}\right)^2 = \xi GM\left[\frac{2}{r^3} + \frac{12(a^2-c^2)}{10r^5}\right] + \mu\xi \qquad [7]$$

$$\frac{d^2\eta}{dt^2} + 2\frac{d\xi}{dt}\frac{d\theta}{dt} + \xi\frac{d^2\theta}{dt^2} - \eta\left(\frac{d\theta}{dt}\right)^2 = \eta GM\left[\frac{1}{r^3} + \frac{3(a^2-c^2)}{10r^5}\right] + \mu\eta \qquad [8]$$

Since the center of gravity of the cluster describes a circle about the Earth, we have $r = d$ (constant), $d\theta/dt = n$ (constant). Centripetal acceleration in the oblate Earth's equatorial plane is of the form

$$\frac{v^2}{d} = dn^2 = GM\left[\frac{1}{d^2} + \frac{3(a^2-c^2)}{10d^4}\right] \qquad [9]$$

The centripetal acceleration in any orbital plane of the spherical Earth is given by the expression

$$\frac{v^2}{d} = dn_0^2 = \frac{GM}{d^2} \qquad [10]$$

Received May 25, 1959.

[1] Design Engineer, Applied Research Section. Member ARS.

[2] Webster, A. G., "Dynamics of Particles and of Rigid, Elastic, and Fluid Bodies," G. E. Stechert and Co., N. Y., 1942, 3rd ed.

where $n_0 = d\theta/dt$. Consequently

$$n^2 = n_0 + \frac{3MG(a^2 - c^2)}{10d^5} \quad [11]$$

Introducing Equations [10 and 11] into Equations [7 and 8] yields the equations

$$\frac{d^2\xi}{dt^2} - 2n\frac{d\eta}{dt} + \xi(2n_0^2 - 5n^2 - \mu) = 0 \quad [12]$$

$$\frac{d^2\eta}{dt^2} + 2n\frac{d\xi}{dt} - \eta(2n^2 + \mu) = 0 \quad [13]$$

Let

$$\xi = A\cos(pt + \alpha) \quad [14]$$

$$\eta = B\sin(pt + \alpha) \quad [15]$$

where A, B and α are real constants. We obtain from Equations [12 and 13], after eliminating A and B, the determinantal equation

$$(p^2 + 2n^2 + \mu)(p^2 + 5n^2 - 2m^2 + \mu) - 4n^2p^2 = 0 \quad [16]$$

If p^2 is real and positive, the globe will be stable. This condition will be satisfied if

$$|\mu| > 5n^2 - 2n_0^2 \quad [17]$$

or

$$|\mu| > 3n_0^2 + \frac{3MG(a^2 - c^2)}{2d^5} \quad [18]$$

We may write Equation [18] as

$$\frac{m}{b^3} > \frac{3n_0^2}{G} + \frac{3M(a^2 - c^2)}{2d^5} \quad [19]$$

Let D denote the density of the globe. The condition that the globe is stable is therefore

$$D > \frac{9M}{4\pi d^3} + \frac{9M(a^2 - c^2)}{8\pi d^5} \quad [20]$$

It is of interest to compare the first and second terms of Equation [20]. We have

$$\frac{9M(a^2 - c^2)/8\pi d^5}{9M/4\pi d^3} < 0.003 \quad [21]$$

A stable globe in the equatorial plane at a central distance equal to four times the equatorial radius would be required to have a density greater than 0.05 gm cm^{-3}, whereas a stable equatorial globe at a central distance equal to 11/10 the equatorial radius would have a density greater than 11 gm cm^{-3}, which is about the density of lead.

Optimum Radiator Temperature for Space Power Systems

EDWARD T. PITKIN[1]

Marquardt Aircraft Co., Van Nuys, Calif.

A NUMBER of articles have recently appeared (1 to 3)[2] in which the optimum radiator temperature for a power converter to be used in space is discussed. In (1), the desired radiator temperature to obtain maximum overall efficiency of a solar powered converter is discussed, while (2 and 3) are concerned with minimum radiator weight for a given power output. The purpose of this note is to discuss the radiator temperature for minimum system weight when power source weight varies as a function of power output, and the radiator weight is a function of temperature.

Consider an energy conversion system which takes thermal energy from a heat source, converts a portion to available mechanical or electrical energy, and discharges the unavailable energy through a radiative heat sink. This analysis will apply to any system where the useful power output P_o is equal to the product of a conversion efficiency factor η, the Carnot efficiency η_c and the thermal power output of the source P_s

$$P_o = \eta\eta_c P_s = \eta_t P_s \quad [1]$$

where

$$\eta_c = 1 - T_r/T_m \quad [2]$$

This relation will hold for most systems which employ recirculating working fluids with conventional heat engine cycles. It is further assumed that the energy source weight is proportional to the thermal power output raised to an exponent, and that the radiator weight is proportional to its surface area. Other weight-producing components of the system will be motors, generators and connecting structure. The total weight of these components may be assumed directly proportional to the useful power output as a first order approximation.

The energy source weight may then be expressed

$$W_s = W_{s1}\left(\frac{P_s}{P_{s1}}\right)^N = W_{s1}\left[\frac{P_o/\eta_s}{(P_o/\eta_t)_1}\right]^N \quad [3]$$

where η_t, the thermal efficiency, is the product of the Carnot efficiency and the conversion efficiency. Let the reference condition denoted by subscript 1 be the case of 100 per cent thermal efficiency, and divide by an arbitrarily fixed power P_o, while noting that this power is identical to the thermal power of the source at the reference condition (i.e., $P_o = P_{o1} = P_{s1}$)

$$\frac{W_s}{P_o} = \frac{W_{s1}}{P_{s1}}\frac{1}{\eta_t^N} \quad [4]$$

An energy balance on the system gives the heat rejected by the radiator

$$P_r = \frac{1 - \eta_t}{\eta_t}P_o \quad [5]$$

This is equated to the heat removed by radiation by use of the Stefan-Boltzman relation while assuming the radiator surface and fluid temperatures are essentially the same. Also, the heat sink is assumed to be at absolute zero temperature as a reasonable approximation for the space environment

$$P_r = A_r\sigma\epsilon T_r^4 \quad [6]$$

If a temperature gradient exists over the radiator surface, Equation [6] may be interpreted as defining an appropriate mean temperature. This might apply to systems utilizing noncondensing fluids. The radiator area is easily determined as

$$A_r = \frac{(1 - \eta_t)P_o}{\sigma\epsilon\eta_t T_r^4} \quad [7]$$

Let K_r be the proportionality constant between radiator weight and area, and K_g be the constant relating weight of motor, generator and connecting structure to power. The weight to power ratio of the conversion system then becomes

$$\frac{W}{P_o} = \frac{W_{s1}}{P_{s1}}\frac{1}{\eta_t^N} + \frac{K_r(1 - \eta_t)}{\sigma\epsilon\eta_t T_r^4} + K_g \quad [8]$$

Received May 1, 1959.

[1] Research Specialist, ASTRO, A Division of the Marquardt Aircraft Co. Member ARS.

[2] Numbers in parentheses indicate References at end of paper.

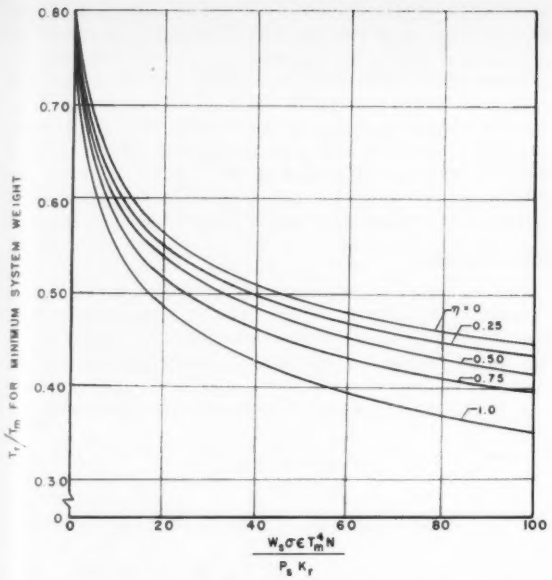

Fig. 1 **Effect of converter efficiency on optimum radiator temperature**

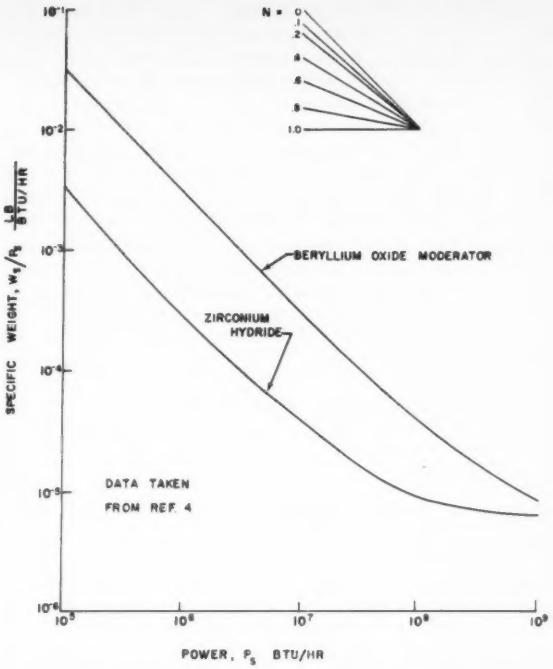

Fig. 2 **Weight characteristics of typical gas-cooled reactors**

Differentiating with respect to T_r at constant power to obtain a minimum gives

$$\left[\frac{W_{s1}}{P_{s1}}\frac{N}{\eta_t^{N+1}} + \frac{K_r}{\sigma\epsilon T_r \eta_t^2}\right]\frac{\partial \eta_t}{\partial T_r} + \frac{4K_r(1-\eta_t)}{\sigma\epsilon T_r^5 \eta_t} = -\frac{\partial(W/P_s)}{\partial T_r}\bigg|_{P_s} = 0 \qquad [9]$$

Also remember that

$$\eta_t = \eta\left(1 - \frac{T_r}{T_m}\right) \qquad [10]$$

The conversion efficiency η is not likely to be a function of T_r so

$$\frac{\partial \eta_t}{\partial T_r} = \frac{-\eta}{T_m} \qquad [11]$$

Substitution of Equations [10 and 11] into Equation [9] and algebraic rearrangement yields an implicit expression for the radiator to maximum temperature ratio T_r/T_m which gives minimum system weight

$$\frac{W_{s1}}{P_{s1}}\frac{\sigma\epsilon T_m^4 N}{K_r} = \frac{(T_m/T_r)^4}{\eta^{1-N}}\left\{4\frac{T_m}{T_r}\left[\left(1-\frac{T_r}{T_m}\right)^N - \eta\left(1-\frac{T_r}{T_m}\right)^{N+1}\right] - \left(1-\frac{T_r}{T_m}\right)^{N-1}\right\} \qquad [12]$$

Equation [3] may now be used to show

$$\frac{W_{s1}}{P_{s1}} = \frac{W_s}{P_s}\left[\eta\left(1-\frac{T_r}{T_m}\right)\right]^{N-1} \qquad [13]$$

This is then substituted into Equation [12] to yield

$$\frac{W_s}{P_s}\frac{\sigma\epsilon T_m^4 N}{K_r} = \left(\frac{T_m}{T_r}\right)^4 \times \left\{4\frac{T_m}{T_r}\left[\left(1-\frac{T_r}{T_m}\right) - \eta\left(1-\frac{T_r}{T_m}\right)^2\right] - 1\right\} \qquad [14]$$

This equation is best solved for T_r/T_m by plotting the right-hand side for given values of T_r/T_m and η. Typical values of optimum temperature ratio are plotted in Fig. 1 vs. the parameter given in the left-hand side of Equation [14] for different values of efficiency factor η. The independent variable is composed of factors which can initially be estimated quite closely in a preliminary design study. As an example take $N = 0.2$, and assume the following values of the other parameters: $T_m = 2000$ R, $\epsilon = 1.0$, $K_r = 1$ lb/ft^2 and $W_s/P_s = 10^{-2}$ lb-hr/Btu. These values combine such that Fig. 1 is entered at an abscissa of 55. Then $0.40 < T_r/T_m < 0.48$, depending on the conversion efficiency. The Carnot efficiency can then easily be determined from Equation [2], and the power output is established by Equation [1].

It is interesting to look at the case where $N = 0$, i.e., power source weight is independent of output. In this case, minimum system weight corresponds to minimum radiator area, the case treated in (2 and 3). Letting N go to zero in Equation [14] gives

$$4\frac{T_m}{T_r}\left[\left(1-\frac{T_r}{T_m}\right) - \eta\left(1-\frac{T_r}{T_m}\right)^2\right] - 1 = 0 \qquad [15]$$

This can be rearranged as a quadratic in T_r/T_m

$$\frac{T_r^2}{T_m^2} - \frac{8\eta - 5}{4\eta}\frac{T_r}{T_m} - \frac{1-\eta}{\eta} = 0 \qquad [16]$$

The solution is

$$\frac{T_r}{T_m} = \frac{8\eta - 5 \pm \sqrt{25 - 16\eta}}{8\eta} \qquad [17]$$

where only the positive sign is retained, since negative values of temperature will otherwise occur. Substitution of efficiency values $0 \leq \eta \leq 1$ into Equation [17] will show that the radiator to maximum temperature ratio for minimum radiator surface area varies between the relatively narrow limits $0.80 \leq T_r/T_m \leq 0.75$. Note that Equation [17] becomes indeterminate for $\eta = 0$, requiring use of L'Hospital's rule to obtain the limit. This numerical result has been previously stated in (2) without a supporting derivation.

The value of N for a given design study must be determined from the power source weight characteristics. As an example, the thermal power to weight characteristics of some typical nuclear reactor designs taken from (4) are plotted in Fig. 2. The proper value of N for use in any particular design study may be obtained from the slope of the thermal power to weight characteristic of the power source in the power range of interest. Slopes for different values of N are shown on the figure. It may be expected that in the case of nuclear power sources, N will approach zero with low power reactors where criticality requirements govern size. In very large reactors, one may expect heat transfer surface area, which is proportional to thermal power output, to govern weight. In this case N could approach 1.

Nomenclature

A = area, ft²
K = weight constant, lb/ft² and lb/Btu/hr
P = power, Btu/hr
N = weight exponent
T = temperature, R
W = weight, lb
σ = Stefan-Boltzman constant, 0.173×10^{-8} Btu/hr-ft²-R⁴
ϵ = emissivity
η = efficiency

Subscripts

1 = reference condition of 100 per cent thermal efficiency
c = Carnot
g = generator + motor
m = maximum
o = output
r = radiator
s = source
t = thermal

References

1 Cross, C. A., "The Fundamental Basis of Power Generation in a Satellite Vehicle," *J. British Interplanet. Soc.*, vol. II, no. 3, May 1952, pp 117–125.

2 Buesard, R. W. and DeLauer, R. D., "Nuclear Rocket Propulsion," McGraw-Hill, New York, 1958, p. 336.

3 Fisher, J. H. and Menetry, W. R., "Problems Associated with Power Requirements for a Mars Mission," ASME Paper no. 59-AV-18, Jan. 26, 1959.

4 Kovacik, V. P. and Ross, D. P., "Performance of Nuclear Electric Propulsion Systems," IAS Rep. no. 59-25, Jan. 1959.

Optimum Proportioning of Two Propellants to Obtain Maximum Burnt Velocity

R. H. OLDS[1]

Lockheed Aircraft Corp., Palo Alto, Calif.

Theory indicates that certain combinations of two propellants have greater propulsive capability than either propellant alone. Optimum performance results from a suitably programmed variation of propellant proportions throughout burning. Results applicable to the first stage of a rocket are presented.

THE USE of variable propellant characteristics during burning has potentialities that have not yet been exploited to any great extent. Lorell and Hibbs (1)[2] by variational methods demonstrated benefits resulting from the use of varying proportions of two propellants during burning. The variational problem requires consideration of four cases. In (1), two of the cases were treated. This paper reports results from an extension of the analysis to include all four cases.

Continuous variation of the relative proportions of two propellants during burning is schematically represented by Fig. 1 in which x corresponds to the volume fraction of total propellant consumed, and y designates the volume fraction of the more dense propellant in the burning mixture. In actual practice a somewhat more sophisticated means of combining the two propellants would probably be required.

Received May 13, 1958.

[1] Staff Scientist, Missiles and Space Division. Member ARS.

[2] Numbers in parentheses indicate References at end of paper.

Basic Equations

The evaluation of performance is based upon the motion of a rocket in the absence of gravity and aerodynamic drag. The effective exhaust velocity varies during burning, so the familiar expression for the burnt velocity in terms of the logarithm of the mass ratio is not valid here. It is necessary to go back to first principles to express the burnt velocity

$$v_f = -\int_m^{m_f} u_E \frac{dm}{m} \qquad [1]$$

The mass of the rocket at any time during burning is expressed by

$$m = m_f + V\int_x^1 \rho dx \qquad [2]$$

Specific impulse is an experimentally measurable propellant characteristic which we choose to relate to the effective exhaust velocity and the effective specific enthalpy in the following way

$$u_E = \sqrt{2JH} = g_0 I_{sp} \qquad [3]$$

In dealing with mixtures of two propellants, let subscript A identify the more dense propellant while subscript B designates the less dense propellant. The density and effective specific enthalpy of a mixture are assumed to be volumetrically related to the densities and effective specific enthalpies of the separate propellants by

$$\rho = \rho_A y + \rho_B(1 - y) \qquad [4]$$

$$\rho H = \rho_A H_A y + \rho_B H_B(1 - y) \qquad [5]$$

in which y represents the volume fraction of propellant A.

It is convenient to employ the following dimensionless parameters

$$a = \frac{\rho_A}{\rho_B} - 1 \qquad [6]$$

$$b = \frac{\rho_A H_A}{\rho_B H_B} - 1 \qquad [7]$$

$$c = \frac{m_f}{\rho_B V} \qquad [8]$$

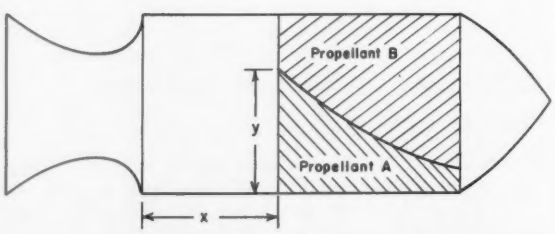

Fig. 1 Schematic representation of a rocket with a variable mixture of two propellants burning simultaneously in the same chamber

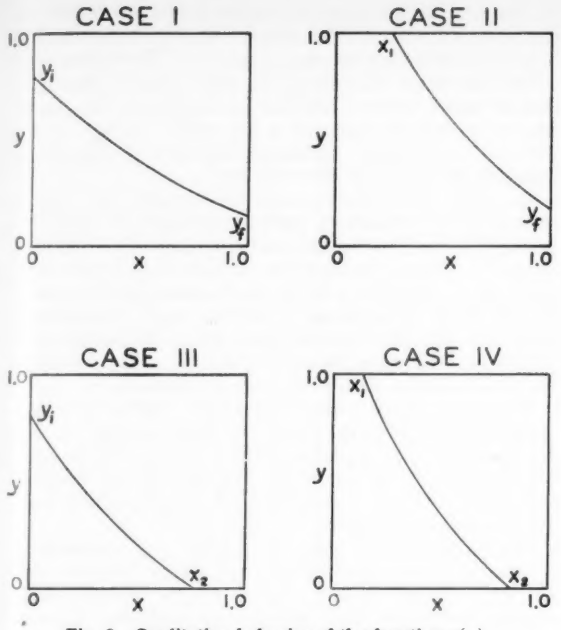

Fig. 2 Qualitative behavior of the function $y(x)$

By means of a combination of the foregoing relationships, Equation [1] can be expressed in the form

$$v_f = \sqrt{2JH_B}\int_0^1 \frac{\sqrt{(1+ay)(1+by)}}{c+\int_x^1 (1+ay)dx}\,dx \qquad [9]$$

The problem is to find the function $y(x)$ that maximizes the integral in Equation [9] and to find the maximum value of v_f.

The four cases to be considered are represented in Fig. 2. They are distinguished by various combinations of boundary conditions involving one or both of the propellants at the beginning and the end of burning. Cases I and III were treated in (1).

Results

Case I

$$y_i = -\frac{a+b}{2ab} \qquad [10]$$

$$y_f = \frac{(a+b)c - a + b}{a(a-b-2bc)} \qquad [11]$$

$$y(x) = -\frac{a+b}{2ab} + \frac{(a-b)^2 x}{2ab\sqrt{(a-b)^2x^2 - 4bc(a-b-bc)}} \qquad [12]$$

$$v_f = \sqrt{2JH_B}\left(\sqrt{\frac{a-b-bc}{ac}} - \sqrt{\frac{-b}{a}}\right) \qquad [13]$$

Case II

$$x_1 = \frac{a+b+2ab}{a-b}\sqrt{\frac{(a-b-bc)c}{a(1+a)(1+b)}} \qquad [14]$$

$$y_f = \frac{(a+b)c - a + b}{a(a-b-2bc)} \qquad [15]$$

When $x_1 \le x \le 1$

$$y(x) = -\frac{a+b}{2ab} + \frac{(a-b)^2 x}{2ab\sqrt{(a-b)^2x^2 - 4bc(a-b-bc)}} \qquad [16]$$

$$v_f = \sqrt{2JH_B}\times \left[\sqrt{\frac{a-b-bc}{ac}} - \sqrt{\frac{1+b}{1+a}}\left(1+\ln\frac{a-b}{2a(1+b)}\right)\right] \qquad [17]$$

Case III

$$y_i = -\frac{a+b}{2ab} \qquad [18]$$

$$x_2 = \frac{(a+b)(1+c)}{2a} \qquad [19]$$

When $0 \le x \le x_2$

$$y(x) = -\frac{a+b}{2ab} + \frac{(a-b)x}{2b\sqrt{a^2x^2 - ab(1+c)^2}} \qquad [20]$$

$$v_f = \sqrt{2JH_B}\left[1 - \sqrt{\frac{-b}{a}} + \ln\frac{(a-b)(1+c)}{2ac}\right] \qquad [21]$$

Case IV

$$x_1 = \frac{(a+b+2ab)(1+c)}{2a\sqrt{(1+a)(1+b)}} \qquad [22]$$

$$x_2 = \frac{(a+b)(1+c)}{2a} \qquad [23]$$

When $x_1 \le x \le x_2$

$$y(x) = -\frac{a+b}{2ab} + \frac{(a-b)x}{2b\sqrt{a^2x^2 - ab(1+c)^2}} \qquad [24]$$

$$v_f = \sqrt{2JH_B}\left[1 + \ln\frac{(a-b)(1+c)}{2ac} - \sqrt{\frac{1+b}{1+a}}\left(1+\ln\frac{a-b}{2a(1+b)}\right)\right] \qquad [25]$$

Discussion

Which of the four cases one has to deal with in any particular situation is most easily determined by evaluating the quantities y_i, y_f, x_1 and x_2. Only those with values between zero and unity have physical significance. This requirement generally eliminates all but one case. There are extreme situations in which none of the y's or x's have physically permissible values. In these situations, only the propellant with the greater impulse per unit volume should be used.

It is of interest to note that the expression for y_i represents the mixture of two propellants with the greatest impulse per unit volume. In all cases, the propellant or mixture of propellants with maximum impulse per unit volume is used at the start of burning.

It can be shown that the effective exhaust velocity increases at exactly the same rate as the velocity of the rocket during those intervals when both propellants are being burned. This is a curious result that is no doubt closely related to a similar result obtained by an energy optimization process treated in an earlier paper (2).

The possible benefits from practical applications of results reported here become significant when one admits the use of propellants with greatly different densities. The feasibility of doubling the density of a solid propellant by addition of large amounts of heavy material, e.g., lead oxide, while retaining good physical properties and combustibility has been demonstrated (3). Even though the resulting propellant has a rather poor specific impulse, it can be shown that combinations of the dense propellant with the initial undoctored propellant have propulsive capabilities greater than either propellant alone.

The analysis that yielded the results reported here has been extended to include the second stage of a multistage rocket

(4). It appears that the range of useful applicability of variable propellant properties is much more restricted in the second stage than it is in the first stage.

Nomenclature

a, b, c = dimensionless parameters defined by Equations [6, 7 and 8], respectively
g_0 = factor for converting specific impulse to velocity, 32.174 (fps)²
H = effective specific enthalpy, Btu/lb
I_{sp} = specific impulse, sec
J = factor for converting specific enthalpy to velocity, 2.503×10^4 (fps)² lb/Btu
m = rocket mass
u = exhaust velocity, fps
v = rocket velocity, fps
V = initial propellant volume, ft³
x = volume fraction of propellant consumed
y = volume fraction of propellant A in burning mixture
ρ = propellant density, lb/ft³

Subscripts

A = the more dense propellant
B = the less dense propellant
f = final value
i = initial value
1 = beginning of variable propellant mixture for cases II and IV
2 = end of variable propellant mixture for cases III and IV

References

1 Lorell, J. and Hibbs, A., "The Effect of Variation of Propellant Density on Rocket Performance," Jet Propulsion Lab Rep. 20-66, July 15, 1952.
2 Olds, R. H., "Optimum Variation of Exhaust Velocity During Burning," Jet Propulsion, vol. 28, 1958, pp. 405–406.
3 Lee, R. J. and Warren, F. A., "Impulse Measurements for a High-Density Double-Base Solid Propellant," NOTS Tech Memo 1525, Nov. 1954, Naval Ordnance Test Station, China Lake, Calif.
4 Parks, J. and Olds, R. H., "Optimum Programming of Propellants to Obtain Maximum Velocity from a Two-Stage Rocket," to be published.

Augmentation of Nuclear Rocket Specific Impulse Through Mechanical-Electrical Means

MARTIN GOLDSMITH[1]

Rand Corp., Santa Monica, Calif.

IN A RECENT paper by Ackeret (1)[2] it is pointed out that a conventional chemical or nuclear rocket operating in space has available to it an essentially infinite expansion ratio. Theoretically, therefore, one could obtain complete conversion of the thermal energy of the hot propellent gas into directed kinetic energy. This would, of course, require a nozzle of infinite area ratio, hence this ideal situation is precluded by practical considerations.

Ackeret further points out that isothermal expansion of the rocket exhaust leads to improved performance as compared to adiabatic expansion for a given expansion ratio. This, of course, requires the addition of heat to the gas during the expansion. This result is difficult to achieve in a practical system, especially if one is limited by permissible material temperatures.

However, Ackeret suggests a stratagem by which the availability of the large permissible expansion ratio is exploited to obtain a quasi-isothermal expansion of the exhaust gas in a series of turbines. The gases are assumed to be reheated by a temperature-limited nuclear reactor. The turbine work is then converted into electricity, which is used directly to heat the gases further after their last heating in the reactor and before they are expanded in the exhaust nozzle. In this way, the temperature limitations imposed by the reactor materials are partially circumvented.

To clarify this proposed cycle, the sequence of events is restated. The propellant, perhaps hydrogen or helium, is passed through a reactor or a part of a reactor at some initial pressure. The heated gas is then expanded through a turbine, and is then returned to a reactor at the lower exhaust pressure for reheating to the original limiting reactor temperature. This cycle may be repeated many times, mechanical complexity and size being the limiting criteria as the pressure of the gas is reduced through continued expansion.

The turbine work is converted into electricity by conventional means. After the gas has made its last pass through the reactor, it may then be heated to a temperature above that possible in the reactor by discharge of the electricity through it. The gas is then expanded through a thrust nozzle in the conventional fashion.

The purpose of this note is to calculate the augmentation of specific impulse possible through use of Ackeret's cycle for some realistic designs. Values will be assumed for the various parameters that enter into the problem. These include: Number of reheat cycles, turbine inlet temperature, initial pressure, turbine pressure ratio, turbine adiabatic efficiency, maximum reactor gas temperature, nozzle pressure ratio. Obviously, covering a wide range for each variable in the calculations would lead to a prohibitive number of cases; hence typical single values will be chosen for most of them. The use of hydrogen as a working fluid will be assumed. The appropriate equilibrium value of dissociation is assumed to occur through the cycle.

For example, the thrust nozzle expansion ratio is assumed to be 1000:1 in all cases. This corresponds to a nozzle area ratio of roughly 40:1. Each turbine is taken to operate at 70 per cent of isentropic efficiency with a pressure ratio of 10:1. Maximum permissible turbine inlet temperature is taken to be 1500 K. The turbine output is considered to be entirely converted into electricity. Pumping and flow losses are neglected.

Specific impulse is calculated for a range of reactor exit temperatures from 2500 to 3500 K. Two initial pressures to the nozzle are considered, 1 atm and $\frac{1}{10}$ atm. The performance for one and two reheat cycles, as well as the conventional case of no reheat cycling is shown in Fig. 1 for the listed conditions. Sample calculations are shown below for two typical cases, using the thermodynamic properties of hydrogen given in (2).

Case 1

Initial nozzle pressure = 1 atm
Reactor exit temperature = 3500 K
No reheat cycle:
h (enthalpy) at 1 atm and 3500 K = 29.4 kcal/gm
h after adiabatic expansion to 10^{-3} atm = 8.6
enthalpy difference (Δh) = 20.8
$I_{sp} = (1/g)\sqrt{2} \times 4.186 \times \Delta h = 1350$ sec

Case 2

Initial nozzle pressure = 0.1 atm
Reactor exit temperature = 3000 K
Two reheat cycles:
h at 10 atm, 1500 K = 5.2 kcal/gm
h after isentropic turbine expansion to 1 atm = 2.6
isentropic turbine work = 2.6
heating energy available = 0.70 × isentropic turbine work = 1.8

Received April 30, 1959.

[1] Engineer, Aero-Astronautics Department. Member ARS.
[2] Numbers in parentheses indicate References at end of paper.

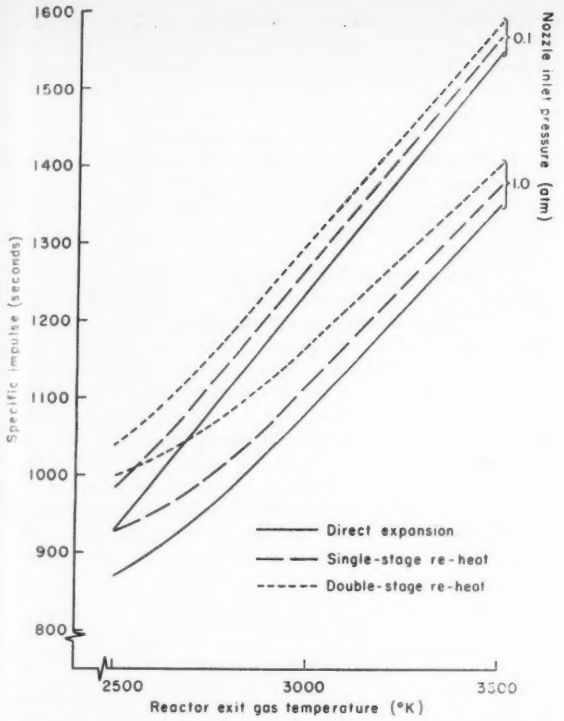

Fig. 1 Specific impulse performance of the Ackeret cycle

h at 1 atm, 1500 K, after reheat = 5.2
h after isentropic turbine expansion to 0.1 atm = 2.8
isentropic turbine work = 2.4
heating energy available = 0.70 × isentropic turbine work = 1.7
h at 0.1 atm, 3000 K = 24.9
total electrical heating energy = 3.5
total h at 0.1 atm before nozzle = 28.4
h after nozzle expansion to 10^{-4} atm = 9.0
enthalpy difference (Δh) = 19.4
$I_{sp} = (1/g)\sqrt{2} \times 4.186 \times \Delta h = 1300$ sec

Certain trends may be observed in the data shown in Fig. 1. The reheat cycle is of most benefit at lower reactor temperatures. The large energies absorbed by dissociation at higher temperatures reduce the effect of the electric afterheating. Likewise, at the lower nozzle inlet pressure, the consequent increased level of dissociation further accentuates this trend.

Therefore, tentative conclusions may be drawn as to the value of the reheat cycle in increasing engine performance. If the permissible reactor temperature is quite high, only a marginal increase in performance is available, unless many reheat stages are used. Mechanically this is probably not feasible.

At the lower end of the temperature spectrum, it is seen that even two stages of reheat offer a worthwhile increase in specific impulse. Only a complete analysis of the performance of the engine and vehicle will indicate whether overall performance is increased and, if so, whether to a degree commensurate with the necessary increase in engine complexity.

It is interesting to compare these results to the performance obtained through isothermal expansion of hydrogen gas in a nozzle, where heat is continually added to the flowing gas. For an infinite pressure ratio in isothermal expansion, the specific impulse, according to simplified analysis, becomes infinite. However, in Table 1, the realistic case of a 1000:1 pressure ratio, starting at a nozzle inlet pressure of 1 atm, is shown for several temperature levels.

Table 1 Specific impulse for isothermal expansion of hydrogen

Temp, K	I_{sp}, sec
2500	1270
3000	1610
3500	1910

A substantial amount of the heat added during isothermal expansion is consumed in the dissociation energy of the gas. Unlike the case of adiabatic expansion, this energy is not useful in the expansion process and represents dead loss.

References

1 Ackeret, J., "A System of Rocket Propulsion Using Reactors and Gas Turbines," unpublished manuscript, Swiss Federal Institute of Technology, Zurich.

2 Krieger, F. J., "Parametric Investigation of Nuclear Rocket Propellants," The Rand Corp., Santa Monica, Calif., to be published.

Beamed Electromagnetic Power as a Propulsion Energy Source

MARTIN I. WILLINSKI[1]

Hughes Aircraft Co., Culver City, Calif.

A novel rocket propulsion system, utilizing an external energy source in the form of beamed electromagnetic power, is proposed. A comparison is made with solar energy. Its application to propulsion fluid heating and electric rockets, as well as to the conversion of a portion of the beamed energy into propellant mass, is discussed. The problems of electromagnetic power beaming are reviewed, and some potential solutions discussed. The possibility of utilizing iconospheres as a means of beaming power over astronomical distances is suggested.

THE PURPOSE of this paper is to suggest and discuss a novel rocket propulsion system which might permit the achievement of currently difficult objectives of space travel. Although this discussion is speculative in nature, it is believed appropriate in view of anticipated technological progress and the long lead time required between the conception and realization of advanced systems.

Two basic limitations to the achievement of many of the future objectives of space travel are:

1 The limit of the total quantity of energy which can be stored in a space vehicle, whether it be nuclear or chemical, for eventual conversion into power in the vehicle's reaction jet.

2 The limit of the vehicle specific power which may be expressed as power in reaction jet divided by vehicle weight (1,2).[2]

For example, the magnitude of both of these propulsion system characteristics must be extremely high for vehicles capable of short duration interplanetary (3) and interstellar flights. Even the most energetic power sources, such as the fission and fusion fuels, have been shown to be limited in these respects (4).

A method for circumventing these limitations is the utilization of a rocket propulsion energy source *external* to the vehicle. This has been suggested previously only in the form of

Received May 25, 1959.

[1] Advanced Planning Staff, Systems Development Laboratories. Member ARS.

[2] Numbers in parentheses indicate References at end of paper.

natural energy sources, such as solar energy (5, 6). Although this utilization of solar energy would overcome the limitation of total required energy, it does not appear capable of overcoming the specific power limitation. This is a result of the constant value of intercepted power per unit solar energy collector area at any given distance from the sun.

A different type of external propulsion energy source is proposed here to overcome the specific power as well as total energy limitations previously discussed. This is an *artificial* energy source in the form of beamed electromagnetic power. For a beamed power energy source, the intercepted power may be increased as long as the transmitted power is increased. A comparison of beamed and solar energy on an intercepted power basis is shown in Fig. 1. It should be noted that the solar energy regime would vary in area with variations of distance from the sun.

Potential Utility

Beamed power is seen as being utilized as a rocket propulsion energy source in two ways:

1 The beamed power would be utilized to heat a propulsion fluid, such as hydrogen, ammonia, gasoline or even water, which would then be expanded through a nozzle to produce thrust.

2 The beamed energy would be converted into electrical power suitable for powering an ion or plasma rocket. It is noteworthy that the use of beamed electromagnetic power as a propulsion energy source for an airborne vehicle powered by an aeropulse-type engine has been proposed (7).

The first method appears to offer the performance advantages of a nuclear propulsion fluid heating type rocket with a considerable reduction in onboard shielding problems. In addition, any method of utilizing a beamed power propulsion energy source has the advantages of a fixed primary power installation.

The receiving antenna could take the form of a large inflated balloon, in which case drag considerations would limit such a system to essentially vacuum conditions and hence vehicle upper-stage operation. Also, the skin of the vehicle itself could possibly be utilized as a surface antenna, thereby allowing operation in the atmosphere. Beam transmission ranges up to several hundred miles, and 500 to 1000 megawatts of power received and utilized for propulsion would be suitable for an upper stage of a satellite booster using such a system.

The application of beamed power to ion rocket propelled vehicles may offer a means of attaining vehicle accelerations orders of magnitude greater than those which have been proposed in past design studies of such vehicles (2, 8, 9). One such vehicle might be a high velocity "artificial comet" for reconnaissance in the vicinity of the outer planets of the solar system. For this application, beam transmission ranges of up to 100,000 miles with approximately 10 megawatts of power received and utilized for propulsion would be required. In this case, the power would be beamed from multiple stations during the vehicle's single powered maneuver in the vicinity of the Earth.

The beam ranges and power levels required for minimum duration interplanetary trajectories and interstellar flight trajectories could possibly be orders of magnitude greater than that required for an "artificial comet." A use of beamed power for the more distant future might involve the conversion of some fraction of the intercepted beamed energy into propellant mass which would be accelerated from ion motors powered by the remaining energy intercepted from the beam.

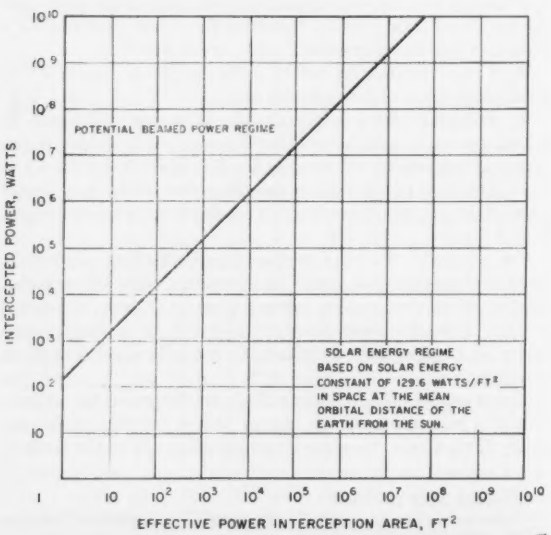

Fig. 1 Solar and beamed power regimes

Problem Areas

The current engineering limitations on the problem of beaming large amounts of electromagnetic energy appear most formidable. This becomes apparent from the basic beamed power equation[3]

$$\frac{P_R}{P_T} = \frac{GA_R}{4\pi d^2} \qquad [1]$$

Ideal far-zone antenna gain, as used in Equation [1], is given by

$$G = 4\pi A_T/\lambda^2 \qquad [2]$$

It has been shown that far-zone gain may be retained under certain circumstances in near-zone operation of antennas by application of a focusing principle (10). It has also been shown that there is an optimum size for an antenna operated under otherwise fixed conditions (11).

As can be seen from Equations [1 and 2], the quantity of power received varies inversely as the square of the antenna separation distance. Some quantitative indication of possible resulting power efficiencies is shown in Fig. 2 where the ratio KP_R/P_T is plotted as a function of the antenna separation distance for a range of values of transmitter antenna gain and receiving antenna diameter.

Although the antenna gains shown in Fig. 2 are not representative of what has been achieved, they do represent values which are theoretically attainable under certain conditions. There are many problems which will be encountered in the development of antennas having such high gain. For example, the actual gain of an antenna is dependent on the antenna fabrication tolerances. For maximum gain, a paraboloid dish antenna reflector should be constructed with a tolerance of approximately $\frac{1}{10}$ of the operating wave length. This tolerance might be difficult to achieve for very large size antennas. The maximum gain is also affected by the environment in which the antenna is operating; higher gains should be attainable in space than within the Earth's atmosphere.

The desirability of lower wave length is apparent from Equation [2]. However, there are factors which tend to limit the maximum usable transmitting frequency. For example, the maximum power obtainable from any particular type of known power transmitting tube decreases with increasing frequency (12). Also, power attenuation by the water vapor and oxygen in the atmosphere generally increases with decreasing wave length starting at a wave length of approximately 10 cm.

[3] This equation is derived from geometrical optics, and therefore the ratio P_R/P_T will, in practice, be reduced by the antenna aperture efficiency factor K which depends upon several of the design parameters of the antenna system.

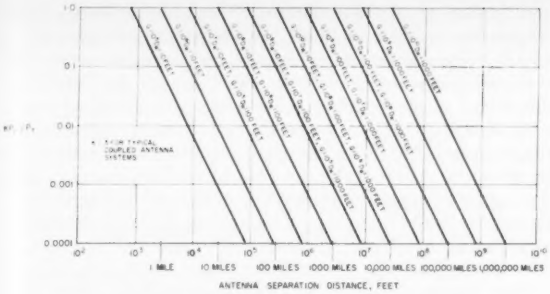

Fig. 2 Beamed power reduction with distance

An additional problem area is the voltage breakdown of the atmospheric constituents. This phenomenon would limit the maximum power density of the beam. Completely new approaches may be required for the solution to some of these and other problems associated with beaming electromagnetic power.

Outlook

There are several prospects for obtaining solutions to these difficult problems. Current and suggested future studies concerning space communications may result in techniques for constructing larger high gain antennas in space than may be possible on Earth. This, in turn, suggests the possibility of "frequency switching," in which one frequency, selected with consideration of atmospheric attenuation, would be used for a "shorter" surface-to-space antenna link and another higher frequency for the "longer" space antenna-to-space vehicle power transmission link.

If enormous quantities of cheap electrical power become available for propulsion purposes, extremely low beam power efficiencies would become usable. Thus the ratio of received-to-transmitted power may be reduced to an extremely small quantity, thereby permitting operation at extreme ranges. The eventual harnessing of fusion energy provides a hopeful solution to the problem of providing enormous quantities of electrical power for propulsion purposes. It is believed that when controlled fusion power becomes a reality, fusion powerplants will produce considerably more electrical power than is produced by conventional or nuclear fission-type powerplants (13).

One approach to the problem of antennas for beaming power over astronomical distances might be the utilization of a natural electromagnetic radiation focusing device as suggested by Berger (14). This natural focusing device is termed an iconosphere by Dr. Berger and may be defined as a series of spherical, optically-real focal surfaces concentrically surrounding a spherical body. Thus, the spherical body acts as a positive lens on incident electromagnetic radiation by refraction, diffraction and/or gravitation. He suggests the use of the iconosphere of the Earth, or even the sun, as a means for communicating over interstellar distances. The prospect of applying iconospherics to the problem of beaming power for propulsive energy purposes appears intriguing; indeed, iconospheric lenses, combined with beamed power, might prove to be the key to the accomplishment of interstellar travel.

Conclusion

The realization of propulsion systems utilizing beamed power energy sources would represent a significant advance in the areas of propulsion and space travel. It is hoped that the concepts discussed here will stimulate research toward the solution of the many problems associated with the successful development of beamed electromagnetic power as a propulsion energy source.

Nomenclature

A_R = effective area of receiving antenna
A_T = effective area of transmitting antenna
d = distance between the transmitting and receiving antennas
D_R = physical diameter of receiving antenna
G = transmitting antenna gain
K = antenna aperture efficiency factor
P_R = power received
P_T = power transmitted
λ = wave length of transmitted power

References

1 Shepherd, L. R. and Cleaver, A. V., "The Atomic Rocket, Further Possibilities: The Ion Rocket," *J. British Interplanet. Soc.*, vol. 8, 1949, p. 59.
2 Spitzer, L., Jr., "Interplanetary Travel between Satellite Orbits," *J. British Interplanet. Soc.*, vol. 10, 1951, pp. 249–257.
3 Cole, D. M., "Minimum Time Interplanetary Orbits," Proc. Amer. Astronautical Soc., 1958, paper no. 39.
4 Foelsche, T., "Relativistic Treatment of Rocket Propulsion with Fast Particles and Photons Taking in Consideration Nuclear Data," presented at the American Association for the Advancement of Science, New Mexico Highlands University, Las Vegas, New Mexico, April 28 to May 1, 1958.
5 Ehricke, K. A., "The Solar-Powered Space Ship," ARS perprint 310-56.
6 Garwin, R. L., "Solar Sailing—A Practical Method of Propulsion Within the Solar System," JET PROPULSION, vol. 28, March 1958 pp. 188–190.
7 Early, H. C., "Ionic Wind Tunnel," University of Michigan, Aeronautical Research Center Rep. EMD-4. Jan. 14, 1949.
8 Stuhlinger, E., "Electrical Propulsion System for Space Ships with Nuclear Power Source" *J. of Astronautics*, Winter 1955, Spring 1956, Summer 1956.
9 Willinski, M. I. and Orr, E. C., "Project Snooper, A Program for Unmanned Interplanetary Reconnaissance," JET PROPULSION, vol. 28, Nov. 1958, pp. 723–729.
10 Bickmore, R. W., "On Focusing Electromagnetic Radiators," *Canadian J. Phys.*, vol. 35, 1957, pp. 1292–1298.
11 Bickmore, R. W., "A Focusing Criterion for Rectangular Apertures", Hughes Aircraft Co., Systems Development Laboratories, Technical Memorandum no. 376, Oct. 31, 1954.
12 Staff, Radio Research Laboratory, Harvard University, "Very High Frequency Techniques," McGraw-Hill Book Co., New York, 1947, p. 473.
13 Herold, E. W., "Controlled Thermonuclear Fusion—Its Meaning to the Radio and Electronic Engineer," *RCA Review*, vol. 19, June 1958, pp. 162–186.
14 Berger, W. J., "Celestial Iconospherics, the Ultimate Astronomy," JET PROPULSION, vol. 28, May 1958, pp. 337–338.

Utilization of Stored Energy in Solid Material as an Added Energy Source

JOHN J. NEWGARD[1]

Thiokol Chemical Corp., Reaction Motors Division, Denville, N. J.

AN ATTEMPT has been made to survey two types of solid-state phenomena in order to determine the capacity inherent in these phenomena for energy storage (1).[2] The first process to be discussed is analogous to energy storage via an order-disorder transformation known to exist in some metallic alloys: Disordered material is ordered; energy is added and stored in the ordered structure; upon combustion the ordering energy as well as the combustion energy is released. The second mechanism is that of interstitial-vacancy formation. Interstitials and vacancies are created by heat and irradiation. Somehow these are retained until combustion. Upon combustion, the energy associated with the interstitials' recombination with vacancies is released along with the normal combustion energy.

Specific examples and orders of magnitude associated with both phenomena are given. The conclusions of this study can be given now. Even if an order-disorder or interstitial-

Received May 25, 1959.
[1] Supervisor, Atomic Technology.
[2] Numbers in parentheses indicate References at end of paper.

vacancy phenomenon existed in readily combustible materials, the energy added to combustion is small (approximately 30 per cent) under the most reasonable conditions assumed in the addition of stored energy to these materials.

If one assumes the existence of a perfectly ordered compound AB, it can be shown that the ratio under ideal circumstances (that the interaction energies of any postulated lattice configuration for nearest neighbor atoms in ordered alloy V_{AB} is much greater than the interaction energy between nearest neighbor atoms V_{AA} and V_{BB} in the disordered alloy), the ratio of ordering energy to internal energy before ordering is equal to unity. Internal energy before ordering may be expressed as

$$(AB)_{\text{disordered solid}} \xrightarrow{E_{MP}} (AB)_{\text{melting point}} \xrightarrow{E_F} (AB)_{\text{melt}}$$

where

E_{MP} = energy required to reach melting point of AB
E_F = energy required to melt AB (fusion energy)
$U_0 = E_{MP} + E_F$

where now U_0 is the internal energy of the solid in question. It can also be shown that the ordering energy of AB is greater than ordering energies associated with AB_n where n is an integer.

If one assumes some order of magnitude parameters, such as average melting points of 100 to 800 C, heat capacities of solid material from 0.1 to 1 cal/gm, heats of fusion of 10 to 100 cal/gm and average molecular weights of substances from 10 to 400, ordering energies can vary from 2×10^2 to 1.2×10^5 cal/mole.

Combustion phenomena give heats of combustion which vary from 2×10^4 to 2×10^7 cal/mole with most substances giving energies upon combustion in excess of 10^5 cal/mole. Hence, the upper order of magnitude of ordering energy and the lower value for heat of combustion of chemical substances have the same magnitude.

Because of the assumption of ideal circumstances in the order-disorder phenomenon, it has been stated that ordering energy is of the same magnitude as internal energy. Based upon more realistic assumptions that $V_{AA} = V_{BB} = \frac{1}{2} V_{AB}$, ordering energy now becomes one third of the internal energy, and hence, if an order-disorder phenomenon can exist, at most a 30 per cent increase over the ordinary combustion energy can be expected in those cases where the combustion energy is as low as 10^5 cal/mole.

Order-disorder phenomena have appeared only in metallic alloys. If a useful propellant alloy, such as MgAl (magnalium) would exhibit order-disorder (to the author's knowledge this alloy hasn't shown the order-disorder phenomenon), the additional energy added to the combustion energy would only be about 15 per cent, since the heat released on "burning" MgAl is greater than 2×10^5 cal/mole. In conclusion then, order-disorder energy addition to combustion energy makes only a small addition to the useful energy attainable from a combustion phenomenon.

Two other stored energy phenomena are those which store energy by Schottky and Frenkel defects. Both these mechanisms store energy by movements of lattice atoms. If the lattice atoms move to the surface, creating a surface atom and a vacancy, a so-called Schottky defect is created. Movement of lattice atoms into interstitial positions in the lattice, creating interstitial atoms and vacancies, is called a Frenkel defect. In both cases this stored energy is assumed released upon combustion.

It has been shown (1) that for the creation of a Schottky defect approximately 1 ev is required (or stored), and approximately 2 ev are required to create a Frenkel defect. However, the number of defects created in either case is proportional to $e^{-E/kT}$, where E is the energy required to create the defect, and T is the temperature. It can be shown for both Schottky and Frenkel defects that, in order to increase the energy upon combustion by 8000 cal/mole, approximately one third of all lattice atoms must appear on the surface or in interstitial positions (assuming no recombination, i.e., surface atoms or interstitial atoms returning to their lattice positions), and the temperature at which this occurs is 11,600 K. At ordinary temperatures (300 K), only one atom in 10^5 is either a Schottky or a Frenkel defect. Hence, these phenomena, even if they did exist in useful combustible material at reasonable temperatures, would represent a minute fraction of the energy available from ordinary combustion.

A special case may be made for neutron radiation-induced energy storage in graphite (2). High energy neutrons in passing through a graphite lattice elastically transfer approximately 1/1000 of their initial energy to carbon atoms. These subsequently move to higher energy interstitial positions (creating vacancies) not unlike Frenkel defects. By this means energy storage as high as 540 cal/gm at 30 C has been obtained experimentally, using reactor neutrons at integrated fluxes of 2×10^{21} nvt (reactor flux times time in units of $1/cm^2$).

Graphite is the only substance showing such a large energy storage effect at ordinary temperatures without the effects annealing out. A semi-empirical model (2) predicts saturation in energy storage between 600 and 700 cal/gm. For normal graphite oxidizing in air at 25 C, the reaction is

$$C + O_2 \rightarrow CO_2$$

and the heat of reaction is 2140 cal/gm. Hence, the maximum increase to be expected in "combustion" energy at 25 C if graphite is to store energy due to neutron irradiation is about 30 per cent.

References

1 Kittel, C., "Introduction to Solid State Physics," John Wiley and Sons, Inc., New York, 1956.

2 Newgard, J. J., "Simple Semi-Empirical Model for Neutron Induced Stored Energy in Graphite," *J. Appl. Phys.*, in publication.

Optimum Magnetic Field for Stagnation Heat Transfer Reduction at Hypersonic Velocities

ROBERT GOULARD[1]

Bendix Products Division, South Bend, Ind.

The application of a magnetic field to the stagnation area of a blunt body has two contrary effects: It reduces convective energy transfer, but increases radiation energy transfer. Consequently, for very high speeds, when this latter effect is existent but not dominant ($q_R^{(o)} < 0.4 q_c^{(o)}$), an optimum magnetic field exists which insures minimum energy transfer. At still higher speeds, radiation is dominant, and the application of a magnetic field always increases the energy transfer to the stagnation area or the nose. This argument closely parallels the well-known argument on the existence of an optimum radius. The existence of an optimum magnetic field is shown, in fact, to depend on the choice of a nose radius below its optimum value.

AS SHOWN in recent papers, the application of a magnetic field at the blunt nose of a hypersonic vehicle reduces the convective heat transfer to the surface of the nose.

Received April 21, 1959.

[1] Consultant, Applied Sciences Laboratory; also Assistant Professor, School of Aeronautical Engineering, Purdue University. Member ARS.

This is due essentially to the retarding effect imposed on the particles streaming past the wall behind the detached shock, resulting also in an increased shock layer thickness.

At high temperature, however, radiative flux becomes an appreciable part of the total energy flux, and its value increases proportionately to the shock layer thickness (3).[2] The presence of a magnetic field will therefore have two opposite effects on the two components of the total energy flux. As a result, a minimum energy flux will usually be achieved for a certain optimum value of the magnetic field. Higher values will, in fact, cause an increase of the energy flux at the wall.

These two opposite effects have been analyzed in (1), where they are illustrated in two cases of hypervelocity flight (u_∞ = 8 and 10 km/sec). An order of magnitude discussion, suggested by Miele, will be used here to present in simple form the main conclusions of (1).

Optimum Magnetic Field

It has been shown in (2) that the application of a magnetic field at the stagnation point of a blunt body reduces the convective heat transfer q_c according to the expression

$$q_c = q_c^{(o)}\, Z^{0.4} \qquad [1]$$

where Z is a magnetic parameter. We note that Z, and therefore q_c, decreases when the applied magnetic field B increases. Similarly, it is shown that the velocity gradient varies in proportion to Z. Hence, by continuity, the shock layer thickness is roughly inversely proportional to Z, and so is the energy radiated by the shock layer

$$q_R \simeq q_R^{(o)}\, Z^{-1} \qquad [2]$$

One recognizes the opposite effects of the magnetic parameter Z on the two components of the total heat transfer q. A minimum value of q is obtained by the condition $dq/dZ = 0$, which is satisfied by the optimum value of Z

$$Z_{opt} \simeq \left(\frac{1}{0.4}\,\frac{q_R^{(o)}}{q_c^{(o)}}\right)^{1/1.4} \qquad [3]$$

with $0<Z<1$.

Hence, whenever radiation heat transfer is present, we conclude to the *existence of an optimum value of the applied magnetic field* corresponding to a minimum total heat transfer. For instance, it is shown in (1) that for u_∞ = 26,200 fps, altitude = 120,000 ft, R = 1 ft, the optimum value of B will be of the order of 3×10^4 gauss ($\zeta \simeq 4$), corresponding to a 20 per cent reduction of the total energy transfer to the hemisphere nose.

We also note that, by definition, $Z < 1$. It follows from Equation [3] that for flight configurations such that

$$q_R^{(o)}/q_c^{(o)} > 0.4 \qquad [4]$$

there will be no such optimum; in this case, the application of a magnetic field will actually increase the total heat transfer to the nose.

Optimum Nose Radius

The values of $q_c^{(o)}$ and $q_R^{(o)}$, on the other hand, are known (3) to be of the form

$$q_c^{(o)} \simeq a_c \left(\frac{\rho_\infty}{R}\right)^{1/2} u_\infty^{\,3} \qquad [5]$$

$$q_R^{(o)} \simeq a_r \alpha_w \rho_\infty^{\,3/2}\, R\, u_\infty^{\,10} \qquad [6]$$

By inspection, it can be concluded that condition $q_R^{(o)}/q_c^{(o)} < 0.4$ will not be maintained for "black" surfaces at very high velocities, large radii or low altitudes. A magnetic field, in this case, would not reduce the total heat transfer. This situation is shown in (1 and 3) to be typical of the direct reentry of circumlunar vehicles ($\sim$10 km/sec, $q_R^{(o)} \simeq q_c^{(o)}$).

It is interesting to note, in Equations [5 and 6], that for a given aerodynamic situation, the nose radius R has also an opposite effect on the two terms of the total heat transfer $q^{(o)}$. This leads to the well-known argument on the possible existence of an optimum radius, which exists for $\partial q^{(o)}/\partial R = 0$, corresponding to

$$q_R^{(o)}/q_c^{(o)} = 0.5 \qquad [7]$$

Conclusion

Comparison of Equations [4 and 7] shows that the application of a magnetic field at the nose will be conducive of energy transfer reduction *only* if the nose radius is less than a value inferior to its optimum value. In other words, if a decrease of q is to correspond to an increased magnetic field B, *the radius of the nose must be such that further thickening of the shock layer will bring a decrease of the energy flux.*

This conclusion illustrates, in particular, the common effect of radius increase and magnetic field application, which is the thickening of the shock layer. In terms of energy transfer, the presence of a magnetic field can be considered as equivalent to the fictitious substitution of a larger nose radius. This magnetic field can be adjusted to the various optimum requirements of a given flight. The overall effect on the drag and the trajectory is briefly discussed in (1).

Nomenclature

a_c, a_r	=	constants
B	=	magnetic field
q_c, $q_c^{(0)}$	=	convective heat flux, with and without magnetic field
q_R, $q_R^{(0)}$	=	net radiation heat flux, with and without magnetic field
q	=	total energy flux, $q_c + q_R$
R	=	nose radius
u	=	velocity
x	=	distance from the stagnation point along the nose
Z	=	$-\zeta/2 + (1 + \zeta^2/4)^{1/2}$
α_w	=	wall absorptivity coefficient
ζ	=	$\dfrac{\sigma B^2}{\rho_{es}} \left(\dfrac{\partial u_{es}}{\partial x}\right)^{-1}_{B=0}$
ρ	=	density
σ	=	electrical conductivity

Subscripts

es	=	stagnation
∞	=	upstream of shock

References

1 Goulard, R., "An Optimum Magnetic Field for Stagnation Heat Transfer Reduction at Hypersonic Velocities," Bendix Products Division, Applied Science Laboratory, South Bend, Ind., Feb. 15, 1959.

2 Lykoudis, P. S., "The Matching of the Viscid and Inviscid Regions for the Stagnation Magnetic Flow," *J. Aero/Space Sci*, vol. 26, May 1959, p. 315.

3 Meyerott, R. E., "Radiation Heat Transfer to Hypersonic Vehicles," Third AGARD Combustion and Propulsion Panel Colloquium, Palermo, Sicily, March 17–21, 1958.

[2] Numbers in parentheses indicate References at end of paper.

Technical Comments

Evaluation of Conical Nozzle Thrust Coefficient

G. V. R. RAO[1]

Rocketdyne, Canoga Park, Calif.

THE THRUST of a nozzle based on one-dimensional flow of ideal gas is given by

$$F_i = (w/g)V_e + (p_e - p_a)A_e \qquad [1]$$

This formula is derived under the assumption that at the exit section A_e we have uniform flow of velocity V_e parallel to nozzle axis. The pressure of the gas in the exit plane and the ambient pressure are denoted by p_e and p_a, respectively. In (1)[2] it is shown that the exit flow of a conical nozzle can be represented by a source-type flow, i.e., across the spherical area A_s, as shown in Fig. 1, one can assume a constant velocity V_s and flow direction normal to the spherical surface.

Upon integration, one obtains thrust of a conical nozzle as

$$F_{\text{conical}} = \lambda(w/g)V_s + (p_s - p_a)A_e \qquad [2]$$

where

$$\lambda = \frac{1 + \cos\alpha}{2}$$

In this equation, V_s and p_s are the velocity and pressure corresponding to expansion of the gases to area A_s, given by

$$A_s = (1/\lambda)A_e$$

The use of Equation [2] was clarified in (2), and the effect of using incorrect area A_e was discussed. One obtains different values for exit momentum depending upon whether the exhaust gases starting from the throat section are assumed to expand to exit area A_e or A_s. However, the importance of the critical flow area, which is generally less than the geometric throat area, in determining V_s and p_s was not discussed in (2).

The influence of the nozzle wall at the throat causes nonuniform flow conditions in the throat region. The consequent sonic line configuration is treated in (3). In the linearized treatment of the transonic flow, the shape of the sonic line turns out to be parabolic and depends upon the ratio of throat radius to the radius of curvature of the nozzle wall. One can compute the mass flow crossing the throat section and find that it is less than the critical flow corresponding to uniform flow conditions across the plane area A_t. Let A^* denote the critical area corresponding to the mass flow w/g through the nozzle

$$\frac{w}{g} = \rho^* V^* A^* = \int_0^{R_t} \rho V \cos\theta 2\pi R dR = D\rho^* V^* A_t \qquad [3]$$

The coefficient D in Equation [3] takes into account the loss in theoretical mass flow obtained for ideal gases, because of the influence of nozzle walls. This coefficient should be distinguished from the discharge coefficient of a rocket nozzle, caused by nonideal properties of gases in addition to the wall effect.

The flow coefficient D is always less than unity. Assuming $\gamma = 1.23$, this coefficient is computed for various values of nozzle wall curvature and is shown in Fig. 2. For the sake of comparison, the values of D for $\gamma = 1.4$ are also shown in the figure.

Since critical area is less than throat plane area, the theoretical estimate of mass flow can be modified as

$$\frac{w}{g} = Dp_c A_t \frac{\gamma[2/(\gamma+1)]^{(\gamma+1)/2(\gamma-1)}}{\sqrt{G\gamma RT_c}} \qquad [4]$$

where p_c and T_c denote the chamber pressure and temperature, respectively. γ is the isentropic exponent, and R is the gas constant of the exhaust gases.

Rearranging terms in Equation [2] one obtains

$$F_{\text{conical}} = \lambda p_s A_s(1 + \gamma M_s^2) - p_a A_e$$

or in terms of thrust coefficient

$$F_{\text{conical}} = \lambda p_c A^* C'_{F_{\text{vac}}} - p_a A_e \qquad [5]$$

In the above equation $C'_{F_{\text{vac}}}$ represents one-dimensional thrust coefficient of a nozzle discharging into a vacuum at an area expansion $\epsilon' = A_s/A^*$.

The following formula is widely used in computing the thrust of a conical nozzle

$$F_{0_{\text{conical}}} = \lambda(p_c A_t C_{F_{\text{vac}}} - p_e A_e) + (p_e - p_a)A_e \qquad [6]$$

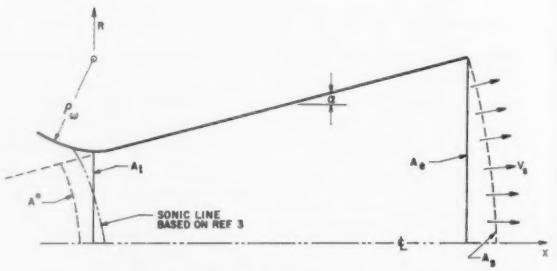

Fig. 1 Conical nozzle parameters

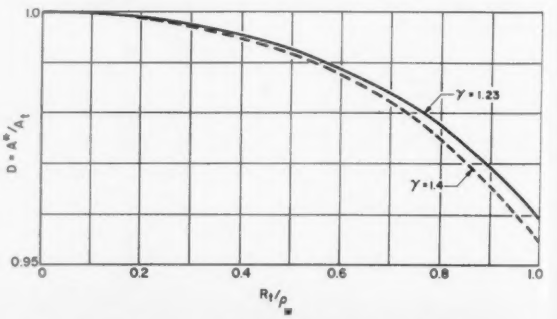

Fig. 2 Variation of flow coefficient with wall curvature

Received June 11, 1959.

[1] Engineering Specialist. Member ARS.

[2] Numbers in parentheses indicate References at end of paper.

where $C_{F_{vac}}$ represents one-dimensional vacuum thrust for area expansion $\epsilon = A_e/A_t$. To evaluate the difference between Equations [5 and 6], one observes the following relation derived from the dependence of one-dimensional thrust coefficient on area expansion

$$\frac{C'_{F_{vac}}}{C_{F_{vac}}} = 1 + \frac{\epsilon' - \epsilon}{\epsilon(1 + \gamma M_e^2)} \quad [7]$$

where M_e is the Mach number corresponding to area ratio ϵ. From the definition of vacuum thrust

$$C_{F_{vac}} = (p_e/p_c)\epsilon(1 + \gamma M_e^2) \quad [8]$$

substituting Equations [7 and 8] into Equation [5] gives

$$F_{conical} = \lambda p_c A^* C_{F_{vac}} + \frac{\epsilon' - \epsilon}{\epsilon} \lambda D p_e A_e - p_a A_e$$

ϵ' and ϵ can be expressed in terms of A_e and A_t in this equation, which reduces to

$$F_{conical} = \lambda D p_c A_t C_{F_{vac}} + p_e A_e(1 - \lambda D - p_a/p_e) \quad [9]$$

The thrust computation of a conical nozzle as given in Equation [9] is more accurate than using [6], under the assumptions involved, since Equation [9] includes the effect of nozzle walls in the throat region. Ignoring this effect means assuming critical flow through throat area A_t. Then the factor D becomes unity, and the above equation reduces to Equation [6]. In the first approximation, we will have

$$F_{conical} = D \cdot F_{0_{conical}}$$

the effect being mainly due to change in the critical mass flow as given by Equation [4].

References

1 Malina, F. J., "Characteristics of the Rocket Motor Based on the Theory of Perfect Gases," *J. Franklin Inst.*, vol. 230, 1940, pp. 433–454.

2 Landsbaum, E. M., "Thrust of a Conical Nozzle," ARS JOURNAL, March 1959, pp. 212–213.

3 Sauer, R., "General Characteristics of the Flow Through Nozzles at Near Critical Speeds," NACA TM 1147, 1947.

Stabilized Gaseous Detonation Waves[1]

J. A. NICHOLLS[2]

The University of Michigan, Ann Arbor, Mich.

RECENT years have witnessed the steady increase of interest in the area of detonative combustion and, of particular interest here, the concept of stationary detonation waves. Recently, Gross (1,2)[3] reported on the attainment of strong stabilized detonation waves and made reference to some of our work. In view of his comments, I feel obligated to elaborate on our experimental procedure and results, to question some of the conclusions he has drawn, and to point out that a standing detonation wave (possibly of the Chapman-Jouguet type) was first achieved at the University of Michigan Aircraft Propulsion Laboratory in May 1958.

Personnel of this laboratory have been studying this problem under sponsorship of the Air Force Office of Scientific Research since 1954. This work has resulted in an experimental facility for generating detonation waves, and much experimental information has been obtained. The essential features of the experimental arrangement are shown in Fig. 1. The nozzle is operated highly underexpanded and discharges to the atmosphere. Typical operating conditions are as follows:

Stagnation pressure of the air and hydrogen, 350–765 psia.
Stagnation temperature of the air, 1950–2600 R.
Stagnation temperature of the hydrogen, 550 R.
Mach number into the normal shock, 3.5–6.2.
Static pressure behind the shock, 20 psia.
Equivalence ratios, 0.33–1.5.

Premature combustion of the gases in the nozzle or upstream of the shock is ordinarily precluded by rapid expansion of the gases. Many runs have been made, and as indicated in the figure, a combustion zone is established which is normally located somewhat downstream of the shock front. This configuration is very steady and reproducible. The attainment of this phenomenon was first reported at the 2nd AFOSR Air Breathing Combustion Symposium, held at Fairchild Engine Division, N. Y., in April 1958. A formal paper covering the results of these experiments was presented at the Seventh Combustion Symposium, London, England, August 1958 (3).

The separation between shock and combustion mentioned above corresponds to the ignition time delay for the given pressure, temperature and mixture ratio existing downstream of the shock. This delay is to be expected, and recent theoretical work by the author has substantiated, reasonably well, the delay times observed. These results will be published in the near future. Now ignition time delay is an exponential function of reciprocal temperature, so it is not surprising that in those cases in which partial premature combustion in the nozzle was experienced (3) the delay decreased to shorter times than could be resolved experimentally. In effect, the premature burning served to increase the stagnation temperature of the stream and, accordingly, the temperature downstream of the shock. The delay was thus materially decreased. Another effect of the premature burning is, of course, a change in the gas composition which tends to obscure the reaction under study and which may or may not expedite the initiation of the combustion reaction.

The question naturally arises as to whether the configuration mentioned is to be properly classified as a detonation wave or merely a case of shock ignition. In many cases we have recorded wave patterns wherein the combustion zone has had little or no effect on shock wave position and hence the Mach number of propagation of the wave. If one were to attempt to classify such waves on the basis of the fuel-air ratio and Mach number of propagation (on a one-dimensional basis), it would be found that some waves corresponded to

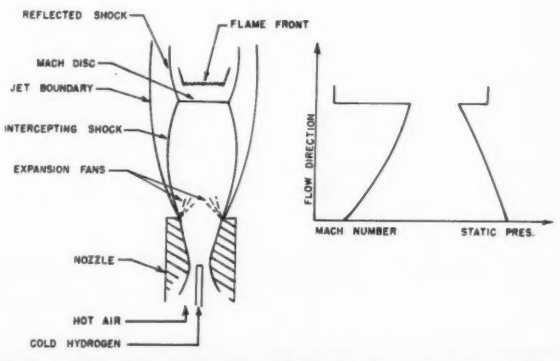

Fig. 1 Standing detonation wave in the open jet of an underexpanded nozzle (schematic)

Received May 28, 1959.

[1] This research was supported by the U. S. Air Force under contract AF 18(600)-1199 monitored by the Air Force Office of Scientific Research, Combustion Dynamics Division, Air Research and Development Command. The work is being continued under contract AF 49(638)-562.

[2] Research Engineer, The University of Michigan Research Institute. Member ARS.

[3] Numbers in parentheses indicate References at end of paper.

strong detonations, some to Chapman-Jouguet, and some would yield no physical solution. It seems apparent that the assumption of a constant-area stream tube breaks down in cases of this type, so that it becomes meaningless to attempt any designation in the conventional manner. Furthermore, with no strong interaction between shock and combustion, it hardly seems plausible that these could rightfully be called detonations. In fact, we have preferred to consider such phenomena as shock ignition. On the other hand, we have observed cases where the onset of combustion has driven the shock upstream to a new lower Mach number of propagation. Such a wave was first observed in May 1958 in which the stagnation temperature of the air was 2600 R, and the stagnation pressure of each stream was 765 psia. The initiation of combustion caused the wave to move upstream from a Mach number of 6.1 to about 5.7 This latter Mach number is close to the Chapman-Jouguet Mach number of detonation under the given conditions This I would refer to as a detonation wave, but will not attempt to define it precisely according to strength in view of difficulties mentioned.

Gross (2) has pointed to the fact that in our experiments light emission is realized for appreciable distances downstream of the wave. On this basis, he expresses some doubt as to whether this could be a detonation wave. Actually, the persistence of the light emission can be attributed to the fact that we inject sodium chloride into the air stream. Furthermore, there will be gradual combustion of the outer portions of the flow that did not pass through the normal shock. Thus, the light emission is irrelevant for either the verification or refutation of the existence of detonation.

As is evident, there is considerable ambiguity surrounding the appropriate description of stabilized shock combustion waves. Certainly, much of this ambiguity is introduced by the finite reaction length required, which subjects the combustion process to externally imposed pressure fields. It is felt, then, that only when the reaction length is small compared to other characteristic dimensions will a true classification of standing detonation waves be possible. This condition can be met at higher temperatures where the kinetics are sufficiently rapid to allow the wave to be treated as a discontinuity.

References

1 Gross, R. A., "Research on Supersonic Combustion," ARS JOURNAL, vol. 29, no. 1, Jan. 1959, pp. 63–64.

2 Gross, R. A. and Oppenheim, A. K., "Recent Advances in Gaseous Detonation," ARS JOURNAL, vol. 29, no. 3, March 1959, pp. 173–179.

3 Nicholls, J. A., Dabora, E. K. and Gealer, R. L., "Studies in Connection with Stabilized Gaseous Detonation Waves," Seventh Symposium (International) on Combustion, Oxford, England, Aug. 1958.

Identification of Inert Objects in Space

LOUIS G. VARGO[1]

Aeronutronic, A Div. of Ford Motor Co., Newport Beach, Calif.

MANMADE objects in space which have ceased to serve their original purpose are variously referred to as "junk" or "debris." These objects are non-emanating and may be considered as lost in the sense that tracking is impossible or unwarranted, or both. There exists a very real possibility, however, that future observations will disclose such objects either by chance or in a search program designed to utilize the inert equipment or structure for other purposes. The period of time that the body remains unobserved may be long indeed. During this period the complex effects of perturbative forces may become of large magnitude, so that radical departures from the original Keplerian orbit will result. It appears important then, to inquire if such objects have some type of "signature" by which they can be positively identified.

Using the reflected radiation characteristics of the body, for example, the radar cross-sectional area, appears not too attractive for several reasons. We will not explore this further except to note that identification by this method has basic difficulties associated with limited resolution capability and the attendant problems of ambiguity.

In 1896, Tisserand[2] addressed himself to a problem which arose in the field of celestial mechanics similar to the one considered here. Cometary orbits, perturbed by a major planet, such as Jupiter, experience large variations in their heliocentric elements between successive observations near perihelion. Since comets are virtually indistinguishable by optical means, the astronomer proposed using the value of an invariant function of the elements, the Jacobi integral, as the identifying characteristic of the body. With certain assumptions, the integral takes the simple form

$$J = \frac{1}{a} + 2\sqrt{a(1 - e^2)}\cos i = \text{constant} \qquad [1]$$

Here a, e and i are, respectively, the semimajor axis, eccentricity and inclination of the Keplerian motion relative to the parent body. The unit of distance is the mean distance of the disturbing body. One merely catalogues values of J for future reference with the knowledge that any variation in J will be orders of magnitude down from changes in the elements themselves.

Several types of missions are currently being considered which result in a situation similar to Tisserand's problem. Among these are terrestrial satellites with perigee distances of several Earth radii and lunar probes that do not impact or escape. These missions give rise to Earth-centered orbits which are dominantly perturbed by the moon. Also, the heliocentric orbit of a nonimpacting planetary probe might well be expected to undergo changes due to the target planet or the Earth on subsequent passages. To date, no artificial objects fall into these classes. One may reasonably anticipate the necessity of having identification methods available.

Received May 19, 1959.

[1] Research Scientist, Astrodynamics Dept. Member ARS.

[2] See Moulton, F. R., "Celestial Mechanics," The Macmillan Co., New York, 1914, pp. 295–298, for a derivation of Tisserand's result.

DYNA-SOAR

Dyna-Soar (for dynamic soaring) is a joint project between the Air Force and the NASA, and is an attempt to solve the technical problems of manned flight in the sub-orbital regions. Advance knowledge on the project indicates how a boost-glide vehicle can operate from the outer fringes of the atmosphere where it can maneuver and be recovered undamaged. Studies show that by varying the original rocket boost, and thus the velocity, and with the control available to the pilot, the Dyna-Soar aircraft can circumnavigate the earth, followed by a normal and controlled landing. Boeing Airplane Company, one of the competing companies for the development contract for the complete boost-glide system, has delegated to RCA the responsibility for the development of important electronic components of Dyna-Soar.

RCA Tmk(s) ®

RADIO CORPORATION of AMERICA

DEFENSE ELECTRONIC PRODUCTS

CAMDEN, N. J.

New Patents

George F. McLaughlin, *Contributor*

Jet engine burner having means for spreading the pilot flame (2,872,785). H. E. Barrett and W. F. Payne, Cedar Grove, N. J., assignors to Curtiss-Wright Corp.

Linear channel members extending from the pilot burner tube to annular channels having an open side facing downstream. Channels have a diameter larger than the tube.

Thermoelectric cooling apparatus (2,872,788). N. E. Lindenblad, Princeton, N. J., assignor to Radio Corporation of America.

Thermocouple element for a heat pump. The element has a pair of bodies of dissimilar thermoelectric material mounted on a plate of conductive material. Members transfer heat between the element and the surrounding air.

Rocket base fuze (2,872,869). V. K. Tasmussen, San Marino, Calif., assignor to the U. S. Navy.

Deceleration discriminating fuze containing a fixed explosive train and a detonator plunger initially held against longitudinal movement. The fuze is detonated at a predetermined reduced deceleration by trigger spring releasing a firing pin.

Igniter squib (2,872,870). W. A. Gey, China Lake, Calif., assignor to the U. S. Navy.

Flame inhibiting means placed upon a cylindrical booster grain of propellant within a housing. The central bore of the grain contains compressed black powder pellets protected from deterioration. The closure is destroyed by burning the igniter propellants.

Solar energy apparatus (2,872,915). W. S. Bowen, Westfield, N. J.

Transparent semicylindrical parabolic mirror forming a closure over a primary semicylindrical parabolic mirror. Both mirrors have the same axis of principal focus. Heat radiated from a heat receiving tube is reflected from both mirrors.

Flight control system (2,873,074). H. Harris, E. B. Hammond Jr., W. T. White and R. M. Giulianelli, North Bellmore, N. Y., assignors to Sperry Rand Corp.

On a dirigible craft, signals are caused by the displacement of the longitudinal axis from a reference direction, and by accelerations normal to the axis. Combined signals are used to control orientation of the craft.

Remote control fluid pressure responsive actuator (2,873,648). C. W. Musser and F. W. Dietsch, Philadelphia, Pa., assignors to the U. S. Army.

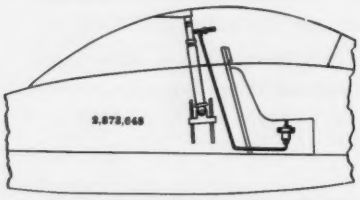

Apparatus for mechanically moving a load by remote control, such as forcibly ejecting an aircraft canopy in an emergency escape. A cartridge actuated thruster is connected by tubing to a cartridge actuated initiator located adjacent to the operator.

Airfoil temperature control means (2,873,933). R. A. Fanti, Springfield, Mass., assignor to United Aircraft Corp.

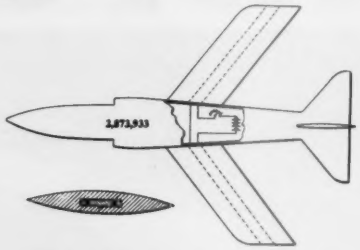

Metal airfoil adapted to be exposed to a high external heat source. Means located in the airfoil for varying the temperature over a minor portion of the chord to maintain a more uniform temperature throughout the chord.

Continuous combustion power plant (2,874,539). H. M. Fox, Bartlesville, Okla., assignor to Phillips Petroleum Co.

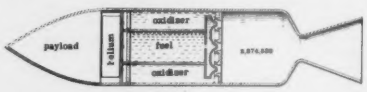

Method of operating a powerplant with a liquid oxidizer selected from the group consisting of white and red fuming nitric acids. The oxidizer and fuel are introduced into the combustion zone in streams at a pressure of 15 to 40 psi greater than the pressure in the combustion zone, so that gentle mixing results.

Substituted furans as hypergolic fuels (2,874,535). A. L. Ayers and C. R. Scott, Bartlesville, Okla., assignors to Phillips Petroleum Co.

Method of developing thrust by the combustion of bipropellant components in a reaction motor. Fuel comprises a hydrocarbon substituted furan. The total number of carbon atoms present in the formula is not greater than 16.

Cooling means for tailpipe (2,874,536). J. A. Benson and G. W. Crosby, Saugus, Mass., assignors to General Electric Co.

Thrust augmentation for a jet engine. Means for permitting axial expansion of the liner between the hot flame area and the afterburner.

Thrust reverser for jet engine (2,874,538). R. G. Laucher and F. A. Coss, Simi, Calif., assignors to Marquardt Aircraft Co.

Variable area exit nozzle composed of segments pivotally connected to the end of the engine. Rearward movement of a shaft forms an opening between a support and a cover through which blocked exhaust gases are expelled to obtain reverse thrust.

Aircraft (2,874,920). G. E. Mallinckrodt, St. Louis, Mo.

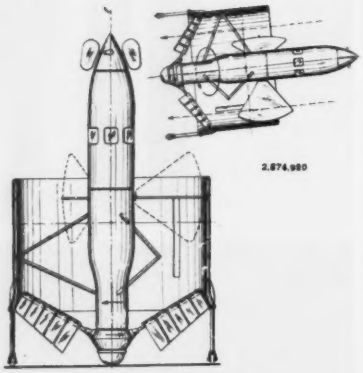

First and second assemblies connected by bearing means adapting them for opposite rotation about an axis of spin. An engine with first and second reactive thrust components, the first attached to a propeller and the second comprising a barrel-shaped wing surrounding the spin axis.

Fuselage shaping to reduce shock waves at transonic and supersonic speeds (2,874,922). R. T. Whitcomb, Hampton, Va.

A first cross-sectional area is taken in a plane perpendicular to the longitudinal axis. A second area is taken in planes tangent to the Mach cone whose axis is on the longitudinal axis, and projected to the airstream, gradually increasing to a maximum and then decreasing from nose to tail.

Variable gear (2,875,628). H. J. Walter, Huntsville, Ala.

Two conically-shaped sets of gears with gradually increased diameters and a single interposed spur gear. One set is mounted on one shaft driven by the driving shaft; the other is mounted on a parallel shaft. The spur gear is shiftable stepwise.

Jet propulsion power plant (2,875,576). J. Endres, Wackersberg, Germany.

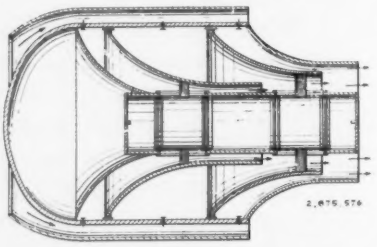

A chamber defined between an inner and an outer cylinder and open at one end to form a discharge nozzle. A pair of opposed pistons operable in the inner cylinder form a central combustion chamber between the pistons and end combustion chambers.

Jet spoiler (2,876,619). A. P. Johnstone, Frimley, England, assignor to Power Jets (Research and Development) Ltd.

Pair of semicircular members at the discharge end of a jet stream. Members may be moved through 90 deg with their concave sides facing upstream to a spoiling position.

EDITOR'S NOTE: Patents listed above were selected from the Official Gazette of the U.S. Patent Office. Printed copies of patents may be obtained from the Commissioner of Patents, Washington 25, D. C., at a cost of 25 cents each; design patents, 10 cents.

The Inquiring Mind at Oldsmobile

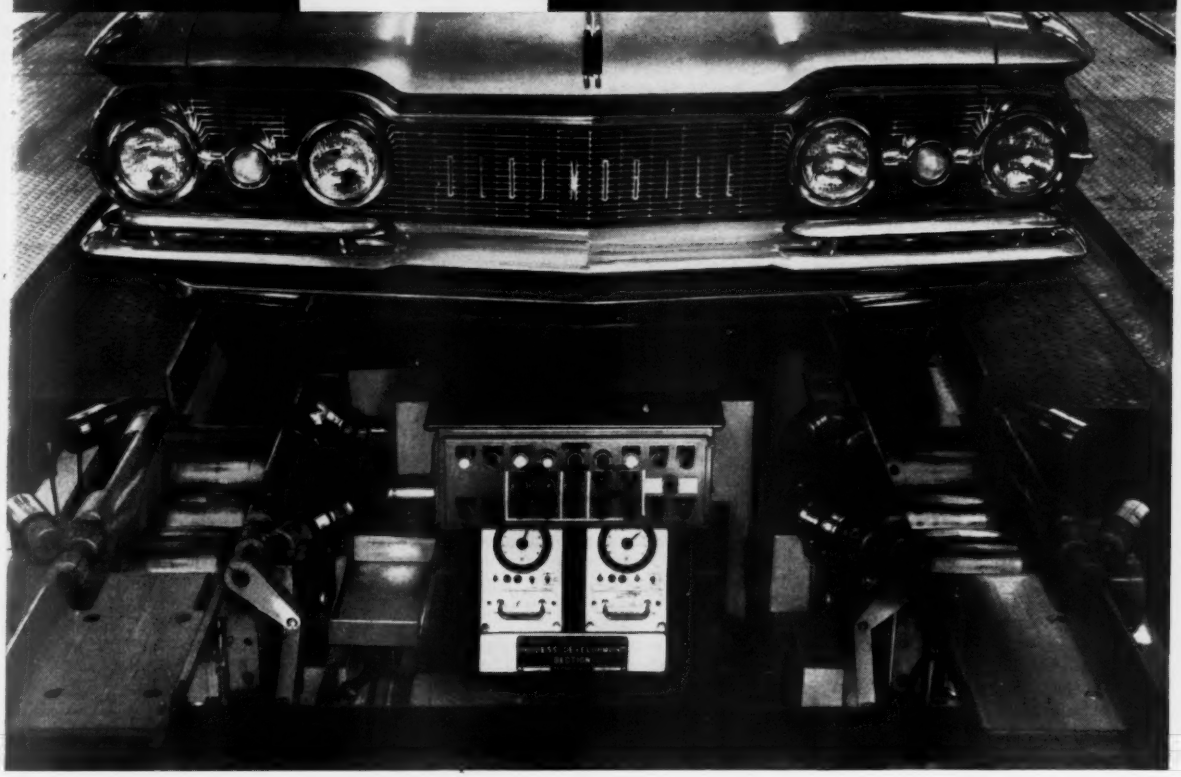

no. 9 OF A SERIES

OLDSMOBILE "TOES THE MARK" ... ELECTRONICALLY!

Oldsmobile Engineering Leadership sets the industry pace with a unique electronic wheel alignment device that dynamically computes "toe-in" measurements for precision steering and handling.

Handling and steering ease depend upon precise, minute measurement and control of front wheel alignment. Because wheels have a tendency to "toe-out" when in motion, they must be adjusted for a slight amount of "toe-in" to eliminate "wheel fight", wander and undue tire wear.

To meet the requirement of rapid, yet extremely accurate measurements on the production line, Oldsmobile engineers developed an electronic computor—a *linear-differential-variable transformer*—that dynamically and accurately measures the average amount of toe-in within .030 inches. As the car is brought into position, the wheels are rotated by rollers to simulate actual driving conditions and to eliminate errors caused by variations in tire run-out. By watching the visual gauges, an operator can quickly make the necessary adjustments to the steering linkage.

By using the most up-to-date electronic measuring techniques in engineering and manufacturing, Oldsmobile is able to offer safe, accurate steering and handling . . . a controlled, comfortable ride. Visit your local Oldsmobile Quality Dealer, take a ride in a '59 Oldsmobile and see why it's the value leader of its class!

OLDSMOBILE DIVISION • GENERAL MOTORS CORPORATION

OLDSMOBILE **Where Proven Quality is Standard!**

Book Reviews

Ali Bulent Cambel, Northwestern University, *Associate Editor*

The Theory and Design of Magnetic Amplifiers, by E. H. Frost-Smith, John Wiley and Sons, Inc., New York, 1958, xix + 481 pp.

Reviewed by G. J. Murphy
Northwestern University

In spite of a statement to the contrary in the Foreword to this book, it does seem a peculiar choice for the first volume in a series on automation and control engineering. Although the book contains much information of value to the designer of magnetic amplifiers, it appears to have been written neither by nor for a control systems engineer.

An elementary introduction is followed by five chapters devoted to the transducer (i.e., the basic amplifying element in a magnetic amplifier). The topics dealt with in these chapters include the basic operation and the characteristics of transductors, the response of a transductor with resistive load to a step input, the steady-state response to a sinusoidal input, the effects of self-excitation and of auto-excitation, and the effect of introducing reactive load components.

Chapter 7, entitled "Closed Loop Control Systems," is simply a very brief (12 pages) treatment of the relation between output and input of single-loop systems with loop transfer functions that have a constant numerator and a denominator of no more than second degree. This chapter is extremely weak and again raises the question of the purpose of including this book in a series of volumes on automation and control engineering.

Chapter 8 is devoted to the transient response and the frequency response of transductors with self-excitation.

The subject of the following three chapters is the use of transductors in various magnetic amplifier circuits. Magnetic modulators are discussed in chapter 12. In chapter 13, the author discusses the construction of magnetic amplifiers, suggests a design procedure, and illustrates the use of the latter in some practical examples.

The fourteenth chapter is devoted to a brief, qualitative treatment of a few systems in which magnetic amplifiers are used. Although a detailed study of some of these systems would be appropriate and of considerable interest, no such study is included.

A short list of references is included, following the appendixes. The references seem to be well-chosen, but the most recent was published in 1955.

The text is supplemented with approximately 20 photographs of equipment, in addition to numerous line drawings.

The impression of this reviewer is that this book may be of considerable interest to the designer of magnetic amplifiers and possibly to an applications engineer, but that it is likely to be very unsatisfying to the theoretically inclined control systems engineer.

Aerodynamics of Supersonic Flight, by Alan Pope, Pitman Publishing Corp., New York, 1958, ix + 243 pp. $6.00.

Reviewed by P. Roy Choudhury
University of Southern California

This is a second edition of "Aerodynamics of Supersonic Flight" which appeared first in 1950. These two editions are very much similar except for an additional chapter on "Performance Calculations" in the second edition. Some new materials are also added in the chapter on "Wind Tunnel Design."

The author has tried "to provide a text at the lowest possible level for a one term course in supersonics," and for that reason, perhaps, he has introduced a great number of topics in a short volume such as this. The topics include fundamental relations, flow in a duct, two-dimensional flow, the oblique shock, approximate theories, supersonic wind tunnels, three-dimensional flow and performance calculations. Like the first edition, the coverage is rather sketchy. At a first glance, the book seems to be a collection of formulas, and many of the explanations seem rather shallow. This is because the author follows a philosophy which educators are currently trying to do away with. He states this philosophy in the preface: "The course treatment is deliberately as non-thermodynamic as possible." In most engineering schools emphasis is placed on the conservation principles (conservation of mass energy and momentum) which form the foundation of most engineering subjects. To try to teach a course in compressible fluids without thermodynamics is not wise and, needless to say, will result in confusion. This is perhaps the weakest point of the text.

The Airglow and the Aurorae, edited by E. B. Armstrong and A. Dalgarno, Pergamon Press, New York, 420 pp. $22.50.

Reviewed by S. F. Singer
University of Maryland

This volume is the fifth one published as a supplement to the *Journal of Atmospheric and Terrestrial Physics*. Volume 1 in this series will be remembered as the highly successful "Rocket Exploration of the Upper Atmosphere." The present volume is very much in the same style. It consists of 53 papers presented at the Conference of Airglow and Aurorae held at the Queen's University of Belfast on September 6–7, 1955, and presents outstanding contributions from workers in all those fields of research which lead to a better understanding of the upper atmosphere.

Following an introductory paper by Prof. Sydney Chapman, the contributions are in seven groups. The first deals with the observations of the airglow, the luminous emission from the upper atmosphere which is produced mainly by photochemical activity. The discussion centers around the emission from excited oxygen atoms, the OH bands and the sodium in the upper atmosphere, particularly the twilight sodium emission.

The next section deals with observations of aurorae and includes a discussion of radio investigations, in addition to the optical measurements.

The next two sections deal with theoretical considerations on how the airglow and aurorae may be excited. Some of the papers deal with the spectroscopic problems of the light emission; others concern the ultimate cause of the aurora. There is, however, no good review of current auroral theories among these contributions.

The next three sections deal with laboratory studies in which luminosities similar to those in the atmosphere are excited, quantal calculations which relate the observed amounts of light to the number of reactions going on, and finally an excellent section on instrumentation, an area in which, as can be imagined, the problems are severe. High speed instruments collect as much of the faint light as possible, and the problem of high resolution is important for measuring the structure of spectral lines and line profiles.

The volume is well-produced, especially the figures, and has subject and name indexes.

A Guide To Nuclear Energy, by R. F. K. Belchem, Philosophical Library, New York, 1958, vii + 77 pp.

Reviewed by J. P. Frankel
University of California

This is a beginners' primer with surprisingly detailed information about reactor principles, process and practice. Its contents range from basic principles of nuclear fission through types of reactors, fuels, fuel elements, materials, reprocessing (no details here) and applications of radiation.

This is the kind of book that can be read by the average high school student in a single sitting; he would benefit greatly from the experience. The rest of us will have to be content with the knowledge that such a book is available to the scientifically uninformed in readable form.

The diction is British; it is a little startling, for instance, to read about ". . .fission products thrown off in the fission process. . ." when one remembers that the mean free path of fission fragments is of the order of millionths of a meter.

The book is recommended for the young scientist-to-be.

Technical Literature Digest

M. H. Smith, *Associate Editor,* **and M. H. Fisher,** *Contributor*
The James Forrestal Research Center, Princeton University

Jet Propulsion Engines

Theoretical and Experimental Study of a Propulsion System, by R. Corelli, *Fusées et Recherche Aéron.*, vol. 3, no. 2, July 1958, pp. 69–73. (In French.)

Contribution to the Study of Normal Combustion in Engines Having Controlled Ignition, by B. Sale, *Inst. Franc. Pétrole, Rév. et Ann. des Combustibles Liquides*, vol. 13, July-Aug. 1958, pp. 1157–1196. (In French.)

A Method for Determining Turbine Design Characteristics for Rocket Turbodrive Applications, by Warner L. Stewart, David G. Evans and Warren J. Whitney, *NACA Res. Mem.* E57K25a, May 1958, 32 pp. (Declassified from Confidential by authority of *NASA Pub. Announcement* 2, p. 17, 12/10/58.)

Rocket Research in Canada, by R. F. Wilkinson, *Inst. Aeron. Sci., Preprint*, 853, Oct. 1958, 22 pp.

EDITOR'S NOTE: Contributions from Professors E. R. G. Eckert, J. P. Hartnett, T. F. Irvine Jr. and P. J. Schneider of the Heat Transfer Laboratory, University of Minnesota, are gratefully acknowledged.

The Rocket Engine Test Facility Sets the Pace, by Benjamin F. Rose Jr., *Inst. Aeron. Sci., Preprint* 840, July 1958, 19 pp.

Design of Ramjet Engine Ground Test Facilities, by S. D. Fasken, *Inst. Aeron. Sci., Preprint* 841, July 1958, 30 pp.

Some Operating Experience and Problems Encountered During Operation of a Free-jet Facility, by John E. McAulay and William R. Prince, *NACA Res. Mem.* E56J02, Feb. 1957, 21 pp. (Declassified from Confidential by authority of *NASA Pub. Announcement* 2, p. 26, 12/10/58.)

Experimental Study of Shock-positioning Method of Ram-jet-engine Control, by Herbert G. Hurrell, George Vasu and William R. Dunbar, *NACA Res. Mem.* E55F21, Aug. 1955, 71 pp. (Declassified from Confidential by authority of *NASA Pub. Announcement* 2, p. 24, 12/10/58.)

Evaluation of Operating Characteristics of a Supersonic Free-jet Facility for Full-scale Ram-jet Investigations, by Carl B. Wentworth, Herbert G. Hurrell and Shigeo Nakanishi, *NACA Res. Mem.* E52I08, Oct. 1952, 27 pp. (Declassified from Confidential by authority of *NASA Pub. Announcement* 2, p. 20, 12/10/58.)

Some Control Considerations for Ramjet Engines, by Seymour G. Himmel, *NACA Res. Mem.* E52F10, Aug. 1952, 40 pp. (Declassified from Confidential by authority of *NASA Pub. Announcement* 2, p. 19, 12/10/58.)

Design and Applications of Mach 4 Turbine Engines, by M. A. Zipkin and R. E. Neitzel, *Inst. Aeron. Sci., Preprint* 859, Oct. 1958, 14 pp.

High-altitude Performance of an Experimental Tubular Prevaporizing Combustor, by Helmut F. Butze, *NACA Res. Mem.* E54I10, Dec. 1954, 29 pp. (Declassified from Confidential by authority of *NASA Pub. Announcement* 2, p. 22, 12/10/58.)

On the Measurement of High Frequency Stability Limits in a Liquid Bipropellant Rocket, by L. Crocco and J. Grey, *Aerotecnica*, vol. 38, June 1958, pp. 135–144. (In Italian.)

An Examination of Solutions of the Underwater Ramjet for Aerial Torpedoes, by Dino Dini, *Aerotecnica*, vol. 38, June 1958, pp. 145–154. (In Italian.)

Gas Turbines . . . Mobile, Flexible Missile Support, by P. B. Garner, *Space/Aeron.*, vol. 30, Dec. 1958, pp. 38–41.

Rocket Throttling: Tricky but Not Impossible, by Kurt R. Stehling, *Space/-*

engineers • scientists

Explore Previously Uncharted Areas in ASTRODYNAMICS and AERODYNAMICS

The Applied Research & Development Division of Republic Aviation is making a multi-disciplined attack on the complex problems posed by advanced and unique flight vehicles. This expanding effort affords you the opportunity to apply your technical imagination and originality in the following areas:

ASTRODYNAMICS
- Space Vehicle Design
- Orbital Mechanics
- Interplanetary Flight
- Re-Entry Flight

AERODYNAMICS
- Missiles & Aircraft Aerodynamics
- Hypersonic Flow
- Physics of Rarefied Gases
- Strong Shock Phenomena

There's a growing atmosphere of technological excitement these days at Republic Aviation Corporation. Accelerating space study contracts plus a number of original proposals in such areas as ICBM's, air-to-surface ballistic missiles and unique aircraft are responsible for this environment that adds incentive for you to use your best thinking. The scope of challenge at Republic ranges from design concept to proof of feasibility. Working within a flexible framework of theoretical and experimental research, you will be able to define your own approach in attaining the requirements of your assignment.

For further information on these positions which combine scientific pioneering with career growth, address your resume to: Mr. George R. Hickman, Engineering Employment Manager, Dept. 10H

REPUBLIC AVIATION
Farmingdale, Long Island, New York

Aeron., vol. 30, Dec. 1958, pp. 66–71.

The World's Aircraft Engines, *Interavia*, vol. 13, Dec. 1958, p. 1279.

Soviet Development of Nuclear Aircraft Engines, by G. N. Nesterenko, A. I. Sobolev and Yu. N. Sushkov, *Space/Aeron.*, vol. 31, Jan. 1959, pp. 132–136.

Aerodynamics of Jet Propelled Missiles

On the Stability of Flow in the Boundary Layer Near the Nose of a Blunt Body, by A. M. Kuethe, *Rand Corp., Res. Mem.* RM-1972 (*ASTIA AD* 150687), Aug. 1957, 13 pp.

Thin Airfoils in Hypersonic Flow with Strong Shocks, by Joseph L. Raymond, *Rand Corp., Paper* P-1189, Dec. 1957, 14 pp.

Sweepback Theory for Shock Waves at Hypersonic Speeds, by J. D. Cole, *Rand Corp., Paper* P-1337, April 1958, 12 pp.

Sweepback Theory for Shock Waves at Hypersonic Speeds, by J. D. Cole, *Rand Corp., Res. Mem.* RM 1991 (*ASTIA AD* 144284), Oct. 1957, 13 pp.

A New Approach to the Theory of Slender Body in Compressible Flow, by Haruo Moriguchi, *J. Phys. Soc. Japan*, vol. 13, Nov. 1958, pp. 1384–1389.

Stability Derivatives for Spinning Bodies of Revolution in the Superaerodynamic Region, by Thomas W. Finch, *Bur. Ordn., TN* 43, 1958, 20 pp

Experimental Studies at Mach Numbers 12 to 19 of Conical and Blunted Bodies at Zero Angle of Attack, by S. M. Bogdonoff and I. E. Vas, *Princeton Univ., Dept. Aeron. Engng., Rep.* 435 (*AFOSR-TN*-58-541; *ASTIA AD* 203181), Sept. 1958, 8 pp.

Theory of Flight of the Sounding Rocket, by V. C. Liu, *ASME, Paper* 58-A-32, Nov. 1958, 3 pp.

Axisymmetric Stagnant Flow of a Viscous and Electrically Conducting Fluid Near the Blunt Nose of a Spinning Body With Presence of Magnetic Field, II: Consideration of Realistic Conditions: Compressible Viscous Layer and Small Magnetic Reynolds Number, by Ching-Sheng Wu, *Princeton Univ., Dept. Aeron. Engng., Rep.* 431 (*AFOSR-TN*-58-711; *ASTIA AD* 162246), Sept. 1958, 36 pp.

Laboratory Studies of Missile Re-entry Aero-thermodynamics, by D. Bershader, *J. Instr. Soc. America*, vol. 5, Nov. 1958, pp. 62–71.

On the Effect of Flow Separation on the Lift of Slender Bodies, by Svetopolk Pivko, *J. Roy. Aeron. Soc.*, vol. 62, Nov. 1958, pp. 832–833.

An Investigation of the Aerodynamic Characteristics of a Series of Cone-cylinder Configurations at a Mach Number of 6.86, by Ralph D. Cooper and Raymond A. Robinson, *NACA Res. Mem.* L51J09, Dec. 1951, 43 pp. (Declassified from Confidential by authority of *NASA Pub. Announcement* 2, p. 27, 12/10/58.)

Generation of High-velocity Projectiles, by Melvin A. Cook and Robert T. Keyes, *J. Appl. Phys.*, vol. 29, Dec. 1958, pp. 1651–1657.

Theoretical Investigation of the Flow Field about Blunt-nosed Bodies in Supersonic Flight, by Roberto Vaglio-Laurin and Antonio Ferri, *J. Aero/Space Sci.*, vol. 25, Dec. 1958, pp. 761–768.

The Effects of Blunt Leading Edges on Delta Wings at March 5,8, by Kenneth F. Nicholson, *J. Aero/Space Sci.*, vol. 25, Dec. 1958, pp. 768–787.

Heat Transfer and Fluid Flow

Heat Transfer in the Turbulent Incompressible Boundary Layer, I: Constant Wall Temperature, by W. C. Reynolds, W. M. Kays and S. J. Kline, *NASA Mem.* 12-1-58W, Dec. 1958, 36 pp.

Heat Transfer in the Turbulent Incompressible Boundary Layer, II: Step Wall-temperature Distribution, by W. C. Reynolds, W. M. Kays and S. J. Kline, *NASA Mem.* 12-2-58W, Dec. 1958, 38 pp.

Heat Transfer in the Turbulent Incompressible Boundary Layer, III: Arbitrary Wall Temperature and Heat Flux, by W. C. Reynolds, W. M. Kays and S. J. Kline, *NASA Mem.* 12-3-58W, Dec. 1958, 52 pp.

Heat Transfer in the Turbulent Incompressible Boundary Layer, IV: Effect of Location of Transition and Prediction of Heat Transfer in a Known Transition Region, by W. C. Reynolds, W. M. Kays and S. J. Kline, *NASA Mem.* 12-4-58W, Dec. 1958, 28 pp.

Air-flow and Thrust Characteristics of Several Cylindrical Cooling-air Ejectors with a Primary to Secondary Temperature Ratio of 1.0, by W. K. Greathouse and D. P. Hollister, *NACA Res. Mem.* E52L24, March 1953, 79 pp. (Declassified from Confidential by authority of *NASA Pub. Announcement* 2, p. 21, 12/10/58.)

Use of IBM 704 Computer for Complicated Thermodynamic Equilibria Calculations, by D. C. Villars, *NAVORD Rep.* 6382 (*NOTS* 2064), July 1958, 12 pp.

Triple Correlations, by M. E. Rose, *AEC*, ORNL-2516, May 1958, 60 pp.

Real Gas Effects on Shock Tube Performance at High Shock Strengths, by J. L. Stollery, *Gt. Brit., Aeron Res. Council, Current Paper* 403, 1958, 12 pp. 12 figs.

The Influence of the Absorption of Radiation in Shock Tube Phenomena, by Jacob Pomerantz, *NAVORD Rep.* 6136, Aug. 1958, 134 pp.

A Study of Some Nearly Free Molecular Flow Problems, by D. Roger Willis, *Princeton Univ., Dept. Aeron. Engng., Rep.*, 440, 1958, 115 pp., 33 figs.

Explosively Induced Nonuniform Oblique Shocks, by John O. Erkman, *Stanford Res. Inst., Poulter Labs., Tech. Rep.* 010–58, June 1958, 17 pp.

The Development of a Variable Mach Number Effuser, by J. B. McGarry, *Gt. Brit., Aeron. Res. Council, Rep. & Mem.* 3097 (Formerly *ARC Tech. Rep.* 19619; *Natl. Gas Turbine Estab., Rep.* R210), 1958, 15 pp.

Static Crucible Investigation of Corrosion and Mass-transfer of Nickel in Molten Sodium Hydroxide with Various Additives, by Americo F. Forestieri and William F. Zelezny, *NACA Res. Mem.* E53F12, Aug. 1953, 25 pp.

Preliminary Investigation of Corrosion by Molten Sodium Hydroxide Flowing in Tubes of AISI 347 Stainless Steel, Inconel, and Nickel Having Average Outer-wall Temperatures of 1500° F and a Circumferential Temperature Gradient of 20° F, by Don R. Mosher and Leland G. Desmon, *NACA Res. Mem.* E51J16, March 1952, 20 pp.

Determination of High Gas Temperatures at High Speeds, II, by E. Neher, *Archiv Für Tech. Messen*, 273, Oct. 1958, pp. 205–208. (In German.)

Solution to the Previous General Motors Institute Classroom Problem: Determine the Static and Total Temperatures of a High Temperature, High Velocity Gas Stream, by Kenneth W. Woodfield and Rodger Bloomfield, *Gen. Motors Engng. J.*, vol. 5, Oct.-Dec. 1958, pp. 47–49.

Unsteady Laminar Boundary Layers in an Incompressible Flow, by Kwang-Tzu Yang, *J. Appl. Mech.*, vol. 25, Dec. 1958, pp. 421–427.

Thermoelectric Effects and Irreversible Thermodynamics, by G. N. Hatsopoulos and J. H. Keenan, *J. Appl. Mech.*, vol. 25, Dec. 1958, pp. 428–432.

Comparison between the Linear and Nonlinear Steady-state Behavior of a Heated Tube, by B. L. McFarland, *J. Appl. Phys.*, vol. 29, Dec. 1958, pp. 1682–1684.

Approximate Three-dimensional Solutions for Transient Temperature Distribution in Shells of Revolution, by Maurice A. Brull and Jack R. Vinson, *J. Aero/Space Sci.*, vol. 25, Dec. 1958, pp. 742–750.

Turbulent Heat Transfer Through a Highly Cooled, Partially Dissociated Boundary Layer, by Peter H. Rose, Ronald F. Probstein and Mac C. Adams, *J. Aero/Space Sci.*, vol. 25, Dec. 1958, pp. 751–759.

On Pitot Pressure in an Almost-free-molecule Flow—a Physical Theory for Rarefied-gas Flows, by V. C. Liu, *J. Aero/Space Sci.*, vol. 25, Dec. 1958, pp. 779–780.

Experimental Mixing Profiles of a Mach 2.6 Free Jet, by Edward T. Pitkin and Irwin Glassman, *J. Aero/Space Sci.*, vol. 25, Dec. 1958, pp. 791–792.

On the Formation of Magneto-hydrodynamic Shock Waves, by S. Segre, *Nuovo Cimento*, vol. 9, Sept. 16, 1958, pp. 1054–1057.

Growth of Electric Space-charge and Radio Waves in Moving Ion Streams, by J. H. Piddington, *Phil. Mag.*, Ser. 8 vol. 3, Nov. 1958, pp. 1241–1248.

The Boundary Layer Equations of Compressible Flow. Separation, by D. Meksyn, *Zeitschr. f. Angewandte Math. u. Mech.*, vol. 38, Sept.-Oct. 1958, pp. 372–379.

Experimental Investigation of Harmonic Oscillations in Rotating Flow, by H. Oser, *Zeitschr. f. Angewandte Math. u. Mech.*, vol. 38, Sept.-Oct. 1958, pp. 386–391. (In German.)

The Exterior Limiting Conditions of the Boundary Layer Differential Equations, by K. Nickel, *Zeitschr. f. Angewandte Math. u. Mech.*, vol. 38, Sept.-Oct. 1958, pp. 400–401. (In German.)

Heat Transfer and Reynolds' Analogy in a Turbulent Flow with Heat Release, by R. R. Hunziker, *Zeitschr. f. Angewandte Math. u. Phys.*, vol. 9a, no. 4, Nov. 11, 1958, pp. 307–315. (In English.)

Low Prandtl-number Free Convection, by J. L. Gregg and E. M. Sparrow, *Zeitschr. f. Angewandte Math. u. Phys.*, vol. 9a, no. 4, Nov. 11, 1958, pp. 383–387. (In English.)

A Simple Relationship Between the Shock and Expansion Pressure Coefficients as a Basis for Studying Two Dimensional Hypersonic Flow, by J. L. Raymond, *Rand Corp., Paper* P-1011, Jan. 1957, 45 pp.

Transport Coefficients of Dissociating and Slightly Ionizing Air, by P. S. Freifinger, *Rand. Corp., Res. Mem.* RM-1794 (*ASTIA AD* 133002), April 1957, 25 pp.

Surface Protection and Cooling Systems for High Speed Flight, by D. J. Mason and C. Gazley Jr., *Rand Corp. Res. Mem.* RM-1735, March 1956, 42 pp.

On the Propagation of Thermal Waves

in Media with Stored Energy, by A. J. E. Foreman, *Gt. Brit., Atomic Energy Res. Estab., AERE T/M* 162, 1958, 10 pp.

Investigation of the Transmission of a Shock Wave Through an Orifice, by Louis L. Monroe, *Calif. Inst. Techn., Guggenheim Aeron. Lab., Hypersonic Res. Proj., Mem.* 46, Sept. 1958, 54 pp.

Combustion, Fuels and Propellants

A Modified Analysis for the Determination of the Burning Velocity of a Gas Mixture in a Spherical Constant Volume Combustion Vessel, by K. H. O'Donovan and C. J. Rallis, *Witwatersrand Univ., Dept. Mech. Engng., Rep* 1/58, May 1958, 30 pp.

Ignition of and Flames above Hydrogen Peroxide Solutions, by Charles N. Satterfield, Ephraim Kehat and Maria A. T. Mendes, *MIT, Dept. Chem. Engng., Rep.* 54, Oct. 1958, 15 pp.

Effect of Fuel Variables on Carbon Formation in Turbojet-engine Combustors, by Edmund R. Jonash, Jerrold D. Wear and William P. Cook, *NACA Rep.* 1352, 1958, 18 pp.

Spontaneous Flammability of Pentaborane and Pentaborane-3-methylpentane Blends, by Edward A. Fletcher, *NACA Res. Mem.* E53I17, Feb. 1957, 11 pp. (Declassified from Confidential by authority of *NASA Pub. Announcement* 1, p. 12,11/14/58.)

Performance Estimation of the Coolant Fuel System, Final Summary Report, *Odin Associates, Tech. Rep.* 100–1 (*AFOSR-TR*-58-43; *ASTIA AD* 154150), Dec. 1957, 23 pp.

Development of a Double Base Propellant Charge for T17E2 JATO, by John Berti and Theodore Zimmerman, *Picatinny Arsenal, Feltman Res. and Engng. Labs., Tech. Rep.* 2540 (*ASTIA AD* 201101), Sept. 1958, 18 pp.

A Pressure Bomb for the Photography of Burning Strands of Solid Propellant, by David R. Margetts and Benjamin V. Connor, *Calif. Inst. Tech., Jet Prop. Lab., Rep.* 20-119, July 1958, 21 pp.

Energy Partition in the Exploding Wire Phenomenon, by F. D. Bennett, *Aberdeen Proving Ground, Ball. Res. Labs., Rep.* 1056, Oct. 1958, 32 pp.

Development and Evaluation of New Nitrometer Reaction Bulb, by Milton Roth, Raymond F. Wegman and George Albansoder, *Picatinny Arsenal, Feltman Res. and Engng. Labs., Tech. Rep.* 2579 (*ASTIA AD* 203400), Nov. 1958, 11 pp.

On the Stability of a Plane Deflagration Wave, by J. Mendes, *Calif. Inst. Tech., Jet Prop. Lab., Progr. Rep.* 20-360, Aug. 1958, 18 pp.

A Contribution to the Theory of Laminar Flames with Radial Symmetry, by J. Menkes, *Calif. Inst. Tech., Jet Prop. Lab., Progr. Rep.* 20-361, Aug. 1958, 29 pp.

An Experimental Investigation on Flame Stabilization in a Heated Turbulent Boundary Layer, by Donald Lawson Turcotte, *Calif. Inst. Tech., Jet Prop. Lab., Progr. Rep.* 20-355, June 1958, 88 pp.

Experiments Concerning the Occurrence and Mechanism of High Frequency Combustion Instability, by Calvin Larue Barker, *Calif. Inst. Tech., Jet Prop. Lab., Progr. Rep.* 20–356, Aug. 1958, 92 pp.

The Effect of Fuel Types and Admission Method upon Combustion Efficiency, by H. M. McManus Jr., W. E. Ibele and T. E. Murphy, *ASME, Paper* 58-A-128, Nov. 1958, 4 pp.

MATHEMATICS

Explore new areas in mathematics at IBM

Creative IBM mathematicians are discovering important, new applications of mathematics in the electronic computer field. With the aid of large-scale computers, for example, one group of mathematicians simulated in a matter of weeks, eight years of engineering work which have yet to begin. Other IBM mathematicians are studying vehicular penetration problems involving thousands of variables. Rewarding careers are now available in such areas as computer system design and analysis; human factors engineering; mathematical and numerical analysis; probability, communication, and information theory; reliability; scientific programming; statistics; and switching theory.

A career with IBM offers advancement opportunities and rewards. You will enjoy professional freedom, comprehensive education programs, and the assistance of skilled specialists. Working independently or as a member of a small team, your contributions are quickly recognized. This is a unique opportunity for a career with a company that has an outstanding growth record.

Qualifications: B.S., M.S., or Ph.D. in Mathematics, Physics, Statistics, Engineering Science, or Electrical Engineering—and proven ability to assume important technical responsibilities in your sphere of interest.

For details, write, outlining background and interests, to:

Mr. R. E. Rodgers, Dept. 572H
IBM Corporation
590 Madison Avenue
New York 22, N. Y.

IBM®

INTERNATIONAL BUSINESS MACHINES CORPORATION

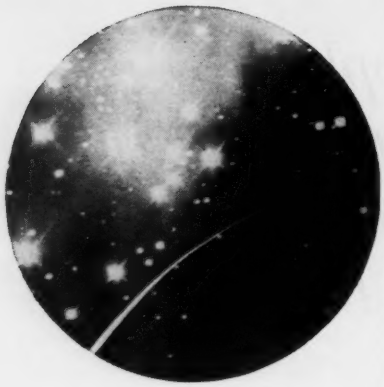

Senior staff openings in basic research

THE BOEING SCIENTIFIC RESEARCH LABORATORIES are engaged in a program of fundamental research designed to make contributions to the progress of the physical sciences. High-level staff positions are open now in the fields of

Gas Dynamics
Plasma Physics
Mathematics
Solid State Physics
Electronics
Physical Chemistry
Geoastrophysics

Boeing grants scientists the latitude and independence needed to achieve and maintain leadership in their special fields. Scientists interested in carrying on their work in this kind of stimulating research environment are invited to communicate with Mr. G. L. Hollingsworth, Director, Boeing Scientific Research Laboratories.

P. O. Box 3822 - JTB
Boeing Airplane Company
Seattle 24, Washington

BOEING

Heat Transfer to Anhydrous Ammonia Flowing Turbulently in an Unsymmetrically Heated Rectangular Tube, by R. Mascolo, *North American Aviation, Inc., Rocketdyne Div., Rep.* R-1155, Nov. 1958, 46 pp.

Cooperative Test Projects of the Joint Army Navy Air Force Panel on Analytical Chemistry of Solid Propellants, Round Robin 4: Ethyl Centralite and Nitroglycerin in Cordite N; Round Robin 5: Heat of Explosion; Round Robin 6: Triacetin in OGK Propellant, by R. H. Pierson, *Naval Ordn. Test Sta., NOTS* 1937, part 3, Feb. 1958, 60 pp.

Halogen Fluorides and Other Covalent Fluorides, Physical and Chemical Properties, by Howard C. Clark, *Chem. Revs.*, vol. 58, Oct. 1958, pp. 869–894.

A Theory for Estimation of Interfacial Energies, II: Application to Surface Thermodynamics of Teflon and Graphite, by Robert J. Good, Louis A. Girifalco and Gerard Kraus, *J. Phys. Chem.*, vol. 62, Nov. 1958, pp. 1418–1421.

The High Temperature Heat Contents of Sodium Ferrite and A-Aluminum Oxide, by John L. Margrave and Robert T. Grimley, *J. Phys. Chem.*, vol. 62, Nov. 1958, pp. 1436–1438.

Heats of Formation of Diborane and Pentaborane, by Edward J. Prosen, Walter H. Johnson and Florence Y. Pergiel, *J. Res. Nat. Bur. Standards*, vol. 61, Oct. 1958, pp. 247–250.

Infrared Emission Spectra of Flames under High Resolution, by Earle K. Plyler and Eugene D. Tidwell, *J. Res. Nat. Bur. Standards*, vol. 61, Oct. 1958, pp. 263–268.

Boron Plus Deuteron Reactions, by R. W. Kavanagh and C. A. Barnes, *Phys. Rev.*, vol. 112, Oct. 15, 1958, pp. 503–511.

Cyclotron Resonance in Flames, by Jürgen Schneider and F. W. Hofmann, *Phys. Rev. Letters*, vol. 1, no. 11, Dec. 1, 1958, pp. 408–409.

Photometric Investigations of Alkali Metals in Hydrogen Flame Gases, III: The Source of the Alkali Metal Continuum by C. G. James and T. M. Sugden, *Proc., Roy. Soc., London*, vol. A248, Nov. 11, 1958, pp. 238–247.

Photometric Investigations of Alkali Metals in Hydrogen Flame Gases, IV: Thermal and Chemiluminescent Effects Produced by Free Radicals, by P. J. Padley and T. M. Sugden, *Proc., Roy. Soc., London*, vol. A248, Nov. 11, 1958, pp. 248–265.

Analytical Evaluation of Effect of Inlet-air Temperature and Combustion Performance of Boron Slurries and Blends of Pentaborane in Octene-1; Supplement I: Influence of New Boric-oxide Vapor-pressure Data on Calculated Performance of Pentaborane, by Leonard K. Tower, *NACA Res. Mem.* E56D02, May 1956, 11 pp. (Declassified from Confidential by authority of *NASA Pub. Announcement* 1, p. 16, 11/14/58.)

Analytical Evaluation of Effect of Inlet-air Temperature and Combustion Pressure on Combustion Performance of Boron Slurries and Blends of Pentaborane in Octene-1, by Leonard K. Tower, *NACA Res. Mem.* E55A31, June 1955, 79 pp. (Declassified from Confidential by authority of *NASA Pub. Announcement* 1, p. 15, 11/14/58).

Materials of Construction

High-temperature Mechanical Properties of Graphite, I: Creep in Compression, by Paul Wagner and Allen R. Driesner, *J. Appl. Phys.*, vol. 30, Feb. 1959, pp. 148–151.

High-temperature Properties of Graphite, II: Creep in Tension, by Paul Wagner, Allen R. Driesner and Larry A. Haskin, *J. Appl. Phys.*, vol. 30, Feb. 1959, pp. 152–154.

New Aspects in Ceramic Coatings, by Paul A. Huppert, ARS JOURNAL, vol. 29, Jan. 1959, pp. 19–21.

Measurements of Total Hemispherical Emissivity of Several Stably Oxidized Metals and Some Refractory Oxide Coatings, by William R. Wade, *NASA Mem.* 1-20-59L, Jan. 1959, 3 pp.

Approximate Equations for Interconverting the Various Mechanical Properties of Linear Viscoelastic Materials, by Thor L. Smith, *Calif. Inst. Tech., Jet Prop. Lab., Mem.* 20-176, Nov. 1958, 27 pp.

State of the Art: Structures and Materials, *Space-Aeron.*, vol. 31, March 1959, pp. 40–41.

Instrumentation, Telemetering, Data Recording

Determination of the Speed of Moving Bodies with the Help of the Doppler Effect, by Siegmund Wintergerst, *Arch. f. Tech. Messen*, No. 275, Dec. 1958, pp. 241–242. (In German.)

New Strain Gages for the Space Age, *ISA J.*, vol. 6, Feb. 1959, pp. 50–51.

Device for Thermal Control of Liquid Hydrogen Bubble Chambers, by Pierre Amiot, *Nuclear Instruments*, vol. 3, no. 5, Nov. 1958, pp. 275–277.

Electronic Apparatus for the Measurement of Dynamic Magnetic Fields, by I. F. Quercia, *Nuclear Instruments*, vol. 3, no. 5, Nov. 1958, pp. 292–297.

Forced Precession of Symmetrical Gyroscopes under Vertical Shock, by F. Weidenhammer, *Zeitschr. f. Angewandte Math. u. Mech.*, vol. 38, Nov.-Dec. 1958, pp. 480–483. (In German.)

Electronic Flow Control, by J. G. Ziegler and N. B. Nichols, *ISA J.*, vol. 6, Jan. 1959, pp. 64, 69.

Avionics, *Aviation Week*, vol. 69, Mid-December 1958, Section C, 106 pp.

Instruments: Key to Missile Program, by F. Leary, *Electronics*, vol. 32, Jan. 16, 1959, pp. 47–51.

Preliminary Development of Telemetry for Aeroballistic Ranges, by M. K. Kingery, *Arnold Engng. Dev. Center, TN*-59-7 (*ASTIA AD* 208692), Feb. 1959, 25 pp.

Electronic Transient Recorder for Tracking of High Speed Projectiles, by D. Ritke and E. White, *Univ. of Maryland, Inst. Molecular Phys.*, IMP-ONR-1, Nov. 1958, 17 pp.

Transducer Frequency Response Evaluation for Rocket Instability Research, by Charles R. Tallman, ARS JOURNAL, vol. 29, Feb. 1959, pp. 119–122.

A New Mass Flow Meter for Liquid Streams, by R. F. Wall, *Ind. Engng. Chem*, vol. 51, Feb. 1959, pp. 69A–70A.

Some Effects of Vibration and Rotation on the Drift of Gyroscopic Instruments, by R. M. Stewart, ARS JOURNAL, vol. 29, Jan. 1959, pp. 22–28.

A Radioactive Ionization Gage Pressure Measurement System, by N. W. Spencer and R. L. Boggess, ARS JOURNAL, vol. 29, Jan. 1959, pp. 68–71.

Guidance Systems and Components

Selection of an Aerodynamic Configuration for Improved Beam Rider Guidance, by Basil Staros, Richard Gretz and Merven Mandel, ARS JOURNAL, vol. 29, Feb. 1959, pp. 115–118.

Guidance for Sputnick III; the Russian Satellite Made Use of Some Very Ingenious Devices, by Richard E. Stockwell, *Ordnance*, vol. 43, Jan.-Feb. 1959, pp. 673–675.

Servomechanisms and Controls

An Attitude Control System for Space Vehicles, by Walter Haeussermann, ARS JOURNAL, vol. 29, March 1959, pp. 203–207.

Spatial Attitude Control of a Spinning Rocket Cluster, by Walter Haeussermann, ARS JOURNAL, vol. 29, Jan. 1959, pp. 56–58.

The Cluster Spin Control System for Jupiter C Missiles, by Niels Jasper and Dieter Teuber, ARS JOURNAL, vol. 29, Jan. 1959, pp. 58–61.

Flight Vehicle Design and Testing

Missile Ground Equipment, by B. J. Meldrum, *SAE Preprint* 5T, Jan. 1959, 8 pp.

Precise Electric Power for Ground Support of Missiles, by David Ginsberg, *SAE Preprint* 7R, Jan. 1959, 5 pp.

Design and Fabrication of a Re-entry Vehicle, by Leon L. Farnham, ASTRONAUTICS, vol. 4, March 1959, pp. 26–27, 57–58.

Heat Protection for Re-Entry Vehicles, by Norris F. Dow, ASTRONAUTICS, vol. 4, March 1959, pp. 28–29, 82, 84, 86.

Missile Reliability Now; Surveillance and Research Programs Must Assure Weapon Dependendability, by T. H. Braunstein, *Ordnance*, vol. 43, Jan.-Feb. 1959, pp. 686–687.

Optimization of Rockets for Maximum Payload Energy, by Dandridge, M. Cole and Michael A. Marrese, ARS JOURNAL, vol. 29, Jan. 1959, pp. 71–73.

Interrelationship of Calculus of Variations and Ordinary Theory of Maxima and Minima for Flight Mechanics Applications, by Angelo Miele, ARS JOURNAL, vol. 29, Jan. 1959, pp. 75–76.

Space Flight

Centimetric Radar Observations of the Russian Satellites, by J. S. Hey and V. A. Hughes, *Proc. Roy. Soc.*, vol. 248A, Oct. 28, 1958, pp. 34–42.

Method for Computations of Satellite Orbits, by L. Jacchia, *Proc. Roy. Soc.*, vol. 248A, Oct. 28, 1958, pp. 43–44.

The Prediction Service of H.M. Nautical Almanac Office, by D. H. Sadler, *Proc. Roy. Soc.*, vol. 248A, Oct. 28, 1958, pp. 45–47.

The Computation of Orbit Parameters from Interferometer and Doppler Data, by E. G. C. Burt, *Proc. Roy. Soc.*, vol. 248A, Oct. 28, 1958, pp. 48–54.

Perturbations of the Orbit of a Satellite Near to the Earth, by D. G. King-Hele, *Proc. Roy. Soc.*, vol. 248A, Oct. 28, 1958, pp. 55–62.

Interested in Systems Engineering?

There are systems

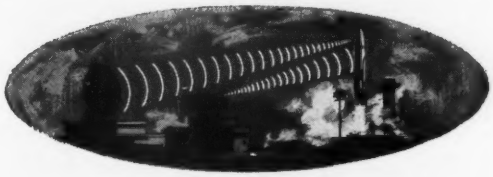

...and systems

...and TOTAL systems in which the big bird and support equipment may rank only as a component.

This difference between systems can make a big difference in your career

IF YOU ARE QUALIFIED and interested in contributing to programs of "total" scope, it will be of value to you to investigate current opportunities with General Electric's DEFENSE SYSTEMS DEPT., whose work lies primarily in providing *total* solutions to large scale defense problems of the next 5, 10 and 20 years.

The work here lies almost entirely in the areas of systems engineering and systems management.

Inquire about these positions:

- Guidance Equation Engineers
- Systems Logistics Engineers
- Electronic Systems Management Engineers
- Operations Analysis Engineers
- Systems Program Engineers
- Data Processing Engineers
- Systems Test Evaluation Engineers
- Engineering Psychologists
- Radar Equipment Engineers
- Weapons Analysis Engineers
- Weapons Systems Integration Engineers
- Engineering Writers

Forward your confidential resume at an early date.

Whereas the growth potential is evident – both for DSD and the engineers who join us – the positions we fill during these early months will carry significant "ground-floor" benefits.

Write fully to Mr. E. A. Smith, Room 8-M.

DSD DEFENSE SYSTEMS DEPARTMENT

A Department of the Defense Electronics Division

GENERAL ELECTRIC

300 South Geddes Street, Syracuse, N. Y.

ENGINEERS and SCIENTISTS

Research Opportunities

Aeronutronic, a new division of Ford Motor Company, has immediate need for qualified people to staff senior positions at its new $22 million Research Center in Newport Beach, Southern California.

The Space Technology Operation offers the highly desirable combination of new facilities and advanced equipment, located in California's finest environment for living and raising a family. Investigate these exceptionally rewarding positions now:

VEHICLE TECHNOLOGY

- Aerodynamic design and testing
- Rocket engine development
- Rocket nozzle and re-entry materials
- High temperature chemical kinetics
- Combustion and detonation theory
- Combustion thermodynamics
- High temperature structural plastics & ceramics
- Advanced structures
- Rocket vehicle systems

MISSILE DEFENSE

- Supersonic aerodynamics
- Aerothermodynamics
- High temperature heat transfer
- Space physics
- Re-entry programs

ASTRO SCIENCES

- Space electronics
- Guidance & control
- Communications
- Instrumentation
- Experimental physics
- Plasma and magneto-hydrodynamics studies

Visit Aeronutronic's exhibit booth 3822-24 at the WESCON show.

Qualified applicants are invited to send resumes and inquiries to Mr. R. W. Speich, Aeronutronic, Dept. 19, Box 451, Newport Beach, California.

AERONUTRONIC

a division of
FORD MOTOR COMPANY

Newport Beach
Santa Ana • Maywood, California

Direction Finding Observations on the 20Mc/s Transmissions from the Artificial Earth Satellites, by F. A. Kitchen, *Proc. Roy. Soc.*, vol. 248A, Oct. 28, 1958, pp. 63–67.

Radio Observations on 20 and 40 Mc/s, by W. C. Bain, *Proc. Roy. Soc.*, vol. 248A, Oct. 28, 1958, pp. 68–71.

Post Office Observations on the First Russian Satellite, by C. F. Booth, *Proc. Roy. Soc.*, vol. 248A, Oct. 28, 1958, pp. 72–75.

The Ionosphere and the Radio Emission from the Satellites, by K. Weekes, *Proc. Roy. Soc.*, vol. 248A, Oct. 28, 1958, pp. 77–79.

The Rocket's Dimensions, by R. d'E. Atkinson, *Proc. Roy. Soc.*, vol. 248A, Oct. 28, 1958, pp. 80–81.

The British Astronomical Association's and Radio Society of Great Britain's Earth Satellite Observations, by J. Heywood, *Proc. Roy. Soc.*, vol. 248A, Oct. 28, 1958, pp. 82–87.

Electric Power for Space Flight, by J. H. Huth, *Rand. Corp., Paper* P-1244, Dec. 1957, 16 pp.

Power in Space, by J. H. Huth, *Rand Corp., Paper* P-1389, May 1958, 13 pp.

Fuel Cells—Current Problems and Potential Usefulness, by J. H. Huth, *Rand Corp., Paper* P-1187, Sept. 1957, 22 pp.

Skin Temperature Variation During Re-Entry of Scientific Satellite, by D. J. Masson, *Rand Corp., Res. Mem.* RM-1693, March 1956, 8 pp.

Heat Transfer Aspects of the Atmospheric Re-entry of Long Range Ballistic Missiles, by Carl Gazley Jr., *Rand Corp., Rep.* R-273, Aug. 1954, 105 pp.

The Penetration of Planetary Atmospheres, by C. Gazley Jr., *Rand Corp., Paper* P-1322, Feb. 1958, 47 pp.

Lunar Trajectory Studies, by H. A. Lieske, *Rand Corp., Paper* P-1293, Feb. 1958, 36 pp.

Lunar Flight Trajectories, by R. W. Buckheim, *Rand Corp., Paper* P-1268, Jan. 1958, 49 pp.

A Discussion of Energy Sources for Space Communications, by J. H. Huth, *Rand Corp., Rep.* P-1318, March 1958, 25 pp.

Propagation Considerations in Space Operations, by Cullen M. Crain, *Rand Corp., Paper* P-1305, March 1958, 17 pp.

Zero Gravity Effects Largely Unknown, by Brig. Gen. Don Flickinger, *Aviation Week*, vol. 70, Jan. 5, 1959, p. 35.

Radio Tracks Orbits of Man-made Moons, by C. A. Schroeder, C. H. Looney Jr. and H. E. Carpenter Jr., *Electronics*, vol. 32, Jan. 2, 1959, pp. 33–37.

Reliability and Stability Most Critical in Satellite Communication, by DuMont Labs, *Space/Aeron.*, vol. 31, Jan. 1959, pp. 38–45.

Atmospheric Attenuation of Space Communication, *Space/Aeron.*, vol. 31, Jan. 1959, pp. 74–75.

Retro-rockets and Drag Devices Teamed for Satellite Recovery, by F. W. Ross, *Space/Aeron.*, vol. 31, Jan. 1959, pp. 180–184.

Three-dimensional Orbits of Earth Satellites, Including Effects of Earth Oblateness and Atmospheric Rotation, by Jack N. Nielsen, Frederick K. Goodwin and William A. Mersman, *NASA Memo* 12-4-58A, Dec. 1958, 85 pp.

Practical Limitations on Orbit Determination, by Robert M. L. Baker Jr., *Inst. Aeron. Sci., Preprint* 842, July 1958, 10 pp.

Some Problems of Space Navigation, by Robert E. Roberson, *Aero/Space Engng.*, vol. 17, Dec. 1958, pp. 39–43.

SFI—A Prime Factor in Space Technology, by Irwin Kane, *Arma Engng.*, vol. 2, Oct.-Nov. 1958, pp. 25–57.

Satellite Survey: Analysis of Their Orbits and Guidance, by Murray Stateman, *Arma Engng.*, vol. 2, Oct.-Nov. 1958, pp. 28–31.

Aerophysics, Astrophysics

The ARDC Model Atmosphere, 1956, by R. A. Minzer and W. S. Ripley, *Air Force Cambridge Res. Center, Geophysics Res. Directorate, Air Force Surveys in Geophys.* 86 (*AFCRC-TN-56-204; ASTIA AD* 110233), Dec. 1956, 201 pp.

Measurements, by Two Methods, of the Equivalent Black Body Radiation Temperature in the Atmosphere and Infrared Divergence Measurements in the Atmosphere with the Double Radiometer, by Roger L. Aagard, *Minnesota Univ., School of Physics*, Dec. 1958, 35 pp.

Variations in the Cosmic-ray Nucleonic Intensity, by J. A. Lockwood, *Phys. Rev.*, vol. 112, Dec. 1, 1958, pp. 1750–1758.

Suprathermal Particle Production by Binary Stars, by D. A. Tidman, *Phys. Rev.*, vol. 112, Dec. 1, 1958, pp. 1759–1762.

Acceleration Cosmic Radiation, by G. S. Murty and R. K. Varma, *Phys. Rev.*, vol. 112, Dec. 1, 1958, pp. 1789–1792.

Unusual Cosmic-ray Intensity Fluctuations Observed at Southern Stations during October 21–24, 1957, by K. G. McCracken and N. R. Parsons, *Phys. Rev.*, vol. 112, Dec. 1, 1958, pp. 1798–1801.

Rapid Decrease of Cosmic Ray Intensity, by J. F. Steljes and H. Carmichael, *Nuovo Cimento*, vol. 10, no. 2, Oct. 16, 1958, pp. 393–394.

International Conference on Cosmic Rays, Varenna, June 1957. Proceedings, *Nuovo Cimento*, Supplement, 2d Quarter, no. 2, 1958, pp. 126–804.

Comparison of High-altitude Rocket and Satellite Density Measurements, by H. E. LaGow and R. Horowitz, *Phys. of Fluids*, vol. 1, no. 6, Nov.-Dec. 1958, pp. 478–479.

Plasma Motions Induced by Satellites in the Ionosphere, by Lester Kraus and Kenneth M. Watson, *Phys. of Fluids*, vol. 1, no. 6, Nov.-Dec. 1958, pp. 480–488.

Free-flight Test of a Technique for Inflating an NASA 12-foot-diameter Sphere at High Altitudes, by Alan B. Kehlet and Herbert G. Patterson, *NASA Mem.* 2-5-59L, Jan. 1959, 18 pp.

An Astronomical Telescope in Space, by R. J. Davis, F. L. Whipple and C. A. Whitney, *Astronautical Sciences Rev.*, vol. 1, no. 1, Jan.–March 1959, pp. 9–12.

IGY Solar Flare Program and Ionizing Radiation in the Night Sky, by Herbert Friedman, ARS JOURNAL, vol. 29, Feb. 1959, pp. 103–107.

U. S. Extension to ICAO Standard Atmosphere Tables and Data to 300 Standard Geopotential Kilometers, by R. A. Minzner, W. S. Ripley and T. P. Condron, *Air Force Cambridge Res. Center, Geophys. Directorate*, 1958, 236 pp.

Atomic Energy

Potentialities and Problems of Nuclear Rocket Propulsion, by T. P. Cotter, *Inst.*

Aeron. Sci., Rep. 59-24, Jan. 1959, 14 pp.

Performance of Nuclear Electric Propulsion Systems, by V. P. Kovacik and D. P. Ross, *Inst. Aeron. Sci., Rep.* 59–25, Jan. 1959, 12 pp.

A Method for Determining Core Dimensions of Heat Exchanger with One Dominating Film Resistance and Verification with Experimental Data, by John N. B. Livingood and Anthony J. Diaguila, *NACA RM* E56K26a, Jan. 1957, 16 pp.

Potentialities and Problems of Nuclear Rocket Propulsion by T. P. Cotter, *Aero/Space Engng.*, vol. 18, Feb. 1959, pp. 50–53.

Kiwa-A to Test Nuclear Rocket Feasibility, by J. S. Butz Jr., *Aviation Week*, vol. 70, Feb. 16, 1959, pp. 48, 49, 51, 53.

Plasma Motors, by Winston H. Bostick, *J. Astron. Sci.*, vol. 5, Summer 1958, pp. 39–44.

Performance Calculations for Hybrid Nuclear-Chemical Rocket Propulsion Systems, by Leon Green Jr. and James M. Carter, ARS JOURNAL, vol. 29, March 1959, pp. 180–186.

NASA Reactor Facility Hazards Summary, Vol. II, by Lewis Res. Center, *NASA Mem.* 12-10-58E, Feb. 1959, 194 pp.

Lockheed's Georgia Nuclear Laboratory, by W. R. Rhoads, *SAE Preprint* 28, Jan. 1959, 7 pp.

A List of United Kingdom Atomic Energy Research Establishment Unclassified Memoranda and Reports on Controlled Thermonuclear Reactions, by C. S. Sabel, *Gt. Brit., Atomic Energy Res. Estab., AERE Inf/Bib* 117, 1958, 6 pp.

Ignition of a Thermonuclear Plasma by High-energy Injection, by Albert Simon, *Phys. of Fluids*, vol. 1, no. 6, Nov.-Dec. 1958, pp. 489–494.

Russian Technical Articles*

Streamlined Bodies in Non-ideal Gas Flows at High Supersonic Speeds, by G. A. Liubimov, *Akademii Nauk SSSR, Izvestiia, Otdelenie Tekhnicheskikh Nauk, Mashinostroenie i Mekhanik*, no. 1, 1959, pp. 173–176. (In Russian.)

Calculation of Slip during Flow of a Viscous Gas around a Semi-infinite Plate, by V. P. Shidlovskii, *Akademii Nauk SSSR, Izvestiia, Otdelenie Tekhnicheskikh Nauk*, no. 9, Sept. 1958, pp. 82–90. (In Russian.)

Radiation Cooling of Air, I: General Description of the Phenomenon and the Weak Cooling Wave, by Ia. B. Zel'dovich, A. S. Kompaneets and Iu. P. Raizer, *Soviet Physics-JETP*, vol. 34(7), no. 5, Nov. 1958, pp. 882–892.

Stabilization of Temperature of Working Substance of Thermal Resistance, by N. P. Udalov, *Abtomatika i Telemekhanika*, vol. 19, no. 11, 1958, pp. 1070–1072. (In Russian.)

Some Problems of the Thermo-elasticity in Convection with Heat Stresses in Turbine Motors, by A. D. Kovalenko, *Akademii Nauk SSSR, Izvestiia, Otdelenie Tekhnicheskikh Nauk*, Oct. 1958, pp. 68–76. (In Russian.)

Application of the Method of Electric Analogy to the Solution of the Problem of Radiant Heat Transfer, by V. N. Adrianov, *Akademii Nauk SSSR, Izvestiia, Otdelenie Tekhnicheskikh Nauk, Energetika i Abtomatika*, no. 1, 1959, pp. 20–25. (In Russian.)

On the Derivations of Basic Equations in the Hydrodynamic Theory of Heat Transfer, by P. N. Pinsker, *Akademii Nauk SSSR, Izvestiia, Otdelenie Tekhnicheskikh Nauk, Energetika i Abtomatika*, no. 1, 1959, pp. 26–32. (In Russian.)

Oblique Shock Waves in a Plasma with Finite Conductivity, by M. I. Kiselev and V. I. Tsepliaev, *Soviet Physics-JETP*, vol. 34(7), no. 6, Dec. 1958, pp. 1104–1106.

Theory of Excitation of Hydromagnetic Waves, by A. I. Akhiezer and A. G. Sitenko, *Soviet Physics-JETP*, vol. 35(8), no. 1, Jan. 1959, pp. 82–86.

Cooling of Air by Radiation II: Strong Cooling Wave, by Ia. B. Zel'dovich, A. S. Kompaneets and Iu. P. Raizer, *Soviet Physics-JETP*, vol. 34(7), no. 6, Dec. 1958, pp. 1001–1006.

Streamlined Conical Flow in Gases Moving at High Supersonic Speeds, by A. L. Gonor, *Akademii Nauk SSSR, Izvestiia, Otdelenie Tekhnicheskikh Nauk, Mashinostroenie i Mekhanik*, no. 1, 1959, pp. 3–40. (In Russian.)

* The Editors of Technical Literature Digest are making a systematic search for pertinent Russian articles, both in the original Russian and in translated form. For the balance of 1959, these will appear in a separate section with this heading, mainly to draw the readers' attention to the new listing. After that, they will appear item by item under the proper subject headings.

CONTINENTAL AVIATION

CAE

RESEARCH
•
DEVELOPMENT
•
PRODUCTION
•

CONTINENTAL AVIATION & ENGINEERING CORPORATION
12700 KERCHEVAL AVENUE
DETROIT 15, MICHIGAN

RESEARCH ENGINEERS

Challenging positions are available in research for men with B.S. to M.S. degrees in Mechanical Engineering, Chemical Engineering, or Aeronautical Engineering with experience in the fields of rocket propulsion, ballistics, and case design.

We offer you an opportunity to use your initiative and creative ability in an atmosphere conducive to accomplishment. These positions afford association with some of the leading engineers in this field.

Excellent employee benefits including liberal vacation policy and tuition free graduate study. Please send resume to:

E. P. Bloch

ARMOUR RESEARCH FOUNDATION
of
Illinois Institute of Technology
10 West 35th Street
Chicago 16, Illinois

SOUTHWEST
"Monoball"
SELF-ALIGNING BEARINGS

CHARACTERISTICS

	ANALYSIS	RECOMMENDED USE
1	Stainless Steel Ball and Race	For types operating under high temperature (800-1200 degrees F.).
2	Chrome Alloy Steel Ball and Race	For types operating under high radial ultimate loads (3000-893,000 lbs.).
3	Bronze Race and Chrome Steel Ball	For types operating under normal loads with minimum friction requirements.

Thousands in use. Backed by years of service life. Wide variety of Plain Types in bore sizes 3/16" to 6" Dia. Rod end types in similar size range with externally or internally threaded shanks. Our Engineers welcome an opportunity of studying individual requirements and prescribing a type or types which will serve under your demanding conditions. Southwest can design special types to fit individual specifications. As a result of thorough study of different operating conditions, various steel alloys have been used to meet specific needs. Write for Engineering Manual No. 551. Address Dept. ARS-59

SOUTHWEST PRODUCTS CO.
1705 SO. MOUNTAIN AVE., MONROVIA, CALIFORNIA

RESEARCH ENGINEERS

Heat and Mass Transfer

Outstanding opportunities exist in our Heat and Mass Transfer Section for men with advanced degrees and experience in this field. Duties will involve working on research programs in Aerodynamic Heating, Thermal Radiation, Heat Transfer in Reactor Design, and Solar Energy.

These positions are non-routine and require men with initiative and creative ability. Excellent employee benefits and tuition free graduate study. Please send resume to:

E. P. Bloch
ARMOUR RESEARCH FOUNDATION
of
Illinois Institute of Technology
10 West 35th Street
Chicago 16, Illinois

Index to Advertisers

AEROJET GENERAL CORP. ..... Back cover
D'Arcy Advertising Co., Los Angeles, Calif.

AERONUTRONIC SYSTEMS, INC. 618
Honig-Cooper, Harrington & Miner, Los Angeles, Calif.

ALLIED CHEMICAL CORP., GENERAL CHEMICAL DIV. 551
Kastor, Hilton, Chesley, Clifford & Atherton, Inc.. New York, N. Y.

ARMOUR RESEARCH FOUNDATION OF ILLINOIS INSTITUTE OF TECHNOLOGY 619, 620

BOEING AIRPLANE CO. 616
Fletcher Richards, Calkins & Holden, Inc., Seattle, Wash.

BULOVA WATCH CO. 549
Duncan-Brooks, Inc., Garden City, N. Y.

CONTINENTAL AVIATION & ENGINEERING CORP. 619
The Hopkins Agency, Detroit, Mich.

CONVAIR, A DIV. OF GENERAL DYNAMICS CORP. ... 3rd cover
Lennen & Newell, Inc., Los Angeles, Calif.

GENERAL ELECTRIC CO., DEFENSE SYSTEMS DEPT. 617
Deutsch & Shea, Inc., New York, N. Y.

GENERAL MOTORS CORP., OLDSMOBILE DIV. 611
D. P. Brother & Co., Detroit, Mich.

GROVE VALVE & REGULATOR CO. ..... 2nd cover
L. C. Cole Co., Inc., San Francisco, Calif.

INTERNATIONAL BUSINESS MACHINES CORP. 615
Benton & Bowles, Inc., New York, N. Y.

JET PROPULSION LABORATORY 552
Stebbins & Cochran, Los Angeles, Calif.

RADIO CORP. OF AMERICA 609
Al Paul Lefton Co., Inc., Philadelphia, Pa.

REPUBLIC AVIATION CORP. 613
Deutsch & Shea, Inc., New York, N. Y.

SOUTHWEST PRODUCTS CO. 620
O. K. Fagan Adv. Agency, Los Angeles, Calif.